Max-Planck-Institut für Metallforschung
Stuttgart

Whisker formation on Sn thin films

Matthias Lukas Sobiech

Dissertation
an der
Universität Stuttgart

Bericht Nr. 232
November 2010

Whisker formation on Sn thin films

Von der Fakultät Chemie der Universität Stuttgart
zur Erlangung der Würde eines Doktors der Naturwissenschaften (Dr. rer. nat.)
genehmigte Abhandlung

vorgelegt von

Matthias Lukas Sobiech

geboren in Zakopane (Polen)

Hauptberichter:	Prof. Dr. Ir. E. J. Mittemeijer
Mitberichter:	Prof. Dr. J. Bill
Prüfungsvorsitzender:	Prof. Dr. E. Roduner
Tag der Einreichung:	07.09.2010
Tag der mündlichen Prüfung:	26.11.2010

MAX-PLANCK-INSTITUT FÜR METALLFORSCHUNG IN STUTTGART
ROBERT BOSCH GMBH IN REUTLINGEN
INSTITUT FÜR MATERIALWISSENSCHAFT DER UNIVERSITÄT STUTTGART

Stuttgart 2010

1. General introduction

The phenomenon of whisker formation on Sn thin films is known since nearly 60 years [1], but only recently the growth of such needle-like Sn single-crystals from the surface of Sn coatings frequently employed in microelectronic industry attracted great technological and, particularly, scientific interest [2, 3]. Conductive filamentary Sn whiskers can bridge the fine-pitched gaps (~ 200 µm) between electrical (Sn-coated) conductors and thereby potentially cause short-circuit failure of the electronic equipment (see Fig. 1.1) [2, 4]. As since July, 1st 2006 the up to now commonly and successfully applied "remedy" against Sn whisker growth in industrial manufacturing, namely Pb-addition to pure Sn, is prohibited by law due to environmental concerns (Pb-free and green legislation) [5], the electronic industry promotes scientific activities to arrive at fundamental understanding of Sn whisker formation in order to implement industrially reliable (accelerated) whisker tests and/or mitigation strategies [4].

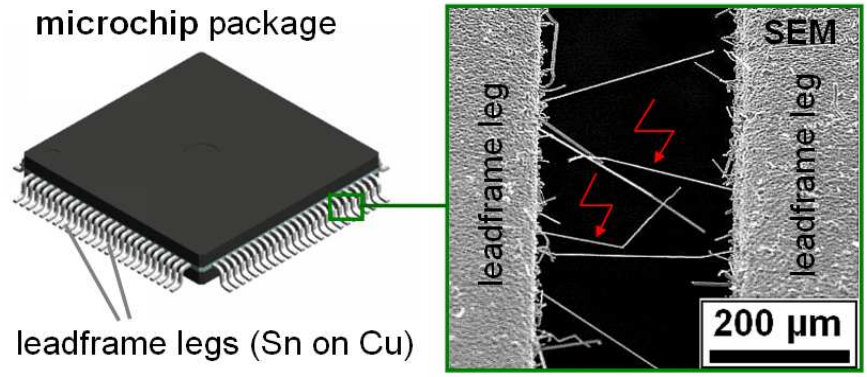

Figure 1.1: Schematic illustration of a common microchip package (left) with leadframe legs consisting of Sn-plated Cu. The spontaneous growth of Sn whiskers from the Sn-plated conductors (right) can cause short-circuits between neighbouring leadframe legs [6].

Against the above described background, the present thesis is addressed in particular to revealing experimentally the driving force for Sn whisker growth in the system Sn on Cu. To this end the room-temperature whiskering behavior of Sn thin films with a thickness of several micrometers deposited on Cu substrates was investigated in detail (see chapters 2-7). Complementary findings were obtained from similar investigations of "whisker-resistant" material systems in order to devise an overall coherent understanding; the whisker-suppressing effects of *i)* the addition of Pb

to pure Sn (see chapter 5), *ii)* the application of a post-plating annealing treatment (see chapters 2 and 6) and *iii)* the application of a particular substrate material (i.e. Si) (see chapter 3) were investigated. Thus, it was shown for the system Sn on Cu that the energetically preferred (see chapter 4) irregular growth of the intermetallic phase Cu_6Sn_5 from the Cu/Sn interface towards the Sn thin film during ageing at room temperature induces mechanical compressive stress as well as mechanical stress gradients in the Sn thin film (see chapters 6 and 7), which provide the driving forces for whisker formation (see chapter 7). Based on interface thermodynamic and kinetic considerations, the irregular (whisker-inducing) growth of Cu_6Sn_5 was explained (see chapter 4) and in combination with detailed microstructural analyses associated whisker mitigation treatments were proposed (see chapters 4 and 5).

1.1. Technological aspects of Sn whisker formation

The digital revolution [7], comprising the change from analog electronic technology to digital technology, takes place since the 1950s and is based on the invention of the microchip (i.e. integrated circuits, e.g. formed by metal-oxide-semiconductor-field-effect-transistors, MOSFETs [8]) and its rapidly ongoing performance increase (the so-called Moore`s law [9]). One major key issue of this technological evolution is the “miniaturization & integration” approach, i.e. a scaling-down process of the components and structures employed in order to realize device miniaturization as well as reduction of production costs by higher packing density of electronic components with more functionalities, faster circuit speed and lower power dissipation. This approach is directly connected to the application and continuous development of functional crystalline and amorphous (micro- and nano-sized) thin film systems (of organic, ceramic, semiconducting and metallic nature) [10, 11] exhibiting outstanding physical and chemical properties, particularly designed by their deliberately tuned surface and interface phenomena [12] for the high-performance demands at the micro- and nanometer scale.[*] The ongoing progress in vacuum technologies, material selection, material deposition techniques, etching processes and

[*] The thin film systems are nowadays widely applied in many industrial sectors, as e.g. *i)* micro-electro-mechanical systems (sensors and actuators in the form of piezoelectric thin films e.g. composed of ZnO or AlN deposited on Si), *ii)* photovoltaics (e.g. Si, $CuInSe_2$, organic films), *iii)* optics (e.g. anti-reflective coatings), *iv)* wear protection (e.g. TiN, AlCrN, Al_2O_3) and *v)* protective and decorative coatings (e.g. Ni, Zn and Cr).

other high-precision material treatments enables technological development to succeed. However, the challenges become increasingly demanding, particularly considering the following limitations:

(i) Limitations related to the "miniaturization" of electronic components

Approaching dimensions of below 20 nm, conventional Si-based (e.g. MOSFET) architectures are expected to fail due physical constraints like thermal fluctuations, quantum effects and power dissipation. On the other hand, technological (e.g. photolithographic techniques) and economic (e.g. increasing production costs) challenges become increasingly relevant [8, 13].

(ii) Limitations related to the "integration" of electronic components

Even though continuous "miniaturization" of single components might be pushed forward industrially, the second vital challenge in industrial manufacturing called "electronic packaging" must also be realized successfully, i.e. mechanical, thermal and electrical "integration" of electronic components on (rigid) substrates (i.e. printed circuit boards) by solder-joint technology [14, 15]. Moreover, the European Union passed on July, 1st 2006 a "green" legislation (called RoHS, restriction of hazardous substances) which restricts the use of Pb (and also the use of the other toxic substances like Hg, Cr^{6+} and Cd) in electronic devices due to environmental and health concerns [5, 15]. Thus it follows that due to the enforced replacement of (the up to now commonly employed) Sn-Pb solder technology with Pb-free solutions and the still associated compliance with the "miniaturization & integration" demands mentioned above (i.e. demands for nano-solders [16]), Pb-free solder alloys (e.g. Sn, Sn-Cu, Sn-Ag, Sn-Cu-Ag, Sn-Zn, Sn-Bi, Sn-In, Sn-Sb, etc.) [15, 17, 18] are considered nowadays as key issue for future technological development, particularly as solder joints represent the "weak points" in electronic systems [19].

With increasing "miniaturization & integration" demands, the following reliability aspects of solder systems, which potentially might lead to device failure, attain particular relevance [2, 18, 20-22]:

- Thermo-mechanical fatigue: Thermally induced mismatch stresses due to difference of the coefficient of thermal expansion of layer (solder) and substrate (conductor).
- External mechanical loading: External damage or high-frequency vibrational stresses.

- Creep deformation: Dislocation- and diffusion-controlled material transport due to mechanical stress relaxation.
- Electromigration: Directional material transport under the influence of electric fields.
- Sn pest: Phase-transformation (α-Sn-cubic $\Leftrightarrow$ β-Sn-tetragonal) induced lost of cohesion.
- Sn whisker formation: Creation of short-circuit induced device-failure due to the growth of conducting filaments of Sn between electrical conductors.

1.2. Historical aspects and societal relevance of "whiskers"

The term "whisker" is generally used for structures exhibiting filamentary growth morphologies, i.e. an aspect ratio significantly larger than one. The growth of filamentary Ag and Cu metals with lengths of several centimetres occurring naturally on mineral argentite (Ag_2S) and chalcosite (Cu_2S), respectively, was already reported in 1580 [23, 24]. However, growth of filamentary metals on metals (i.e. the "actual" phenomenon of whisker growth) was first observed in 1945 due to short-circuit failure of electronic equipment (Cd-electroplated condenser) caused by the growth of conductive Cd filaments [25]. Only three years later, in 1948, the growth of Sn filaments from Sn-plated connectors was also recognized to be responsible for short-circuit failure of telephone transmission lines of the Bell Telephone Corporation [1]. Thus, in-depth scientific activities on this subject were undertaken in order to provide better understanding of Sn whisker formation [2] and even though the physics of the whisker-growth phenomenon were not revealed (even not until today), Arnold made empirically in the early 1960s the following striking discovery: Addition of Pb to pure Sn prevents whisker formation [26]. Since that time SnPb alloys have been employed successfully as "whisker-resistant" solutions for soldering and coating issues of electronic systems. Recently, due to legislative directives for "green manufacturing" (see section 1.1), the electronic industry is forced to replace Sn-Pb with Pb-free finish solutions. However, as nowadays pure Sn and Sn-based alloys are considered as the most suitable candidates to replace effectively and economically SnPb alloys [15, 17], the Sn whisker phenomenon re-emerged as a serious reliability concern of modern interconnection systems and attained recently once again great scientific interest [2, 4].

Since their discovery in 1948 [1] Sn whiskers have caused an enormous financial damage by generation of short-circuit induced failures of electronic equipment. Satellites, computer centers, power plants and military (e.g. weapons) and medical (e.g. heart peacemaker) devices were involved [2, 4, 27]. Against this background and due to the fact that modern microelectronics, particularly in high-reliability applications like antilock-braking-systems in automotive or control units in spacecrafts, are a vital part of our modern society, it thus follows that a fundamental understanding of the whisker growth phenomenon constitutes an issue of considerable societal relevance.

1.3. Scientific aspects of whisker formation in the system Sn on Cu

1.3.1. Growth behavior and morphology

Polycrystalline Sn thin films with thicknesses of several micrometers deposited on Cu substrates are very prone to the spontaneous formation of Sn whiskers during ageing at room temperature [1, 2]. Usually (i.e. for Sn layer thicknesses of several micrometers) whisker formation occurs several days after Sn deposition (i.e. after a certain incubation period) on the surface of the Sn coating. However, it was also reported that the incubation period (of nominally the same Sn on Cu system) can be extended up to several week, months or even years [28], depending on the particular material properties and storage conditions. The same holds for the ageing time when whisker growth comes to a halt. The microstructure (i.e. the grain morphology and the crystallographic texture) of the Sn thin film as well as the native Sn-oxide surface-layer (with a thickness of several nanometers, see e.g. Ref. [29]) remain unchanged during ageing at room temperature (see chapter 2 and Ref. [30]), apart from the growth of the intermetallic phase η'-Cu_6Sn_5 (see phase diagram shown in Fig. 1.2) at the Cu/Sn interface due to interfacial reactions between Sn (layer) and Cu (substrate) [29, 31-34]. The room-temperature formation of Cu_6Sn_5 is directly related to the processes leading to the formation and growth of Sn whiskers (see also section 1.3.2). This fundamental interrelation between growth of Cu_6Sn_5 and generation of Sn whiskers in the system Sn on Cu during ageing at room temperature is a particular focus of the present thesis (see chapters 2-7). Both, experimental (see chapters 2-3) and theoretical

(see chapter 4) investigations were thus undertaken in order to provide a coherent understanding of this fundamental interrelation.

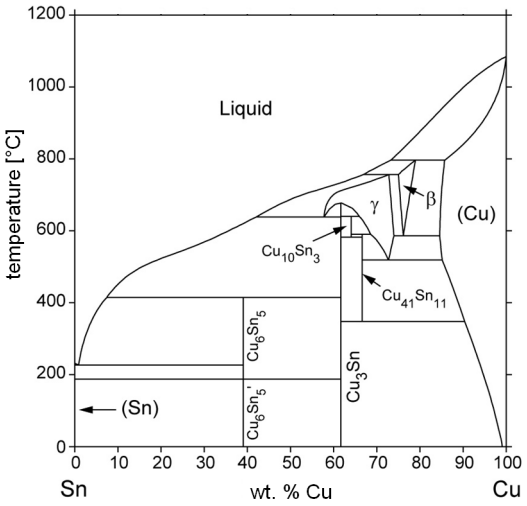

phase	Cu	Sn	η'-Cu_6Sn_5
crystallographic structure	face centered cubic	body centered tetragonal	base centered monoclinic
lattice parameter	a = 0.3615 nm	a = 0.58311 nm b = 0.58311 nm c = 0.31817 nm	a = 1,0913 nm b = 0.721 nm c = 0.9782 nm β = 98.96 °
density	8.92 g/cm³	7.31 g/cm³	8.28 g/cm³
Young's modulus	130 GPa	50 GPa	86 GPa
Poisson's ratio	0.35	0.33	0.3
thermal expansion	$17.7x10^{-6}$ K^{-1}	$23.5x10^{-6}$ K^{-1}	$16.3x10^{-6}$ K^{-1}
melting point	1083.5 °C	232 °C	187 °C

Figure 1.2: left: Calculated equilibrium phase diagram of the system Sn-Cu (modified after Ref. [35]). right: Some relevant properties of Sn [36], Cu [36] and Cu_6Sn_5 [37, 38].

The location of the (potential) whisker nucleation sites on top of the as-deposited Sn thin films cannot be distinguished morphologically prior to onset of whisker formation from surrounding surface-locations which remain whisker-free upon further ageing. It was observed [6] that the initial event of whisker-formation appears to be a "pushing-up" process of pre-existing Sn grains from the Sn matrix (see Fig. 1.3 and chapter 5).

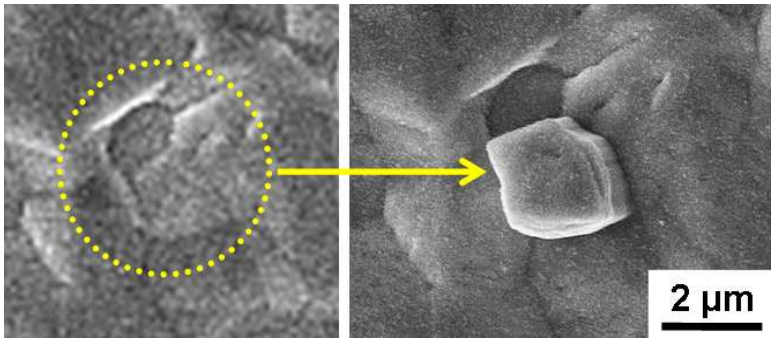

Figure 1.3: Scanning electron micrographs of the Sn grain morphology (in top-view) of a whisker nucleation site observed (left) before (i.e. directly after Sn deposition on Cu) and (right) shortly after onset of whisker formation. The whisker-head is a pre-existing Sn grain.

It is worth noting that the directly adjacent surroundings of the whisker nucleation site remain morphologically unaffected by this whisker-initiation process. The same holds for whisker surroundings exhibiting whisker lengths of several

hundreds of micrometers after prolonged ageing times at room temperature (see chapter 3), i.e. no material depletion around the whisker root occurs.

Sn whiskers are “perfect” single-crystalline filamentary structures of tetragonal symmetry [39-41] (with diameters of about 1-10 μm) growing through continuous addition of material to their base [42] (see Fig. 1.4 left) with growth rates of about 1 Å/s [43-45] and up to 10000 Å/s in the presence of externally applied mechanical stresses [39]. It is also known that other thin metal films with a low melting point (e.g. Cd and Zn) exhibit similar whiskering behaviors [1, 46]. The growth morphologies of whiskers can be very divers (see Fig. 1.4 right); whiskers can be straight, kinked, curved, coiled or they can have a combined morphology, whereas the crystallographic orientation throughout the whisker remains unchanged [41].

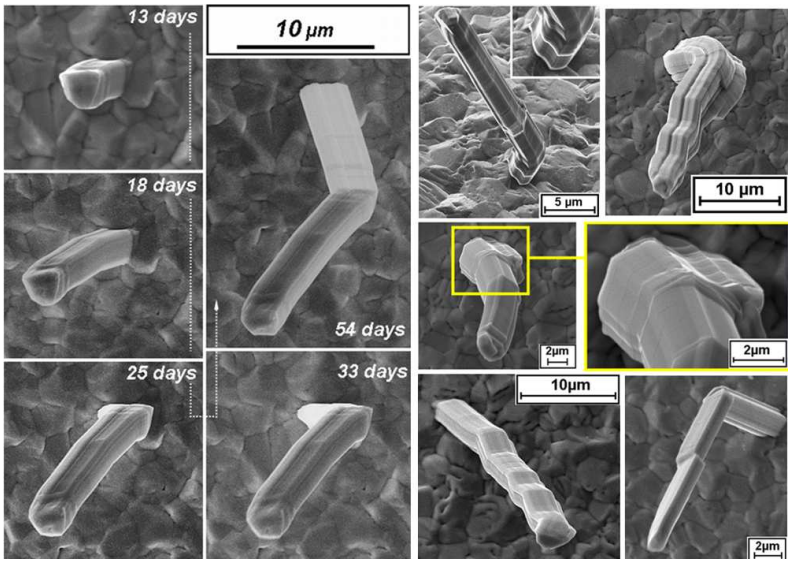

Figure 1.4: left: Scanning electron micrographs of the same Sn whisker taken at different ageing times at room temperature illustrating the growth mechanism from the base. right: Micrographs showing the diversity of possible Sn whisker growth morphologies.

1.3.2. Driving force for Sn whisker formation

Usually the driving force for Sn whisker growth is attributed to the (external and/or internal) build-up of mechanical compressive stress in the Sn coating during and/or after Sn deposition and thus whisker growth is regarded as a stress relief phenomenon [31, 47-49]. Already in 1954, Fisher *et al.* [39] demonstrated that mechanical compressive stress in the Sn thin film can serve as a driving force for whisker growth by applying (controlled) external mechanical loads on the specimen. Basically, the origin for the build-up of mechanical compressive stress in the Sn layer

can be *mechanical* (due to external mechanical loading), *thermal* (due to differences in coefficients of thermal expansion of the substrate and the Sn coating), *intrinsic* (due to the deposition conditions) or *chemical* (phase formations due to chemical reactions between the substrate, the Sn coating and the ambient atmosphere) (see section 1.4).

After Sn deposition on the Cu substrate and during subsequent ageing at room temperature, Cu diffuses rapidly into the Sn thin film by an interstitial mechanism [31, 50] and (only) the formation of the intermetallic compound Cu_6Sn_5 takes place at the Cu/Sn interface [31], preferentially along the Sn grain boundaries intersecting the Cu/Sn interface [49, 51]. The Cu_6Sn_5 formation is accompanied by a specific volume increase and due to the constraint imposed by the (rigid) substrate, residual compressive stress parallel to the surface can be generated in the Sn thin films [30, 49, 52].

The presence of a native surface Sn-oxide layer is conceived by many authors as an important parameter for whisker formation [3, 29, 49, 51-55]. Experimental [29, 52] and theoretical [53, 54] investigations indicate that without the presence of a (passivating) oxide layer the compressive stress generated by Cu_6Sn_5 formation, as described above, could be relaxed uniformly via Coble creep [56] along the entire layer surface, i.e. Sn atoms could diffuse from the columnar grain boundaries to the free surface of Sn [57] (see also chapter 5).

It was speculated that stress gradients in the Sn layer drive the transport of Sn atoms to the whisker root [3, 30, 31, 49, 51, 58]. However, only very recently in the framework of the present thesis (see chapters 6 and 7), sound experimental evidence was presented by (non-destructive) state-of-the-art (laboratory and synchrotron) X-ray diffraction stress analyses (see section 1.5) that the nature of stress *gradients* around a potential whisker-nucleation site is decisive, not the absolute value of the state of stress [59, 60]. It was also shown by means of FIB cross-sectional analysis that these whisker nucleation sites are characterized morphologically by significant Cu_6Sn_5 formation underneath (see Fig. 1.5) [6]. Additionally, finite element simulations were taken into account in order to compare the experimental results mentioned above with the theoretical stress distribution in the Sn layer due to irregular Cu_6Sn_5 formation at the Cu/Sn interface (see Fig. 1.6) [6].

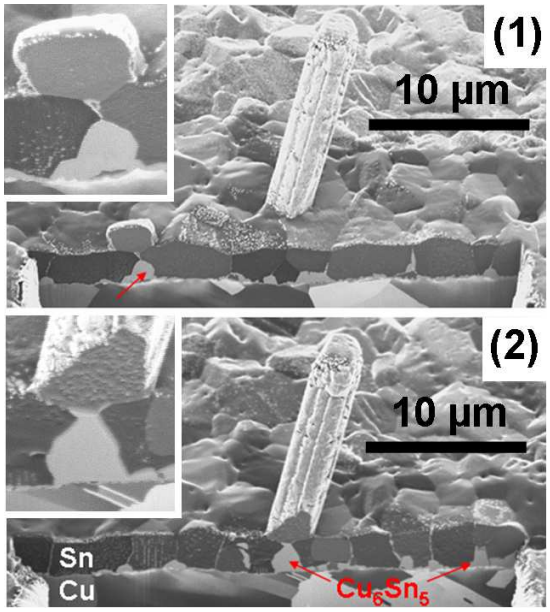

Figure 1.5: Sequence of FIB-cross sectional micrographs taken through the nucleation sites of two whiskers [6]. Significant Cu_6Sn_5 formation at the Cu/Sn interface is clearly visible (see also the respective insets) under both whisker roots.

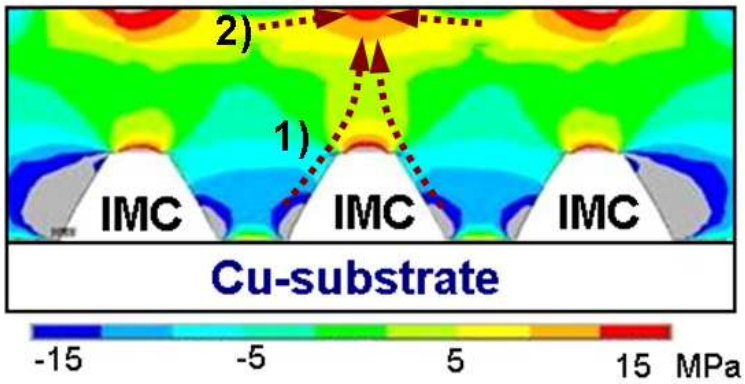

Figure 1.6: Calculated in-plane mechanical stress distribution in a Sn layer due to irregular intermetallic compound formation (IMC, Cu_6Sn_5) at the Cu/Sn interface [6]. The stresses were derived from a finite element simulation considering elasto-plastic material properties. Two types of stress gradients are obvious, 1) with out-of-plane direction and 2) with in-plane direction.

Against the above background, the following mechanism of whisker formation was proposed (see Fig. 1.7 and chapter 7): Formation of Cu_6Sn_5 along the Sn grain boundaries at the Cu/Sn interface induces in-plane compressive stress in the Sn layer, particularly in the depth range of the Sn coating where Cu_6Sn_5 formation proceeds. Then, close to the surface of the Sn layer in-plane tensile stress occurs; most pronouncedly at those surface locations where formation of Cu_6Sn_5 is most distinctive,

as observed underneath a whisker (see Figs. 1.5 and 1.7). As a consequence, both negative out-of-plane residual stress-depth gradients, in the direction of increasing depth and negative in-plane residual stress gradients in the direction from the whisker-nucleation site toward the whisker surroundings occur (see also calculated stress distribution in Fig. 1.6), which provide the driving forces for the transport of Sn atoms to the whisker nucleation site.

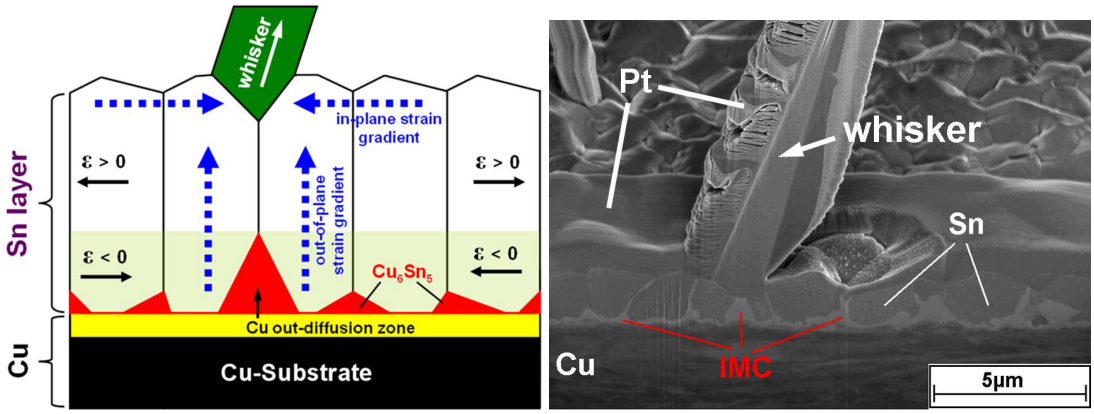

Figure 1.7: left: Schematic model for the driving forces (based on results of the present thesis, see chapter 7) which cause spontaneous Sn whisker growth in the system Sn on Cu. right: FIB cross-sectional micrograph of a whisker nucleation site in order to allow comparison with the proposed model regarding microstructural features.

1.3.3. Growth mechanism of Sn whiskers

The proposed growth models for Sn whiskers in the system Sn on Cu [3, 43-45, 47-49, 51, 53-55, 61-68] are not able to explain the observed whiskering behavior (e.g. moment of whiskering, locations of whisker nucleation and growth kinetics). These models can be subdivided into three groups: *i)* Dislocation models [47-49, 61-63], *ii)* Recrystallization models [43-45, 65, 66] and *iii)* Creep models [3, 51, 53-55, 64, 67, 68]. The dislocation models assume that a suitable dislocation source situated at the whisker root is emitting continuously dislocation loops which glide subsequently to the surface and thus transfer Sn atoms from the Sn layer to the growing Sn whisker. The recrystallization models conceive whisker growth as the outcome of localized (unidirectional) grain growth. The creep models, which are nowadays favored by many authors, describe whisker growth as a special form of localized diffusional creep operating via (long-range) grain-boundary diffusion.

1.3.4. Sn whisker tests and mitigation treatments

(i) Whisker predictability tests

To date (absolutely) reliable (accelerated) whisker predictability tests for assessing the risk of a given material system to from whiskers are not available, because the fundamentals of whisker formation and growth are not discovered yet. However, such tests are of vital importance for the electronic industry [69, 70]. Nowadays the following commonly accepted whisker tests are usually applied in industrial manufacturing for evaluating the whiskering propensity of electronic equipment (note that all tests are based on the presumption that mechanical compressive stress in the Sn layer is precondition for whisker growth) [71]:

- Temperature cycling -55 °C ⇔ 85 °C / 3000-4000 cycles
- Temperature / Humidity storage 30°C / 60 % rel. humidity / 4000 hours
- High temperature / Humidity storage 55 °C / 85 % rel. humidity / 4000 hours

(ii) Whisker mitigation strategies

Several whisker mitigation strategies were proposed for industrial application of the nowadays technologically preferred system Sn on Cu:

- Application of different Sn-alloys (e.g. SnPb [26], SnBi [72], SnAg [73]) and/or Cu-alloys (e.g. CuSn, CuFe, CuNi) [74, 75]).
- Application of diffusion barriers, e.g. interlayers of Ni [72, 75-77] or Ag [78].
- Application of heat treatments (e.g. simulated reflow [2, 77] and post-plating annealing [44, 49, 75, 78-80]).
- Application of conformal surface coatings [4, 81].

The most important and commonly used whisker mitigation treatments are the application of Ni-underlayers (acting as diffusion barriers for Cu) and the post-plating annealing (called 'post-bake' at 150°C for 1 h applied within 24 h after Sn deposition) in combination with a minimum Sn-thickness of about 7 μm [82].

1.3.5. Scientific and technological benefit of understanding whisker formation

The fundamental understanding of the whisker-formation processes is of great scientific relevance. It offers the possibility to investigate transport mechanisms of condensed matter in complex (non-hydrostatic) mechanical stress fields, a topic of long-lasting interest [83-85]. Furthermore, the nearly perfect, single-crystalline nature of whiskers makes them very suitable for the fundamental investigation of single-

phase properties neglecting possible influences resulting from imperfections (see for example Refs. [86, 87].

From a technological point of view the application of (semiconducting and metallic) nano-sized whisker-structures (i.e. nanowires) for the build-up of nanofunctional systems attained recently great interest due to their unique electrical, mechanical, optical and magnetic properties [88, 89]. The fabrication of semiconducting nanowires can nowadays be operated in routine mode [90]. However, the controlled preparation of metallic nanowires appears only recently to make significant progress [91, 92]. It was shown that application of mechanical stress, e.g. thermally-induced stress [93, 94] or electromigration-induced stress [95], can be employed to grow metallic nanowires. Against this background, it is reasonable to conclude that once a thorough understanding of the stress-induced mechanisms controlling Sn whisker formation is established, this knowledge can also be adopted appropriately to fabricate metallic nanowires of desired properties in a controlled fashion.

1.4. Sn whisker growth behavior in "alternative" material systems

As already mentioned in section 1.3.2, mechanical compressive stress (in combination with stress gradients) is the driving force for Sn whisker growth. So far compressive stress generation in the Sn thin film was discussed in terms of (internal) Cu_6Sn_5 formation during ageing at room temperature. However, it is also known that other sources for the generation of compressive stress can initiate whisker formation. Therefore, in the following a compilation of these alternative whisker growth behaviors will be given, in order to provide an overall assessment of the Sn whisker formation process.

(i) Sn whisker growth due to external mechanical loading

Fisher *et al.* in 1954 [39] first demonstrated that mechanical compressive stress in the Sn thin film can serve as a driving force for whisker growth by applying external mechanical loads on the whole specimen (Sn-plated steel; note that here no intermetallic phase formation occurs at room temperature). Moreover, they revealed a direct relation between applied pressure and whisker growth rate (maximal growth rate of 10000 Å/s were observed). Similar findings were made by Glazunova in 1962 [80], Pitt and Henning in 1964 [96], Britton in 1974 [76] and Lin and Lin in 2008 [97]. On

the other hand, it was reported recently, that local contact loading (i.e. indentation) can also induce whisker growth in direct vicinity around the indent [98-101].

(ii) Sn whisker growth due to electromigration

It was demonstrated that the growth of Sn whiskers on Sn [20, 102], Sn-Pb [103, 104] and Sn-Cu-Ag [105] thin films can be triggered and significantly accelerated (up to about 8 Å/s on pure Sn thin films [20]) by electromigration. The following mechanism of whisker formation was proposed: The (directional) electron flow induces Sn migration from the cathode to the anode side, which leads to the build-up of compressive stress, and thus to the formation of Sn whiskers, at the anode end.

(iii) Sn whisker growth due to the presence of rare earth elements

Very recently it was reported that the presence of (reactive) rare earth elements (REE) (e.g. Ce, La, Lu, Nd, Y, Er, etc.) in Sn [106, 107] (but also in Sn-Pb [108] and Sn-Cu-Ag [109, 110]) can accelerate the growth rate of Sn whiskers enormously. The as-casted Sn-REE bulk alloys containing Sn-REE precipitates were stored at room temperature and at 150°C upon ambient atmosphere and whisker formation was observed *only* on the surface of Sn-REE precipitates. Whisker formation was particularly pronounced in Sn-Lu specimens exhibiting growth rates of about 500 Å/s [106]. It was proposed that oxidation of Sn-REE particles leads to the formation of REE-oxides and released Sn, which itself starts to form Sn whiskers, because oxidation is accompanied by generation of compressive stress.

(iv) Sn whisker growth due to oxidation/corrosion

Several authors [76, 111-113] have shown experimentally that oxidation/corrosion-induced whisker formation can occur on the surface of the Sn thin film, independent of the substrate material used. At elevated temperatures and high humidity, e.g. 60°C/93% relative humidity, formation of Sn oxides at the surface of the Sn layer, particularly along Sn grain boundaries takes place, which leads due to volume expansion to the build-up of compressive stress and thus to the formation of Sn whiskers.

(v) Sn whisker growth due to thermally induced stress

The difference of the linear coefficients of thermal expansion of the Sn thin film and the underlying substrate (e.g. Cu, Ni, Fe) leads upon non-ambient temperature conditions to the generation of thermally induced mismatch stresses. It was shown that temperature cycling (e.g. -55 °C ↔ 85 °C) can induce whisker growth on specimens

which were whisker-free during (prolonged) ageing conditions at room temperature [79, 114].

(vi) Sn whisker growth due to intrinsic stress

It was observed that the presence of intrinsic compressive stress (due to deposition conditions) in Sn layers electrodeposited on W [115] (a substrate not forming interfacial intermetallics) as well as evaporated on polymers [116] is sufficient to grow Sn whiskers, however with significantly shorter lengths as compared to the system Sn on Cu [55]. The reason is that once the intrinsic stress component in the Sn layer is relieved in the course of whisker formation, further driving force for continued whisker growth lacks, as it is the case for the system Sn on Cu due to ongoing formation of Cu_6Sn_5.

(vii) Sn whisker growth due to the presence of impurities

The presence of impurities (particularly Cu and Zn; note that both types of atoms can diffuse very fast interstitially in Sn [50, 117]) in the Sn thin film (co-deposited and/or post-plating implemented due to out-diffusion form the substrate, e.g. in the case of CuZn) can accelerate whisker growth significantly [28, 44, 55, 118-121]. It was proposed that in the case of Cu containing Sn layers additional compressive stress is generated due to precipitation of Cu_6Sn_5 along Sn grain boundaries. Moreover, such precipitation of Cu_6Sn_5 lowers the grain boundary mobility of the Sn layer, leading to enhanced whisker formation as sole stress relaxation possibility [55]. In the case of Zn containing Sn layers it was speculated that additional compressive stress results from the accumulation of Zn dissolved in the Sn. It was also assumed that Zn influences the grain boundary mobility of Sn, however, without further explanations [28].

(viii) Sn whisker growth due to particle bombardment

Intensive bombardment of the surface of Sn thin films by neutrons at ambient temperature [122] as well as by He atoms at temperatures below -100 °C [123, 124] was shown to induce significant whisker growth. The high energetic collisions at the Sn surface led to the build-up of compressive stress and thus to whisker formation.

1.5. Focus of the thesis – Methodology and experimental procedures

The present work focuses on uncovering the driving force for Sn whisker growth in the system Sn on Cu. To this end the room-temperature evolution of the Sn

microstructure, the intermetallic phase formation, the residual stress evolution and the associated formation of Sn whiskers on the surface of Sn layers with a thickness of several micrometers (electro- and sputter-) deposited on Cu substrates was investigated during ageing at room temperature by means of scanning electron (SEM) and focused ion beam (FIB) microscopy and (laboratory and synchrotron) X-ray diffraction (XRD) analyses. Whisker-resistant systems (achieved by particular specimen treatments as well as by application of particular material combinations) were also investigated in order to provide an overall coherent understanding. Particularly, the combined approach of SEM and XRD analyses was very suitable to record non-destructively the above mentioned microstructural evolution of the system Sn on Cu during ageing time regarding the precise onset of whisker formation in relation to the measured residual stress development. Furthermore, after different ageing times at room temperature, (destructive) cross-sectional FIB analyses were conducted in order to obtain (3D) microstructural information of the aged Sn microstructure, the intermetallic phase formation at the Cu/Sn interface as well as of the whisker nucleation sites. Thus, it was possible to derive fundamental interrelations between the observed microstructural development, the measured residual stress evolution and the associated phenomenon of Sn whisker formation and on this basis the driving force for whisker growth was established (see chapters 6 and 7).

The focal point of interest was devoted to the non-destructive assessment of the (*though-thickness averaged*, *depth-resolved* as well as *spatially-resolved*) residual stress evolution in Sn thin films deposited on Cu during ageing at room temperature by performing state-of-the-art laboratory (macro) [125] and synchrotron (micro) [126] X-ray diffraction stress analyses.

1.5.1. Macro X-ray diffraction stress analyses

In order to determine (*though-thickness averaged* and *depth-resolved*) residual mechanical residual stresses, macro X-ray diffraction stress measurements were conducted employing parallel-beam laboratory diffractometers (with a Cu Kα X-ray source) equipped with an Eulerian cradle. The determination of residual mechanical stresses was carried out on the basis of the $\sin^2\psi$-method which allows in principle the full assessment of the mechanical state of stress of a specimen under investigation [125, 127, 128]. By means of the Bragg diffraction condition $\lambda = 2d^{hkl}\sin\theta^{hkl}$ (λ as X-

ray wavelength used, d^{hkl} as lattice spacing of the lattice plane *hkl* and θ^{hkl} as corresponding diffraction angle), the lattice spacing d^{hkl} of one or more families of {*hkl*} lattice planes can be measured by monochromatic X-ray diffraction. Then it is possible to calculate the elastic (diffraction) strain ε^{hkl} of the {*hkl*} planes from $\varepsilon^{hkl} = (d^{hkl}-d^{hkl}_0)/d^{hkl}_0$ with d^{hkl}_0 as the strain-free lattice spacing. The measurement of the elastic strain ε^{hkl} of certain {*hkl*} planes at various (tilt and rotation) angles ψ and φ (both angles define the orientation of the diffraction vector m with respect to the specimen frame of reference, see Fig. 1.8, right) provides the experimental data required for diffraction stress analysis, i.e. evaluation of ε^{hkl}-$\sin^2\psi$ plots. In order to derive the mechanical stress from the measured lattice (diffraction) strain of a polycrystalline specimen, suitable (X-ray) elastic constants of the material under investigation are required (see, for example Ref. [125] and references therein). These can be either determined experimentally by applying a known load to a specimen with known stress and measuring the thus resulting lattice strain or by calculation from single-crystal elastic constants adopting a suitable grain-interaction model.

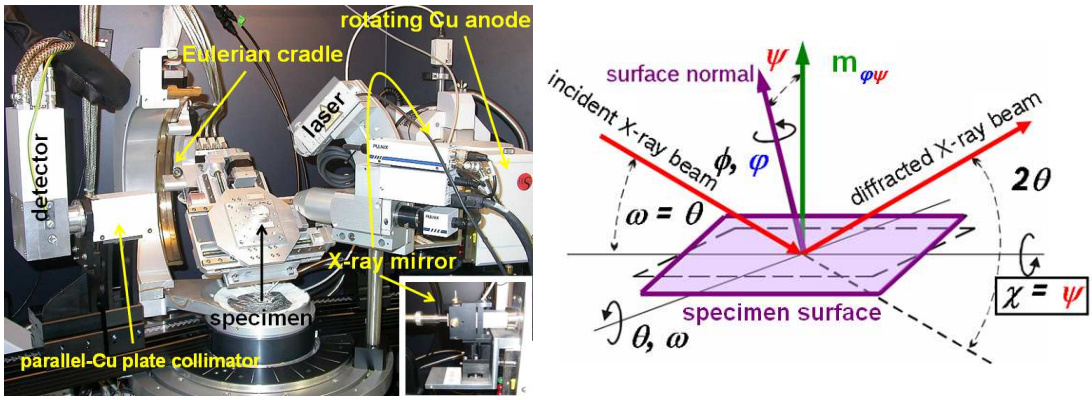

Figure 1.8: left: Laboratory parallel-beam diffractometer (Bruker TXS D8 Discover) used in this work (for a detailed description see Ref. [129]) for the performance of macro-diffraction analyses. right: The corresponding schematic illustration of the diffraction geometry depicting instrumental (ω, χ, ϕ and θ) and measurement (ψ and φ) angles.

Performing conventional X-ray diffraction stress analysis, no measures are taken to control the penetration depth of the X-ray beam during specimen tilting (i.e. in this case averaged stress values within the probed diffraction volume result). However, in order to determine depth-gradients of mechanical stress, X-ray diffraction stress measurements at different but controlled penetration depths are mandatory. Recently a dedicated diffraction strategy was proposed to fix the penetration depth upon (appropriate) specimen tilting

[130]. This diffraction method in combination with a laboratory top-notch instrumentation (in this work a Bruker TXS D8 Discover diffractometer was used, see Fig. 1.8 left) allowed to measure near-surface stress-depth profiles with a depth-resolution of the order of hundreds of nanometers. The particular advantages of this state-of-the-art laboratory diffractometer were the high photon flux with a high brilliance (realized by a rotating micro-focus Cu anode in combination with a single-reflection collimating multilayer X-ray mirror) as well as the favorable characteristics of the conditioned, quasi-parallel X-ray beam allowing to fully neglect instrumental aberrations and to adjust well-defined the incidence angle of the beam (this is particularly relevant for maintaining a constant penetration depth) [129]. As the measured stress-depth profile using X-ray diffraction represents the Laplace transformed stress-depth profile in real space [131, 132], an inverse Laplace transformation was developed and performed in this work using an iterative procedure in order to derive the stress-depth profile in real space.

1.5.2. Micro X-ray diffraction stress analyses

In order to experimentally determine the local residual stress distribution around growing Sn whiskers (i.e. *spatially resolved* with a grain to grain resolution), high-resolution micro Laue X-ray diffraction experiments [133] were conducted employing the synchrotron end-station setup at beamline 34ID-E [134] at the Advanced Photon Source (APS) of the Argonne National Laboratory (Argonne, Illinois, USA) (see Fig. 1.9). A focused, polychromatic (8-24 keV) X-ray beam was used, that emerged from a slightly off-axis undulator source with a high integrated brilliance over the adjusted bandpass. The high-energy X-rays penetrated the whole film thickness of several microns and thus the diffraction data recorded at each probed specimen position contained information from all positions along the penetration depth of the X-rays. By using a pair of reflecting and elliptically bent Kirkpatrick-Baez mirrors [135] all wavelengths of the polychromatic X-ray beam could be focused simultaneously to a sub-micrometer beam size of about 0.3 x 0.3 μm^2. The focused X-ray beam was step-scanned with sub-micron steps around the root of the Sn whisker. Since the size of the Sn grains (~ 2-5 µm) was larger than the focused X-ray beam, each grain could be treated as a single crystal with respect to micro-beam diffraction. In combination with a high-precision CCD area detector for data collection, two dimensional residual stress measurements were performed on the basis of white-beam Laue diffraction. By using computer-automated peak search routines the angular positions of the Bragg reflections were determined and by employing pattern-recognition software the diffraction pattern could be indexed with respect to reference patterns [136]. The

crystallographic orientation and the (deviatoric) strain tensor components were derived directly from the indexed Laue diffraction patterns.

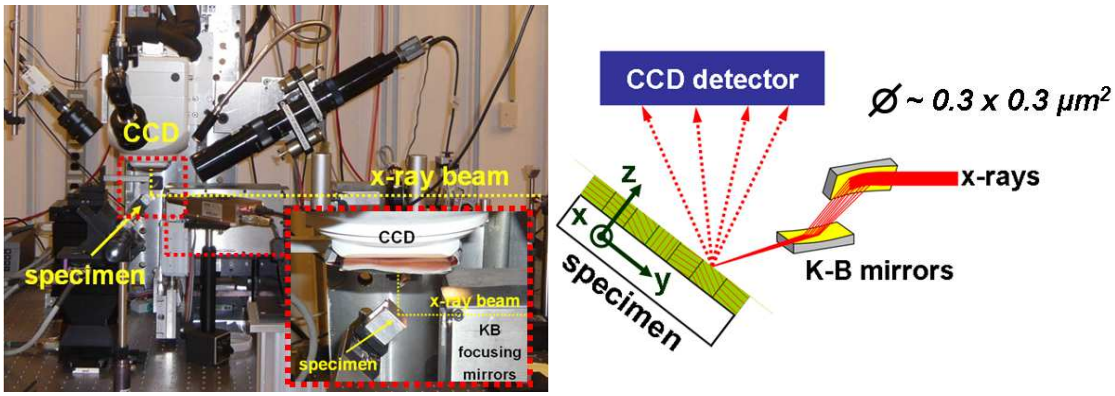

Figure 1.9: left: Synchrotron end-station setup at beamline 34ID-E at the Advanced Photon Source (see for further information Ref. [134]) used for the performance of micro-diffraction experiments. right: Schematic illustration of the micro-Laue diffraction technique [133].

1.6. Outline of the thesis

In chapters 2, 3 and 5 results on the interrelation of microstructural evolution, residual stress development and whisker formation of Sn thin films electro- and sputter-deposited on Cu as well as of SnPb thin films electrodeposited on Cu and Fe are presented. The importance of the Sn grain morphology (i.e. columnar vs. equiaxed) regarding stress relaxation mechanism via whisker formation is discussed and on this basis a whisker mitigation treatment involving microstructural control of the Sn coating is proposed (see chapter 5). The role of (irregular) Cu_6Sn_5 formation (in the system Sn on Cu) for the generation of mechanical compressive stress and thus the associated growth of Sn whiskers is also discussed in detail. In chapter 4 this irregular (whisker-inducing) growth of Cu_6Sn_5 is explained by interface thermodynamic and kinetic considerations and on this basis a (intrinsic) whisker mitigation treatment is proposed. Based on laboratory (macro) and synchrotron (micro) X-ray diffraction stress analyses, the investigations of the (actual) driving forces for whisker growth in the system Sn on Cu are presented in chapters 6 and 7. Additionally, by taking microstructural investigations of whiskers and their surroundings into account, a coherent model for whisker formation is presented (see chapters 5 and 7).

References

[1] Compton K. G., Mendizza A. & Arnold S. M. (1951). *Corrosion* **7**, 327.

[2] Galyon G. T. (2005). IEEE Trans. Electron. Packag. Manuf. **28**, 94.

[3] Tu K. N., Chen C. & Wu A. T. (2007). *J. Mater. Sci. - Mater. Electron* **18**, 269.

[4] Brusse J. A., Ewell G. J. & Siplon J. P. (2002). *in Proc. of the 16th Passive Components Symposium, CARTS EUROPE*, 221.

[5] Directive 2002/95/EC of the European Parliament and of the Council of 27 January 2003 on the restriction of the use of certain hazardous substances in electrical and electronic equipment (2003). *Official Journal of the European Union* **L37**, 19.

[6] Sobiech M., Wohlschlögel M., Welzel U., Mittemeijer E. J., Hügel W., Seekamp A., Garza M., Koyuncu M., Liu W. & Ice G. E. (2009). *Presentation at the 3rd International Symposium on Tin Whiskers in Denmark.*

[7] Barrett C. R. (2006). *MRS Bull.* **31**, 906.

[8] Keyes R. W. (2005). *Rep. Prog. Phys.* **68**, 2701.

[9] Moore G. E. (1965). *Electronics* **38**, 114.

[10] Ohring M. (2002). *Materials Science of Thin Films*. New York: Academic Press.

[11] Abraham U. (1995). *Organic thin films and surfaces: directions for the nineties*. San Diego: Academic Press.

[12] Howe J. M. (1997). *Interfaces in Materials*. New York: Wiley.

[13] Korkin A., Labanowski J., Gusev E. & Luryi S. (2007). *Nanotechnology for electronic materials and devices*. New York: Springer.

[14] Klein Wassink R. J. (1989). *Soldering in Electronics*. Isle of Man: Electrochemical Publications.

[15] Abtew M. & Selvaduray G. (2000). *Mater. Sci. Eng. R - Rep.* **27**, 95.

[16] Shen J. & Chan Y. C. (2009). *Microelectron. Reliab.* **49**, 223.

[17] Chen S. W., Wang C. H., Lin S. K. & Chiu C. N. (2007). *J. Mater. Sci. - Mater. Electron* **18**, 19.

[18] Plumbridge W. J. (2009). *Eng. Fail. Anal.* **16**, 1347.

[19] Plumbridge W. J., Matela R. J. & Westwater A. (2003). *Structural Integrity and Reliability in Electronics* Dordrecht: Kluwer Academic.

[20] Liu S. H., Chen C., Liu P. C. & Chou T. (2004). *J. Appl. Phys.* **95**, 7742.

[21] Zimprich P., Saeed U., Weiss B. & Ipser H. (2008). *J. Electron. Mater.* **38**, 392.

[22] Ma H. & Suhling J. C. (2009). *J. Mater. Sci.* **44**, 1141.

[23] Brenner S. S. (1960). *Sci. Am.* **203**, 64.

[24] Hardy H. K. (1956). *Prog. Met. Phys.* **6**, 45.

[25] Cobb H. L. (1946). Monthly Rev. Am. Electroplaters Soc. **33**, 28.

[26] Arnold S. M. (1966). *Plating* **53**, 96.

[27] http://nepp.nasa.gov/whisker/failures/index.htm.

[28] Dunn B. D. (1987). ESA STR-23 research report.

[29] Kumar K. S., Reinbold L., Bower A. F. & Chason E. (2008). *J. Mater. Res.* **23**, 2916.

[30] Sobiech M., Welzel U., Schuster R., Mittemeijer E. J., Hügel W., Seekamp A. & Müller V. (2007). *in Proc. of the 57th Electronic Components and Technology Conference in Reno, USA,* 192.

[31] Tu K. N. (1973). *Acta Metall.* **21**, 347.

[32] Tu K. N. & Thompson R. D. (1982). *Acta Metall.* **30**, 947.

[33] Tu (1996). *Mater. Chem. Phys.* **46**, 217.

[34] Laurila T., Vuorinen V. & Kivilahti J. K. (2005). *Mater. Sci. Eng. R* **49**, 1.

[35] www.metallurgy.nist.gov.

[36] Gale W. F. (2004). *Smithells Metals Reference Book*. London: Butterworths.

[37] Fields R. J., Low III S. R. & Lucey Jr G. K. (1992). *In: M. J. Cieslak, J. H. Perepezko, S. Kang, M. E. Glicksman, eidtors. Metal science of joining. P. A., Warrendale: The Minerals, Metals & Materials Society*.

[38] Zhou W., Liu L. & Wu P. (2010). *Intermetallics* **18**, 922.

[39] Fisher R. M., Darken L. S. & Carroll K. G. (1954). *Acta Metall.* **2**, 368.

[40] Herring C. & Galt J. K. (1952). *Phys. Rev.* **85**, 1060.

[41] LeBret J. B. & Norton M. G. (2003). *J. Mater. Res.* **18**, 585.

[42] Koonce S. E. & Arnold S. M. (1953). *J. Appl. Phys.; Lett. to Editor* **24**, 365.

[43] Ellis W. C., Gibbons D. F. & Treuting R. C. (1958). *Growth and Perfection of Crystals,* edited by Doremus, R. H., Roberts, B. W. and Turnbull, D. (Wiley, New York, 1958), pp. 102-120.

[44] Glazunova V. K. & Kudryavtsev N. T. (1963). *Russ. J. Appl. Chem.* **36**, 543.

[45] Furuta N. & Hamamura K. (1969). *Jpn. J. Appl. Phys.* **9**, 1404.

[46] Key P. L. (1970). *in Proc. of the 20th Electronic Components Conference,* 155.

[47] Hasiguti R. R. (1955). *Acta Metall.* **3**, 200.

[48] Lindborg U. (1976). *Acta Metall.* **24**, 181.

[49] Lee B. Z. & Lee D. N. (1998). *Acta Mater.* **46**, 3701.

[50] Dyson B. F., Anthony T. R. & Turnbull D. (1967). *J. Appl. Phys.* **38**, 3408.

[51] Tu K. N. (1994). *Phys. Rev. B* **49**, 2030.

[52] Chason E., Jadhav N., Chan W. L., Reinbold L. & Kumar K. S. (2008). *Appl. Phys. Lett.* **92**, 171901.

[53] Buchovecky E. J., Du N. & Bower A. F. (2009). *Appl. Phys. Lett.* **94**, 191904.

[54] Buchovecky E. J., Jadhav N., Bower A. F. & Chason E. (2009). *J. Electron. Mater.* **38**, 2676.

[55] Boettinger W. J., Johnson C. E., Bendersky L. A., Moon K.-W., Williams M. E. & Stafford G. R. (2005). *Acta Mater.* **53**, 5033.

[56] Coble R. L. (1963). *J. Appl. Phys.* **34**, 1679.

[57] Shin J. W. & Chason E. (2009). *J. Mater. Res.* **24**, 1522.

[58] Choi W. J., Lee T. Y., Tu K. N., Tamura N., Celestre S., MacDowell A. A., Bong Y. Y. & Nguyen L. (2003). *Acta Mater.* **51**, 6253.

[59] Sobiech M., Welzel U., Mittemeijer E. J., Hügel W. & Seekamp A. (2008). *Appl. Phys. Lett.* **93**, 011906.

[60] Sobiech M., Wohlschlögel M., Welzel U., Mittemeijer E. J., Hügel W., Seekamp A., Liu W. & Ice G. E. (2009). *Appl. Phys. Lett.* **94**, 221901.

[61] Eshelby J. D. (1953). *Phys. Rev.* **91**, 755.

[62] Frank F. C. (1953). *Philos. Mag.* **44**, 854.

[63] Franks J. (1958). *Acta Metall.* **6**, 103.

[64] Smetana J. (2007). IEEE Trans. Electron. Packag. Manuf. **30**, 11.

[65] Kakeshita T., Shimizu K., Kawanaka R. & Hasegawa T. (1982). *J. Mater. Sci.* **17**, 2560.

[66] Boguslavsky I. & Bush P. (2003). *Proceedings APEX Conference*, pp. S12.

[67] Osenbach J. W. (2009). *J. Appl. Phys.* **106**, 094903.

[68] Hutchinson B., Oliver J., Nylen M. & Hagström J. (2004). *Mater. Sci. Forum* **467-470**, 465.

[69] Reynolds H. L., Osenbach J. W., Henshall G., Parker R. D. & Su P. (2010). *IEEE Trans. Electron. Packag. Manuf.* **33**, 1.

[70] Osenbach J. W., Reynolds H. L., Henshall G., Parker R. D. & Su P. (2010). *IIEEE Trans. Electron. Packag. Manuf.* **33**, 16.

[71] JESD201A J. S. (2008). http://www.jedec.org/standards-documents/results/whisker.

[72] Whitlaw K. & Crosby J. (2002). in Proc. of AESF SUR/FIN Conference, 19.

[73] Yanada I. (1998). in Proc. of the IPC Printed Circuits Expo, 11.

[74] Zhang W., Egli A., Schwager F. & Brown N. (2005). IEEE Trans. Electron. Packag. Manuf. 28, 85.

[75] Whitlaw K. & Crosby J. (2003). in Proc. of the AESF SUR/FIN Conference, 289.

[76] Britton S. C. (1974). Trans. Inst. Metal Finish. 52, 95.

[77] Xu C., Zhang Y., Fan C. & Abys J. A. (2002). *CircuiTree* **15**, 10.

[78] Dittes M., Oberndorff P. & Petit L. (2003). *in Proc. of the 53rd ECTC Electronic Components and Technology Conference,* 822.

[79] Osenbach J. W., Shook R. L., Vaccaro B. T., Potteiger B. D., Amin A. N., Hooghan K. N., Suratkar P. & Ruengsinsub P. (2005). *IEEE Trans. Electron. Packag. Manuf.* **28**, 36.

[80] Glazunova V. K. (1962). *Kristallografiya* **7**, 761.

[81] Woodrow T. A. & Ledbury E. A. (2005). *in Proc. of the 8th IPC/JEDEC Conference,* 18.

[82] Hügel W., Kirchner V., Klein C. & Feufel H. (2005). *Presentation at the 9th IPC/JEDEC Conference in Singapore.*

[83] Larche F. & Cahn J. W. (1973). *Acta Metall.* **21**, 1051.

[84] Ostrovsky A. S. & Bokstein B. S. (2001). *Appl. Surf. Sci.* **175-176**, 312.

[85] Chakraborty J., Welzel U. & Mittemeijer E. J. (2008). *J. Appl. Phys.* **103**, 113512.

[86] Brenner S. S. (1956). *J. Appl. Phys.* **27**, 1484.

[87] Park H. S., Cai W., Espinosa H. D. & Huang H. C. (2009). *MRS Bull.* **34**, 178.

[88] Cui Q., Gao F., Mukherjee S. & Gu Z. (2009). *Small* **5**, 1246.

[89] Alaca B. E. (2009). *Int. Mater. Rev.* **54**, 245.

[90] Wang N., Cai Y. & Zhang R. Q. (2008). *Mater. Sci. Eng. R - Rep.* **60**, 1.

[91] Karim S., Toimil-Molares M. E., Maurer F., Miehe G., Ensinger W., Liu J., Cornelius T. W. & Neumann R. (2006). *Appl. Phys. A.* **84**, 403.

[92] Gunter R., Hillerich K., Gianola D. S., Mönig R., Kraft O. & Volkert C. A. (2009). *Nano Lett.* **9**, 3048.

[93] Saka M., Yamaya F. & Tohmyoh H. (2007). *Scripta Mater.* **56**, 1031.

[94] Shim W., Ham J. H., Lee K. I., Jeung W. Y., Johnson M. & Lee W. (2009). *Nano Lett.* **9**, 18.

[95] Lu Y. & Saka M. (2009). *Mater. Lett.* **63**, 2227.

[96] Pitt C. H. & Henning R. G. (1964). *J. Appl. Phys.* **35**, 459.

[97] Lin C. K. & Lin T. H. (2008). *Microelectron. Reliab.* **48**, 1737.

[98] Shibutani T., Yu Q., Yamashita T. & Shiratori M. (2006). *IEEE Trans. Electron. Packag. Manuf.* **29**, 259.

[99] Moriuchi H., Tadokoro Y., Sato M., Furusawa T. & Suzuki N. (2007). *J. Electron. Mater.* **36**, 220.

[100] Shibutani T., Yu Q., Shiratori M. & Pecht M. G. (2008). *Microelectron. Reliab.* **48**, 1033.

[101] Yang F. & Li Y. (2008). *J. Appl. Phys.* **104**, 113512.

[102] Lin Y. W., Lai Y. S., Tu C. T. & Kao C. R. (2008). *J. Electron. Mater.* **37**, 17.

[103] Wei C. C., Liu P. C., Chen C. & Tu K. N. (2008). *J. Mater. Res.* **23**, 2017.

[104] Liu C. Y., Chen C. & Tu K. N. (2000). *J. Appl. Phys.* **88**, 5703.

[105] Ouyang F. Y., Chen K., Tu K. N. & Lai Y. S. (2007). *Appl. Phys. Lett.* **91**, 231919.

[106] Chuang T. H., Lin H. J. & Chi C. C. (2007). *Scripta Mater.* **56**, 45.

[107] Chuang T. H., Chi C. C. & Lin H. J. (2008). *Metall. Mater. Trans. A.* **39**, 604.

[108] Liu M. & Xian A. P. (2009). *Microelectron. Reliab.* **49**, 667.

[109] Dudek M. A. & Chawla N. (2009). *Acta Mater.* **2009**, 4588.

[110] Hao H., Shi Y., Xia Z., Lei Y. & Guo F. (2009). *Metall. Mater. Trans. A* **40**, 2016.

[111] Osenbach J. W., DeLucca J. M., Potteiger B. D., Amin A., Shook R. L. & Baiocchi F. A. (2007). *IEEE Trans. Electron. Packag. Manuf.* **30**, 23.

[112] Barsoum M. W., Hoffman E. N., Doherty R. D., Gupta S. & Zavaliangos A. (2004). *Phys. Rev. Lett.* **93**, 206104.

[113] Oberndorff P., Dittes M., Crema P., Su P. & Yu E. (2006). *IEEE Trans. Electron. Packag. Manuf.* **29**, 239.

[114] Dittes M., Oberndorff P., Crema P. & Schroeder V. (2003). *in Proc. of the 5th EPTC Conference in Singapore, 183.*

[115] Williams M. E., Moon K.-W., Boettinger W. J., Josell D. & Deal A. D. (2007). *J. Electron. Mater.* **36**, 214.

[116] Chen C. M. & Shih P. Y. (2008). *J. Mater. Res.* **23**, 2668.

[117] Huang F. H. & Huntington H. B. (1974). *Phys. Rev. B* **9**, 1479.

[118] Kawanaka R., Fujiwara K., Nango S. & Hasegawa T. (1983). *Jpn. J. Appl. Phys.* **22**, 917.

[119] Moon K. W., Williams M. E., Johnson C. E., Stafford G. R., Handwerker C. A. & Boettinger W. J. (2001). *in Proc. of the 4th Pacific Rim Conference on Advanced Materials and Proceesing*, 1115.

[120] Sheng G. T. T., Hu C. F., Choi W. J., Tu K. N., Bong Y. Y. & Nguyen L. (2002). *J. Appl. Phys.* **92**, 64.

[121] Woodrow T. A. (2006). *in Proc. of the SMTA International Conference in Rosemont, USA*, 1.

[122] Arnold S. M. (1956). *in Proc. of the 43rd Annual Convention of the American Electroplaters Soc.*, 26.

[123] Poker D. B., Schubert J., Alexandrou A., Fröhlingsdorf J. & Stritzker B. (1987). *Nuckear Instr. and Methods in Phys. Res.* **B19/20**, 185.

[124] Poker D. B., Schubert J. & Stritzker B. (1987). *Mat. Res. Soc. Symp. Proc.* **74**, 529.

[125] Welzel U., Ligot J., Lamparter P., Vermeulen A. C. & Mittemeijer E. J. (2005). *J. Appl. Crystallogr.* **38**, 1.

[126] Ice G. E. & Pang J. W. L. (2009). *Mater. Charact.* **60**, 1191.

[127] Hauk V. (1997). *Structural and Residual Stress Analysis by Nondestructive Methods*. Amsterdam: Elsevier.

[128] Noyan I. C. & Cohen J. B. (1987). *Residual Stress: Measurements by Diffraction and Interpretation*. New York: Springer.

[129] Wohlschlögel M., Schülli T. U., Lantz B. & Welzel U. (2008). *J. Appl. Crystallogr.* **41**, 124.

[130] Kumar A., Welzel U. & Mittemeijer E. J. (2006). *J. Appl. Crystallogr.* **39**, 633.

[131] Dölle H. J. (1979). *J. Appl. Crystallogr.* **12**, 489.

[132] Behnken H. & Hauk V. (2000). *Mater. Sci. Eng. A* **300**, 41.

[133] Larson B. C., Yang W., Ice G. E., Budai J. D. & Tischler J. Z. (2002). *Nature* **415**, 887.

[134] Ice G. E., Larson B. C., Tischler J. Z., Liu W. & Yang W. (2005). *Mater. Sci. Eng. A* **399**, 43.

[135] Ice G. E. (2007). Nucl. Instrum. Methods Phys. Res. Sect. A **582**, 129.

[136] Chung J.-S. & Ice G. E. (1999). *J. Appl. Phys.* **86**, 5249.

2. The microstructure and state of stress of Sn thin films after post-plating annealing; an explanation for the suppression of whisker formation?

M. Sobiech, U. Welzel, R. Schuster, E. J. Mittemeijer , W. Hügel, A. Seekamp and V. Kirchner

Abstract

The post-plating annealing ('post-bake' treatment, annealing at 150°C for 1 h) of pure matte Sn thin films on Cu-based substrates is known to be an effective whisker mitigation treatment. The microstructure and the stress state of Sn thin films on Cu-substrates produced with and without a ‘post-bake’ treatment have been investigated using scanning electron and focused ion beam microscopy (SEM & FIB), X-ray photoelectron spectroscopy (XPS) and ageing time and depth-dependent X-ray diffraction (XRD) stress analyses. A comparison of the measured stress-depth gradients in the near-surface regions of the Sn thin films produced with and without ‘post-bake’ treatment indicates differences that might provide a plausible explanation for the observed long-term resistance against whisker growth of Sn thin films subjected to a ‘post-bake’ treatment. In specimens subjected to a ‘post-bake’ treatment, an almost depth-independent tensile stress state prevails in the surface region even after prolonged ageing.

2.1. Introduction

In the microelectronic industry Sn is the "new" material of choice for soldering and coating of electronic components, as the use of up to now commonly employed SnPb-alloys will be restricted according to the directives of the Pb-free legislation "RoHS" (Restrictions of Hazardous Substances) [1]. Since more than 50 years it is well known that pure Sn thin films deposited on Cu are very prone to spontaneous growth of Sn-whiskers exhibiting growth rates of around 1 Å/s [2] and up to 10000 Å/s in the presence of externally applied mechanical stresses [3]. Sn-whiskers grow through continuous addition of material to their base [4]. Mechanical [5], electrical [6] and transmission electron microscopy investigations [7-10] proved Sn-whiskers to be nearly perfect single-crystalline filamentary structures forming on the surfaces of metals with a low melting point [11]. The diameters of Sn-whiskers are about 1-10 µm, whereas the length can reach values up to 10 mm [12]. As Sn-whiskers are able to carry currents of some tens of milliamperes [13], they represent a serious risk of causing short circuits in low-voltage microelectronic devices.

Several models have been proposed for the mechanism of spontaneous Sn-whisker growth on Cu [2, 14, 15], but none of these is able to explain properly all observed phenomena. The build-up of compressive mechanical stresses parallel to the surface in the Sn thin film, due to the formation of an intermetallic compound (IMC; Cu_6Sn_5) at the Sn grain boundaries, may be proposed as a driving force for whisker growth [7, 16]. The formation of a Sn-whisker can be regarded as a stress relief phenomenon. It has been speculated that a positive stress gradient from the IMC region near the interface with the substrate towards the Sn layer surface, as well as a positive stress gradient on the Sn layer surface from the surroundings towards the whisker-root are the cardinal parameters controlling Sn-whisker growth (see, for example [16-18]). Some authors speculated that the presence of a Sn-oxide layer is decisive for whisker formation [7, 16, 19]: The presence of a stable Sn-oxide layer, disabling vacancy sources and sinks at the surface, would enable the built-up of residual macrostresses. Due to different strains in neighboring grains resulting from different grain orientations, shear stresses would develop and lead to a cracking of the Sn-oxide at 'weak' points, which would then serve as nuclei for the formation of whiskers.

From a practical point of view, reliable whisker mitigation treatments and reliable whisker predictability tests are of great importance. The most important and commonly used whisker mitigation treatments are the application of Ni-underlayers (acting as diffusion barriers for Cu) and the post-plating annealing ('post-bake', 150°C for 1 h) in combination with a minimum Sn-thickness of about 7 µm [13]. The purpose of this work is the investigation of the 'post-bake' treatment on the microstructure and the state of stress of Sn thin films.

2.2. Experimental

The Sn thin films were electrodeposited at near room temperature conditions (~ 40°C) and current densities of 1 A/dm^2 on pure Cu-substrates using industrial electrolytes (see Tab. 2.1). The microstructure was columnar with in-plane grain sizes of around 1-5 µm. Sn thin films with in-plane grain sizes between 1 and 10 µm are termed 'matte' as their generally rough surface is poorly reflecting. In order to obtain through-thickness information of the Sn thin films by use of X-ray diffraction applying Cu-Kα radiation the thickness of the Sn layers was of the order of several microns (~ 4 µm). After Sn deposition the specimens were dried at around 100°C for 5 min and then cooled down to room temperature by means of ambient atmosphere storage. The post-plating annealing (called 'post-bake' in the following) was accomplished directly (within 24 h) after Sn deposition by heating the specimens in ambient atmosphere for about 1 hour to 150°C using a conventional furnace.

Table. 2.1: List of specimens used in this study. The specimens were electroplated with matte Sn layers exhibiting a columnar microstructure with in-plane grain sizes of around 1-5 µm.

	substrate	**film thickness**	**'post-bake' treatment**
specimen I	Cu	~ 4 µm	no
specimen II	Cu	~ 4 µm	yes

Micrographs of the Sn layer surface were obtained with a LEO 1450 VP scanning electron microscope, using an acceleration voltage of 15 kV and a beam current between 100 to 200 pA. The surfaces of the Sn thin films were regularly

checked for the presence of whiskers using a SEM. In order to investigate the Sn microstructure cross sections were prepared with a NOVO 600 NanoLab focused ion beam workstation (FEI).

Time-dependent XRD stress measurements were performed employing a Philips (now: PANalytical) MRD Pro diffractometer. Depth-dependent XRD stress measurements were done employing a Bruker AXS D8 Discover diffractometer. Both diffractometers were operating in parallel beam geometry using Cu-Kα radiation and were additionally equipped with an Eulerian cradle (four-circle goniometer) to allow tilting and rotating the specimen as required for stress and texture measurements. The X-ray source in the Philips MRD Pro diffractometer was a conventional sealed Cu tube (45 kV/ 40 mA) and an X-ray lens was employed for obtaining a parallel beam [20]. In the Bruker AXS D8 Discover diffractometer the Cu-Kα radiation was emerging from the point focus (100 µm x 100 µm under take off angle of 6°) of a rotating micro-focus X-ray anode (50 kV/ 20 mA). The X-rays were converted to a parallel beam by means of a 2D-collimating mirror (Xenocs Fox 2D) [21]. In both diffractometers, the diffracted beam was passed through parallel-foils collimators used as secondary optics. In the case of the Philips MRD diffractometer, a flat graphite monochromator was placed in the diffracted beam path and a proportional counter was used as a detector. In the case of the Bruker AXS D8 Discover diffractometer the diffracted beam was counted by an energy-dispersive detector.

The mechanical macrostress state of the Sn thin films was found to be planar and approximately rotationally symmetric. All stress measurements where done along the same in-plane direction in the specimen frame of reference and thus only one component, $\sigma_{||}$ (stress parallel to the surface), of the stress tensor will be reported. Stresses were calculated from lattice strains measured employing the 321 and 631 reflections on the basis of the $\sin^2\psi$-method. The specimen was assumed to be macroscopically elastically isotropic (quasi-isotropic). As Sn is intrinsically elastically anisotropic, hkl-dependent diffraction (X-ray) elastic constants (XEC) Shkl1 and ½Shkl2 had to be claculated for each reflection using an appropriate grain interaction model [22]. In the present study the XEC were derived from single-crystal data [23] using the Neerfeld-Hill model. For each stress measurement the ψ-range (where ψ denotes the inclination of the diffraction vector with respect to the specimen surface normal) was 0-80° with 8°-steps. The time-evolution at room temperature of the

residual stress was traced by performing stress measurements after different ageing times. For the XRD stress measurements at constant penetration depths, τ, the penetration depth increment was chosen as 200 nm. To control the penetration depth a combined χ , ω and ϕ tilting (χ , ω and ϕ are instrumental angles describing the orientation of the specimen with respect to the laboratory frame of reference) of the specimen was applied. The complete strategy for diffraction stress measurements at fixed penetration depths has been described in detail elsewhere [24].

2.3. Results and Discussion

2.3.1. Residual stress evolution in Sn thin films upon ageing at room temperature

The residual macrostress evolution of the Sn thin films as a function of ageing time at room temperature is shown in Fig. 2.1.

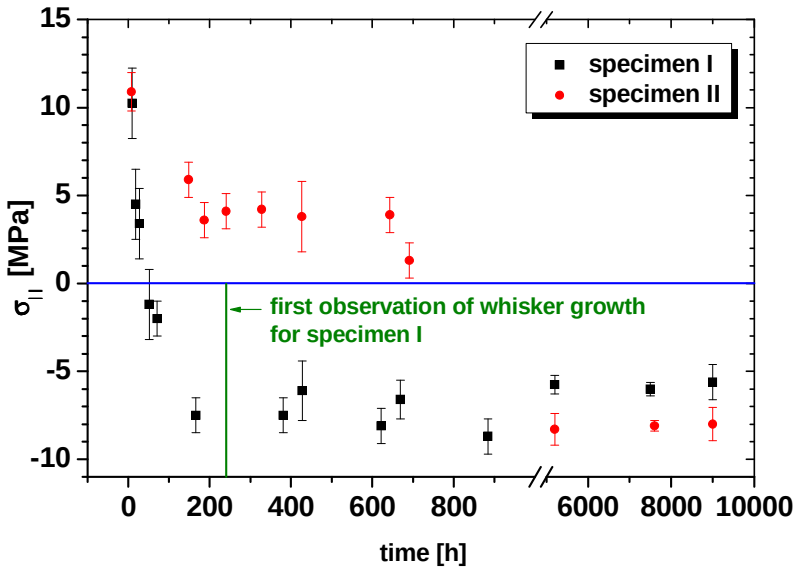

Figure 2.1: Residual macrostress evolutions of the Sn thin film of specimens I and II as a function of ageing times at room temperature. The time of the first observation of whisker growth for specimen I has been marked with the green vertical line.

A tensile stress of around 10 MPa is observed shortly after layer deposition. The initially tensile stress state incorporates intrinsic (growth) stresses arising during electrodeposition and thermal stresses generated during cooling from the temperature of the galvanic deposition bath (about 40°C) to room temperature. Note that the coefficient of thermal expansion of Sn ($23*10^{-6}$ K^{-1}) exceeds the coefficient of

thermal expansion of Cu ($17*10^{-6}$ K^{-1}) [23] and thus tensile thermally induced stresses of about 7 MPa develop in the Sn coatings upon cooling. To some extent, the drying operation after deposition, during which temperatures of about 100°C were employed, may also contribute to the generation of tensile stresses as a consequence of a partial relaxation of compressive stresses generated during heating to the drying temperature. These considerations make likely that the intrinsic growth stresses are in any case small.

The stress of specimen I changed after about 50 h from tensile to compressive and attained after about 200 h a plateau value of -8 MPa. The first whiskers were observed for this specimen after 240 h. Representative SEM pictures of Sn-whiskers of specimen I are shown in Fig. 2.2. The micrographs were taken several months after the Sn deposition. The generation of compressive stresses at room temperature in specimen I is due to the formation of the intermetallic compound (IMC; Cu_6Sn_5) preferably along the Sn grain boundaries orientated more or less perpendicular to the interface/surface. The occurrence of a compressive stress plateau may be interpreted as that the built-up of compressive stress by the growth of the intermetallic phase is compensated by the relief of compressive stress due to the formation of whiskers.

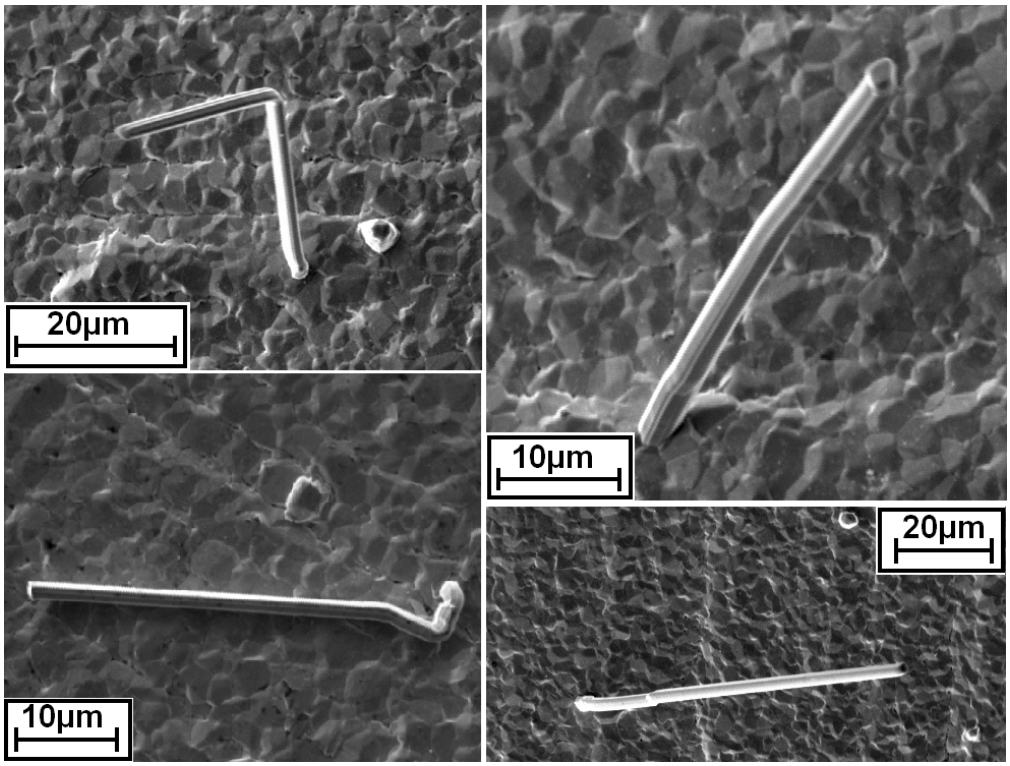

Figure 2.2: SEM images of several Sn-whiskers grown at the surface of specimen I after ageing at room temperature for several months.

The stress of specimen II remained tensile up to an ageing time of about 700 h and apparently reached a plateau at about 2-4 MPa. The next stress data for specimen II was collected 4300 h later, i.e., at 5200 h after deposition. A compressive stress of about -8 MPa was found. The, as compared to specimen I, delayed transition from tensile to compressive stresses in specimen II is also ascribed to the formation of the intermetallic compound (IMC; Cu_6Sn_5) along the Sn grain boundaries at room temperature upon prolonged specimen ageing. Throughout the entire observation period, no whiskers could be detected.

The occurrence of a plateau in the tensile stress regime and the absence of whisker formation for specimens subjected to a 'post-bake' treatment were reported previously in the literature (cf. Ref. [7] for maximum ageing time of 700 h). The above result indicates that specimens subjected to a 'post-bake' treatment may develop a compressive stress upon long-term ageing at room temperature. Hence, the presence of compressive mechanical stresses as such does not appear to be a sufficient condition for whisker growth. It will be shown below that in the light of different stress-depth distributions of specimens I and II a plausible explanation for the different whiskering propensities can be found.

2.3.2. Microstructure

The microstructures of as-deposited and 'post-baked' (cf. 'Experimental') Sn thin films were investigated by SEM, FIB cross-section micrographs, XRD phase analysis and XRD texture measurements.

XRD phase analyses (not shown) and XRD texture measurements (see Fig. 2.3) revealed that neither the phase composition (apart from the occurrence of Cu_3Sn after 'post-bake') nor the crystallographic texture of the Sn thin films were affected significantly by the 'post-bake' treatment.

SEM plane-view investigations revealed that the average in-plane grain size was not affected by the 'post-bake' treatment. Representative FIB-cross sectional micrographs of the Sn thin films obtained before and after a 'post-bake' treatment have been gathered in Fig. 2.4.

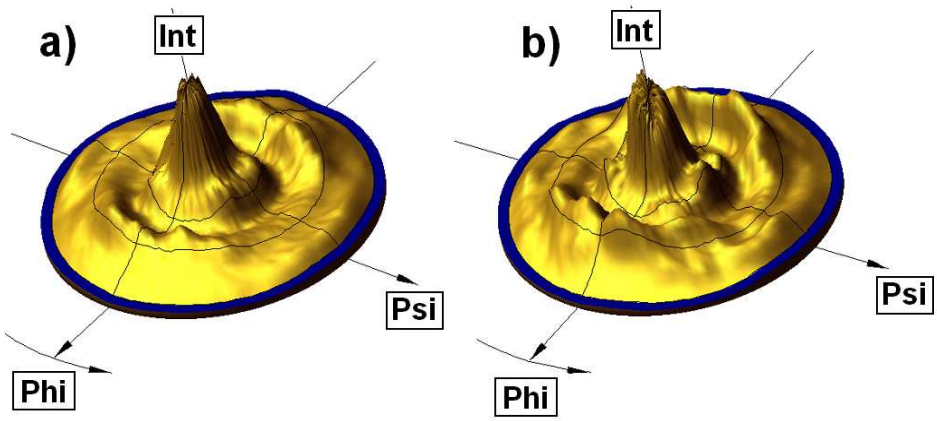

Figure 2.3: Pole figures showing the {321}-fibre texture of matte Sn thin films before (a) and after (b) 'post-bake' (specimens I and II). The pole figures of the 321 reflections of both specimens show no significant changes. The discontinuity in the development of the rotationally symmetric fibre texture for higher ψ angles is most likely due to influences of the underlying Cu-substrate exhibiting a rolling texture.

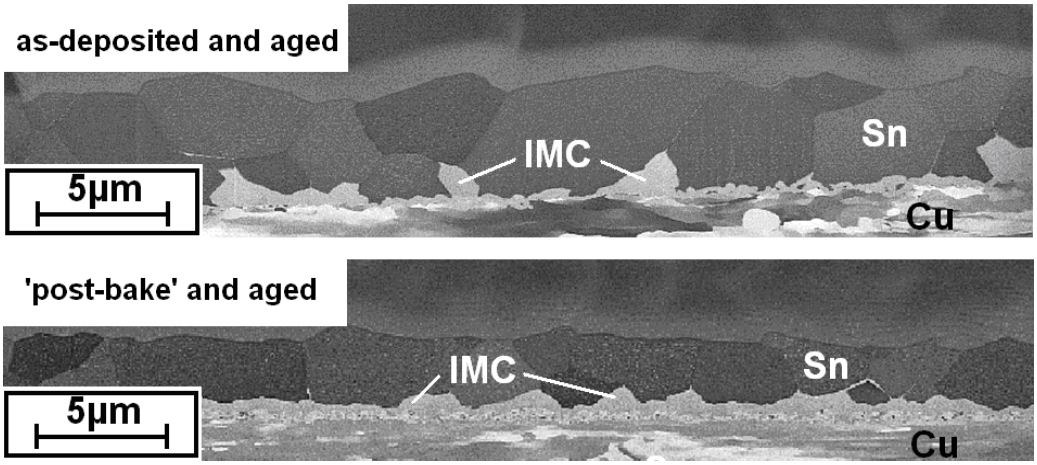

Figure 2.4: FIB-cross sections of matte Sn thin films on Cu-substrates after ageing at room temperature for several months. Top: specimen I. Bottom: specimen II.

The most striking difference between the different specimens is the morphology of the IMC at the Cu/Sn-interface, which is more regular and more planar in the specimen subjected to the 'post-bake' treatment. At room temperature Cu_6Sn_5 forms; the formation of Cu_3Sn progresses only at temperatures exceeding 60°C [25] (see Fig. 2.5).

It may be suggested that, due to predominant bulk-diffusion of Cu in Sn at elevated temperatures, an initially flat IMC double layer consisting of Cu_6Sn_5 and Cu_3Sn formed during 'post-bake'. Then the transition from tensile to compressive

stress upon ageing at room temperature, ascribed to the growth of the IMC along the Sn grain boundaries, occurs at a later stage for the 'post-baked' specimen, due to the presence of the 'post-bake'-induced comparatively thick IMC layer acting as a diffusion barrier for Cu [26].

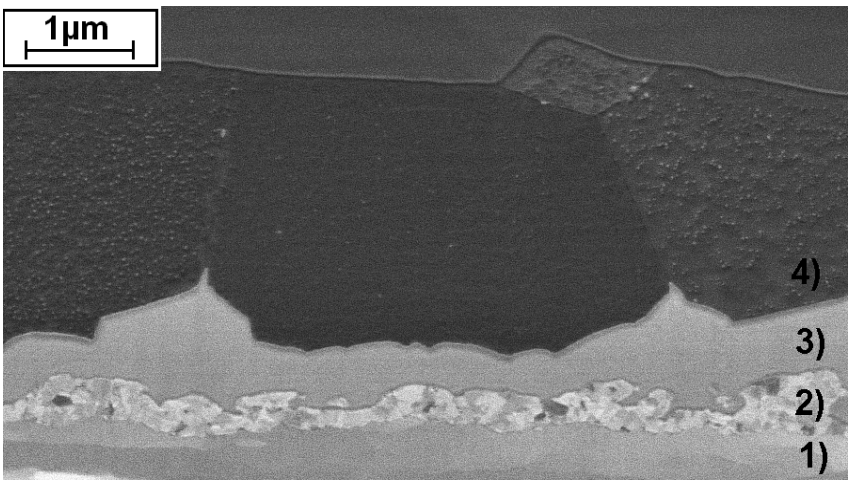

Figure 2.5: FIB-cross section of the matte Sn thin film 4) (specimen II) on a Cu-substrate 1) after 'post-bake' and subsequent ageing at room temperature for several months. The IMC double layer consists of Cu_6Sn_5 3) and Cu_3Sn 2).

2.3.3. Thickness of the surface oxide layer on Sn

The depth-distributions of the elements C, O and Sn in the near-surface regions (~ 15 nm) of the specimens I and II were investigated by use of XPS in combination with successive sublayer removal employing Ar^+ sputter-depth profiling (see Fig. 2.6).

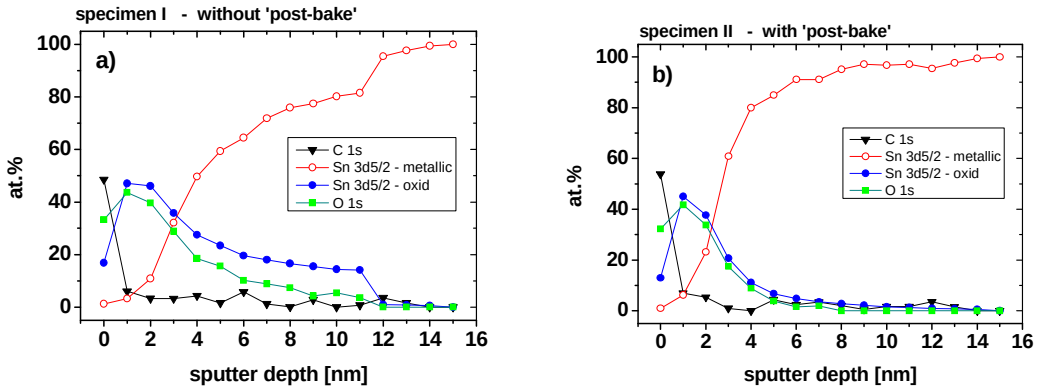

Figure 2.6: XPS sputter-depth profiles of the near-surface regions of Sn thin films before (a) and after (b) 'post-bake' treatment (specimen I and II).

After each sublayer removal step the layer surface was excited by Al-Kα radiation with a spot size of about 0.15 mm^2 and the characteristic binding energies corresponding to the escaping photoelectrons C 1s, O 1s and Sn 3d were detected. For both specimens the Sn-oxide layers exhibit similar average thicknesses of a few nanometres. At sputter depths of around 2-3 nm for both specimens the oxide Sn-peak has disappeared, indicating the transition from the Sn-oxide phase to the metallic Sn thin film. The obtained data indicate that the Sn-oxide phase has a composition of SnO.

The XPS sputter-depth profiles (see Fig. 2.6) did not reveal significant differences among as-deposited specimens and specimens subjected to a 'post-bake' treatment. This makes likely that the 'post-bake' treatment does not affect the whiskering propensity via a thickening of the Sn oxide film, as one may naively assume (cf. 'Introduction').

2.3.4. Stress-depth profiles

The time-dependent XRD stress data shown in Fig. 2.1 were obtained without controlling the penetration depth τ. The results represent through-thickness averaged stress values for the Sn thin films (τ varies between about 1600 nm at ψ = 0° and 600 nm at ψ = 80° in these measurements). For investigating stress-depth gradients in the near-surface region, XRD stress measurements at different controlled penetration depths τ were performed for specimens with and without 'post-bake' treatment after ageing for several months at room temperature. The stress-depth profiles of the specimens indicate that a significant stress gradient occurs in the specimen without 'post-bake' treatment (see Fig. 2.7).

It has been speculated (see, for example Ref. [17]) that such a stress gradient is crucial for the stress-induced Sn-diffusion towards the Sn surface. If this is true, then the current findings make likely that the absence of a significant stress gradient in the surface region of the specimen subjected to a 'post-bake' treatment is responsible for the non-occurrence or suppression of whisker formation. The above reported microstructural observations (see section 2.3.2) make also likely that the region in which compressive stresses are generated upon long-term ageing by IMC development along the Sn grain boundaries orientated more or less perpendicular to

the interface/substrate is located closer to the layer-substrate interface in specimens subjected to a 'post-bake' treatment.

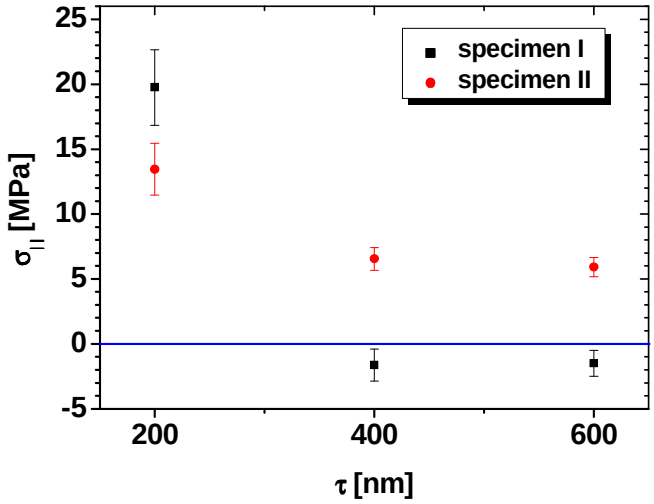

Figure 2.7: The dependence of stress on penetration depth, τ, for specimen I (as-deposited) and specimen II ('post-baked') after ageing at room temperature for several months.

2.4. Summary

- The internal macrostress evolution in Sn thin films of thickness ~ 4 µm, on pure Cu-substrates, produced with and without 'post-bake' treatment, was investigated using X-ray diffraction stress analysis.
- The as-deposited Sn thin films exhibited initially tensile stresses parallel to the surface that became compressive after ageing for about 50 h at room temperature. This stress transition was accompanied by the formation of whiskers on the surface after reaching a stress value of about -8 MPa.
- The stress of the 'post-baked' Sn thin film remained tensile for several hundreds of hours of ageing at room temperature (2-4 MPa). Upon continued, long-term ageing (~ 4000 h) a transition from tensile to compressive stresses occurred. Yet, no whiskers were observed throughout the entire observation period lasting about 9000 h.
- The most striking effect of a 'post-bake' treatment on the microstructure concerns the morphology of the IMC: Whereas the interface of the IMC to the Sn layer is jagged with IMC regions extending deeply into the Sn grain boundaries in the as-deposited specimens without a 'post-bake' treatment, a more planar interface

occurs for the specimen subjected to ‘post-bake’. These findings make likely that the compressive stresses resulting from the growth of the IMC upon long-term ageing at room temperature are concentrated in the interface region for the specimen subjected to a ‘post-bake’ treatment. Indeed, the stress-depth profile in the near-surface region of the specimen subjected to a ‘post-bake’ treatment indicates no significant stress gradient to be present, which could explain the suppression of whisker formation.[20]

Acknowledgment

The authors would like to thank Dr L.P.H. Jeurgens (Max Planck Institute for Metals Research, Stuttgart) for performing the XPS measurements.

References

[1] Directive 2002/95/EC of the European Parliament and of the Council of 27 January 2003 on the restriction of the use of certain hazardous substances in electrical and electronic equipment (2003). *Official Journal of the European Union* **L37**, 19.

[2] Ellis W. C., Gibbons D. F. & Treuting R. C. (1958). *In Growth and Perfection of Crystals,* edited by Doremus, R. H., Roberts, B. W. and Turnbull, D. (Wiley, New York, 1958), pp. 102-120.

[3] Fisher R. M., Darken L. S. & Carroll K. G. (1954). *Acta Metall.* **2**, 368.

[4] Koonce S. E. & Arnold S. M. (1954). *J. Appl. Phys.* **25**, 134.

[5] Herring C. & Galt J. K. (1952). *Phys. Rev.* **85**, 1060.

[6] Dunn B. D. (1976). *Circuit Wolrd* **2**, 32.

[7] Lee B. Z. & Lee D. N. (1998). *Acta Mater.* **46**, 3701.

[8] Sheng G. T. T., Hu C. F., Choi W. J., Tu K. N., Bong Y. Y. & Nguyen L. (2002). *J. Appl. Phys.* **92**, 64.

[9] LeBret J. B. & Norton M. G. (2003). *J. Mater. Res.* **18**, 585.

[10] Liu S. H., Chen C., Liu P. C. & Chou T. (2004). *J. Appl. Phys.* **95**, 7742.

[11] Compton K. G., Mendizza A. & Arnold S. M. (1951). *Corrosion* **7**, 327.

[12] Key P. L. (1970). *In Proc. of the 20th Electronic Components Conference,*155.

[13] Hügel W., Kirchner V., Klein C. & Feufel H. (2005). *Presentation at the 9th IPC/JEDEC Conference in Singapore*.

[14] Eshelby J. D. (1953). *Phys. Rev.* **91**, 755.

[15] Furuta N. & Hamamura K. (1969). *Jpn. J. Appl. Phys.* **9**, 1404.

[16] Tu K. N. (1994). *Phys. Rev. B* **49**, 2030.

[17] Galyon G. T. & Palmer L. (2005). *IEEE Trans. Electron. Packag. Manuf.* **28**, 17.

[18] Choi W. J., Lee T. Y., Tu K. N., Tamura N., Celestre S., MacDowell A. A., Bong Y. Y. & Nguyen L. (2003). *Acta Mater.* **51**, 6253.

[19] Tu K. N., Suh J. O., Wu A. T., Tamura N. & Tung C. H. (2005). *Mater. Trans.* **46**, 2300.

[20] Leoni M., Welzel U. & Scardi P. (2004). *J. Res. Natl. Inst. Stand. Technol.* **109**, 27.

[21] Wohlschlögel M., Schüli T. U., Maier G., Welzel U. & Mittemeijer E. J., accepted for publication in the Proc. of EPDIC10.

[22] Welzel U., Ligot J., Lamparter P., Vermeulen A. C. & Mittemeijer E. J. (2005). *J. Appl. Crystallogr.* **38**, 1.

[23] Gale W. F. (2004). *Smithells Metals Reference Book*. London: Butterworths.

[24] Kumar A., Welzel U. & Mittemeijer E. J. (2006). *J. Appl. Crystallogr.* **39**, 633.

[25] Tu K. N. (1973). *Acta Metall.* **21**, 347.

[26] Osenbach J. W., Shook R. L., Vaccaro B. T., Potteiger B. D., Amin A. N., Hooghan K. N., Suratkar P. & Ruengsinsub P. (2005). *IEEE Trans. Electron. Packag. Manuf.* **28**, 36.

3. Evolution of microstructure and stress of and associated whisker growth on Sn layers sputter-deposited on Cu substrates

M. Sobiech, C. Krüger, U. Welzel, J. Y. Wang, E. J. Mittemeijer and W. Hügel

Abstract

After sputter-deposition of Sn (layer thickness of 350 nm) on Cu substrates and during subsequent ageing at room temperature, Cu and Sn reacted to form the intermetallic phase Cu_6Sn_5 in the Sn layer at the Cu/Sn interface, which led within a few hours of ageing to the development of a compressive stress parallel to the Cu/Sn interface in the Sn layer. One day after ageing at room temperature whisker formation occurred on the surface of the Sn layer. It was shown that whisker growth is associated with long-range Sn diffusion parallel to the Cu/Sn interface. Sn layers of the same thickness sputter-deposited on pure Si substrates exhibited throughout the same ageing time at room temperature a tensile stress parallel to the Cu/Sn interface (no intermetallic phase formation took place) and whisker formation did not occur. The interrelationship of intermetallic compound formation, stress development and whisker growth was discussed.

3.1. Introduction

Nowadays pure Sn is the material of choice for use as “surface finish” (it provides surface passivation and solder reactions with the leadframe) of electronic components, as application of the until recently commonly employed Sn-Pb alloys (introduced in industrial manufacturing in the middle 1960s [1]) has become unacceptable according to legislative directives (RoHS, Restrictions of Hazardous Substances) for “green manufacturing” (e.g. Pb-free soldering) in electronic industry [2]. However, since more than 50 years it is well known that pure Sn thin films deposited on Cu are very prone to the formation of Sn whiskers [3] (lengths of several millimeters [4] can be achieved) which can lead to short-circuit failure of the electronic equipment [5] and thus the whisker-growth phenomenon attained recently great technological and scientific interest. Countermeasures like “post-bake” (a post-plating annealing treatment) and application of diffusion barriers (e.g. Ni) were proposed [5].

Whiskers can exhibit growth rates of about 1 Å/s [6-8] and up to 10000 Å/s in the presence of externally applied mechanical stresses [9]. Whiskers are nearly perfect single-crystalline filamentary structures [9-11] (with diameters of about 1-10 μm) growing through continuous addition of material to their base [12] on the surface of thin metal films with a low melting point (e.g. Cd, Zn and Sn) [3]. The morphologies of whiskers can be very divers; they can be straight, kinked, curved, coiled or they can have a combined morphology (i.e. the morphological growth orientation of the whisker can change with respect to the specimen frame of reference), whereas the crystallographic orientation throughout the whisker remains unchanged [11].

None of the until now proposed mechanisms of formation and growth of Sn whiskers on the surface of Sn layers deposited on Cu [6-8, 13-28] has been able to explain all observed key features of whisker growth, as the moment of whiskering, the locations of whisker nucleation and the growth kinetics. These proposed models can be subdivided into three groups: *i)* the dislocation models [13-17, 19], *ii)* the recrystallization models [6-8, 23, 24] and *iii)* the creep models [18, 20-22, 25-28]. The dislocation models assume that a suitable dislocation source (e.g. a Frank-Read dislocation source [13]) situated at the whisker root continuously emits dislocation loops which glide to the surface and thus transfer Sn atoms from the Sn layer to the growing Sn whisker. The recrystallization models conceive whisker growth as the

outcome of localized (unidirectional) grain growth [6]. The creep models, which are nowadays favored by many authors [25, 27], describe whisker growth as a special form of localized diffusional creep operating via long-range (grain-boundary) diffusion.

Usually the driving force for Sn whisker growth is attributed to the build-up of mechanical compressive stress parallel to the surface in the Sn coating during and/or after Sn deposition and thus whisker growth can be regarded as a stress relief phenomenon [15, 17, 19, 29]. The origin for the build-up of compressive stress can be *mechanical* (due to external mechanical loading), *thermal* (due to difference of the coefficients of thermal expansion of the Cu substrate and the Sn coating), *intrinsic* (due to the deposition conditions) or *chemical* (phase formation by chemical reaction of the Cu substrate, the Sn coating and, possibly, the ambient atmosphere, e.g. oxidation).

Upon ageing at room temperature Cu diffuses into the Sn thin film [29, 30] and formation of the intermetallic compound (IMC) Cu_6Sn_5 takes place only at the Sn side of the Cu/Sn interface [29, 31, 32] and, preferentially, along the Sn grain boundaries intersecting the Cu/Sn interface [18, 19]. The Cu_6Sn_5 formation is accompanied by a specific volume increase and, due to the constraint imposed by the (rigid) substrate, residual compressive stress parallel to the surface can be generated in the Sn thin films [19, 31, 33], in particular in the depth range of the Sn coating where Cu_6Sn_5 formation proceeds [34].

It has been speculated that stress gradients in the Sn layer drive the transport of Sn atoms to the whisker root [18-20, 29, 34, 35]. Only very recently sound experimental evidence was presented demonstrating not only that *compressive* stress is not a prerequisite for whisker formation but, in particular, that, instead, the nature of stress *gradients* in three dimensional space around a potential whisker-nucleation site is decisive for whisker formation [36, 37]. It was shown that *negative out-of-plane residual stress gradients* in the direction from the Sn surface towards the Cu/Sn interface in combination with local *negative in-plane residual stress gradients* around the root of growing Sn whiskers can be conceived as the driving forces for the transport of Sn atoms to the whisker-nucleation site and thus control Sn whisker growth.

The role of formation of the intermetallic compound Cu_6Sn_5 in the system Sn on Cu, during ageing at room temperature, for spontaneous whisker growth (as described above) was first proposed by Tu in 1973 [29]. However, corresponding,

direct experimental evidence lacked until now: In particular, a time-resolved analysis of the evolution of microstructure, state of stress and, possibly, whiskering of Sn layers deposited on Cu and on an inert substrate, upon ageing at room temperature, is needed. The current project aims to provide such data. In the present work the room temperature evolution of the microstructure, the state of stress and the whiskering behavior of (high-purity) Sn coatings with a thickness of about 350 nm sputter-deposited on Cu and Si substrates were investigated in detail. Of particular importance is that the high-purity (6N) of the Sn layers investigated excludes possible influences (controversially discussed, see Ref. [38]) of co-deposited organic and inorganic impurities, in contrast with the commonly used electrodeposited Sn films.

3.2. Experimental

3.2.1. Specimen preparation

Polycrystalline Sn coatings with a thickness of about 350 nm were deposited on pure Cu (commercial leadframe material) and Si (commercial Si {100} wafer covered with thin amorphous SiO_2 (~ 50 nm) and (on top) Si_3N_4 (~ 50 nm) barrier layers) substrates by direct current magnetron sputtering (base pressure of about 2.1 x 10^{-3} mbar) employing Ar (at 5 x 10^{-3} mbar; corresponding to 5% Ar-flow) as sputter gas and a magnetron power of 50 W. The purity of the Sn target from MaTeck© was 6N. Prior to Sn deposition the Cu and Si substrates were surface-treated in the following way: *i)* wet cleaning, i.e. rinsing in acetone and alcohol followed by an ultra-sound bath treatment; *ii)* drying, i.e. treatment with N_2 and CO_2-snow jet streams and *iii)* radio frequency sputter cleaning. During Sn deposition the substrate temperature increased to about 50-80°C. After Sn deposition all specimens were aged at room temperature without controlling the ambient atmosphere.

3.2.2. Microstructural analyses

Micrographs of the surface of the Sn layer were recorded using a LEO 438 VP scanning electron microscope (SEM), operating at an acceleration voltage of 15 kV, a beam current between 100 and 200 pA and a working distance of 16 mm. The surfaces of the Sn layers were regularly checked during ageing at room temperature for the presence of whiskers using the SEM.

In order to prepare and image cross sections of the Sn layers and of Sn whiskers a dual-beam FEI Nova NanoLab 600 work station was employed, which allowed cutting the specimen with a focused Ga-ion beam (FIB) and imaging subsequently the prepared cross-section by means of a focused electron beam in scanning mode (SEM). Prior to preparation of cross-sections of the Sn layer by FIB cutting, a Pt capping double-layer (see also Fig. 3.2) was deposited onto the specimen (by decomposition of a metal-organic precursor gas by the action of the ion beam) in order to protect the specimen surface during ion-beam treatment. The FIB work station was also used for isolating Sn whiskers from the Sn coating (not covered by a Pt capping double layer) as follows (see also section 3.3.4): First the whisker was brought into direct contact with a tungsten needle used as micro-manipulator (see Fig. 3.8a). Next, Pt was deposited onto the contact point between needle and whisker and subsequently the whisker was isolated from the surface of the specimen by cutting through the whisker root using the ion beam. Thereafter the tungsten needle with the attached whisker (see Fig. 3.8b) was moved towards a Si substrate (see section 3.2.1; also present in the vacuum chamber). Pt was deposited on the contact point of whisker and Si substrate, in order to fix the whisker on the Si substrate and finally the Si substrate with the whisker on it was transferred from the FIB apparatus to the AES instrument for compositional analysis (see section 3.2.4).

3.2.3. X-ray diffraction phase and stress analyses

Diffraction analysis was performed employing a Philips (now: PANalytical) MRD Pro diffractometer operating in parallel beam geometry (parallelization was realized by means of a polycapillary X-ray lens, see Ref. [39]) with an X-ray beam size of 4 x 4 mm^2 and Co Kα radiation emerging from the point focus of a conventional sealed X-ray tube working at 40 kV / 40 mA. The specimen was mounted onto an Eulerian cradle which allowed tilting and rotating the specimen as required for X-ray diffraction stress analysis. The diffracted beam was passed first through a parallel-plate collimator, then through a flat graphite monochromator and subsequently the diffracted signal was recorded by a proportional counter. Qualitative X-ray diffraction phase analysis was performed after several ageing times in conventional ($\theta/2\theta$) diffraction geometry within the 2θ-range of 30-100°, with a step size of 0.04° 2θ and a step time of 1 s.

Based on direction- and position-dependent X-ray diffraction stress measurements, the mechanical macrostress state of the Sn thin films in the specimen frame of reference was found to be planar, rotationally symmetric and laterally (more or less) homogeneous and thus only one component, $\sigma_{\parallel}$ (= σ_{11} = σ_{22}; the stress parallel to the Cu/Sn interface) occurs. Mechanical stresses were calculated from lattice strains measured employing the 321 reflection on the basis of the $\sin^2\psi$-method [40]. The specimen was assumed to be macroscopically elastically *quasi-isotropic* and thus the *hkl*-dependent (X-ray) diffraction stress factors reduce to the (X-ray) diffraction elastic constants (XEC) $S^{hkl}{}_1$ and $\frac{1}{2}S^{hkl}{}_2$ [41], which were calculated here from the single-crystal elastic constants [42], adopting the Neerfeld-Hill approach [40]. For each stress measurement the investigated ψ-range (where ψ denotes the inclination of the diffraction vector with respect to the specimen-surface normal) was 0-80°, in steps of 8°. One stress measurement took about 20 h. The evolution of the residual stress during ageing at room temperature was traced by performing stress measurements after different ageing times.

The residual stress of the intermetallic compound Cu_6Sn_5 forming at the Cu/Sn interface was measured at three different times of ageing at room temperature. Lattice strains employing the $24\bar{1}$ reflection of Cu_6Sn_5 were measured on the basis of the $\sin^2\psi$-method [40] and the mechanical stress was assessed using elastic constants obtained from polycrystalline specimens [43], as single-crystal elastic constants are not available for Cu_6Sn_5.

3.2.4. Compositional analysis of whiskers

Composition-depth profiles of individual whiskers were measured employing Ar ion sputter-depth profiling in combination with Auger electron spectroscopy (AES) applying a JEOL JAMP 7830F field emission scanning Auger microprobe (base pressure of about 8.0 x 10^{-10} mbar) equipped with a hemispherical (high-resolution) analyzer. The Ar ion beam (energy of 1 keV) used for sputtering was directed at an incidence angle of about 40° with respect to the whisker-surface normal. Sputter-depth profiling (perpendicular to the (longitudinal) growth axis of the whisker) at 1 kV and with a sputtering rate of 6 nm/min (according to standard calibration with Ta_2O_5) was conducted using the discontinuous step-mode, i.e. after each sputtering step a point AES analysis (lateral position control was realized by automatic comparison of SEM

images taken before and after sputtering), roughly in the middle of the whisker (see Fig. 3.8a), was performed. AES analysis was conducted with an electron beam (with diameter of about 15 nm) of 10 keV and 20 nA. The chemical composition of the Sn whisker with a diameter of about 0.5 μm (see Fig. 3.8) along an overall sputter-depth of about 180 nm was recorded by monitoring the Auger lines Si-LVV (92 eV), Ar-LMM (210 eV), C-KLL (270 eV), Sn-MNN (430 eV), O-KVV (503 eV) and Cu-LMM (920 eV).

3.3. Results and Discussion

3.3.1. Microstructure and phase formation

The sputter-deposited Sn layers had a high surface roughness due to the formation of laterally partly isolated Sn islands with in-plane sizes of about 1 μm (see Figs. 3.1a and e). FIB top-view (see Fig. 3.1e) and FIB cross-sectional (see Fig. 3.2a) micrographs show that the island-type Sn microstructure exhibited occasionally trenches extending to the substrate between Sn islands and thus the Sn coating appears as a "network" of interconnected Sn islands. The polycrystalline nature of the Sn island network is revealed clearly by the ion-beam induced channeling contrast, as shown in Fig. 3.1e.

Directly after Sn deposition and during subsequent ageing at room temperature SEM investigations of the Sn surface were performed regularly. It followed that the morphology of the Sn layer did not change with ageing time, but whisker formation did occur on the Sn surface of Cu/Sn specimens, after about one day of room temperature ageing. A representative top-view SEM image of the "early" whisker-formation stage is shown in Fig. 3.1d), where a small whisker with a length of about 2 μm had grown out of an isolated Sn island. The SEM micrograph shown in Fig. 3.1a) illustrates more clearly that the nucleation site of whiskers is located on top of the Sn islands (this finding could be confirmed on many whisker-nucleation sites).

FIB cross-sectional investigations (see Fig. 3.2b) as well as phase analysis by X-ray diffraction (see Fig. 3.3) reveal that small amounts of Cu_6Sn_5 had already developed at the Cu/Sn interface one day after Sn deposition, which agrees with recent findings [31, 44]. Upon continued ageing at room temperature more Cu_6Sn_5 formed at

the Cu/Sn interface (see Fig. 3.3), thereby extending into the Sn layer (see Figs. 3.4b and 4c).

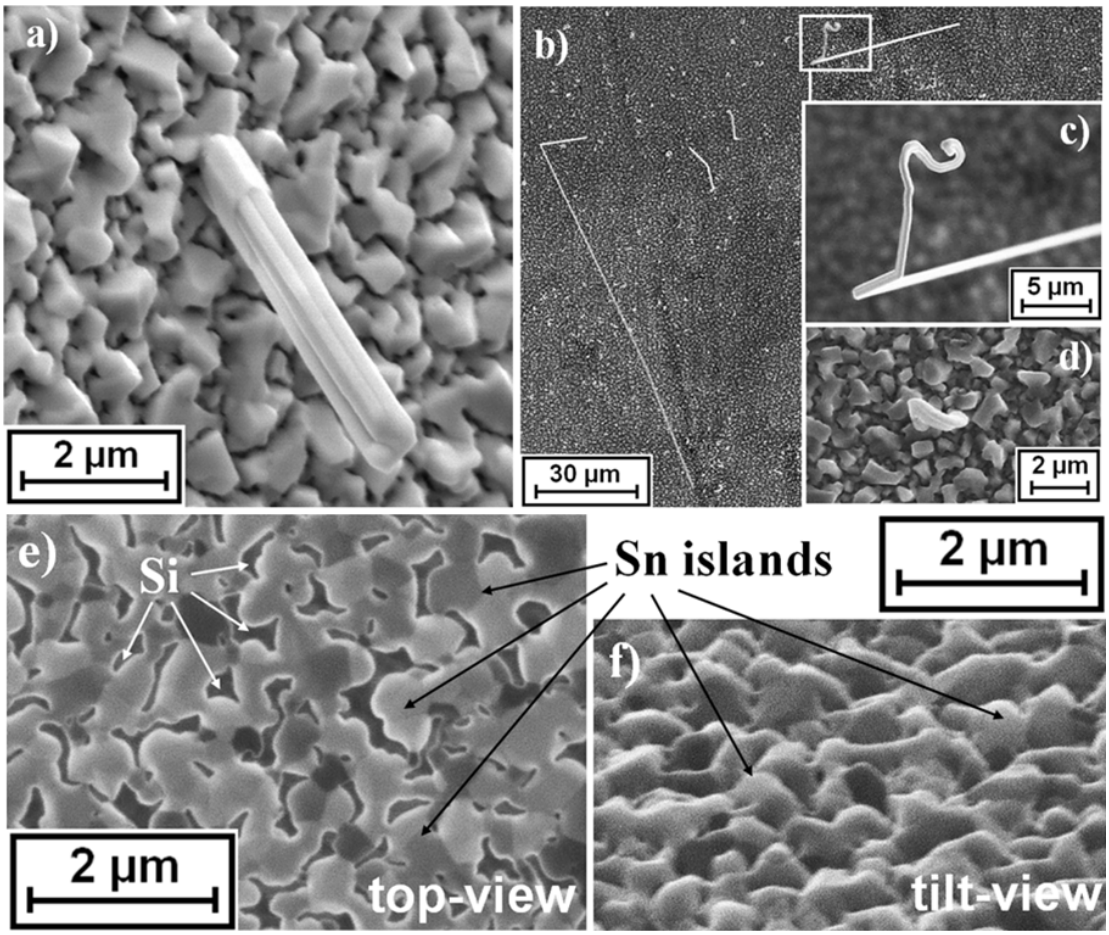

Figure 3.1: SEM image (tilt-view) of the surface of a Sn coating sputter-deposited on Cu taken several days after Sn deposition. The island-type morphology of the Sn coating and a Sn whisker are visible. b)-c) SEM images of several Sn whiskers of a Cu/Sn specimen showing different whisker-growth morphologies and whisker lengths of more than 100 µm; micrographs were taken about 50 days after Sn deposition. d) SEM image of the Sn surface showing the "early" whisker-formation stage, as recorded about 2 days after Sn deposition. e)-f) FIB micrographs (top- and tilt-view, respectively) of the Sn coating sputter-deposited on Si taken after treating the surface for a few seconds with the ion beam. Particularly the very fine-grained Sn in-between the Sn islands was removed during sputtering (compare with images a) and d)). Thus the network of Sn islands is even more obvious due to the bright appearance of Sn, as compared with Si which appears darker. The polycrystalline nature of the Sn island network is clearly visible due to the ion-beam induced channeling contrast, i.e. each Sn grain exhibits a particular shade of grey.

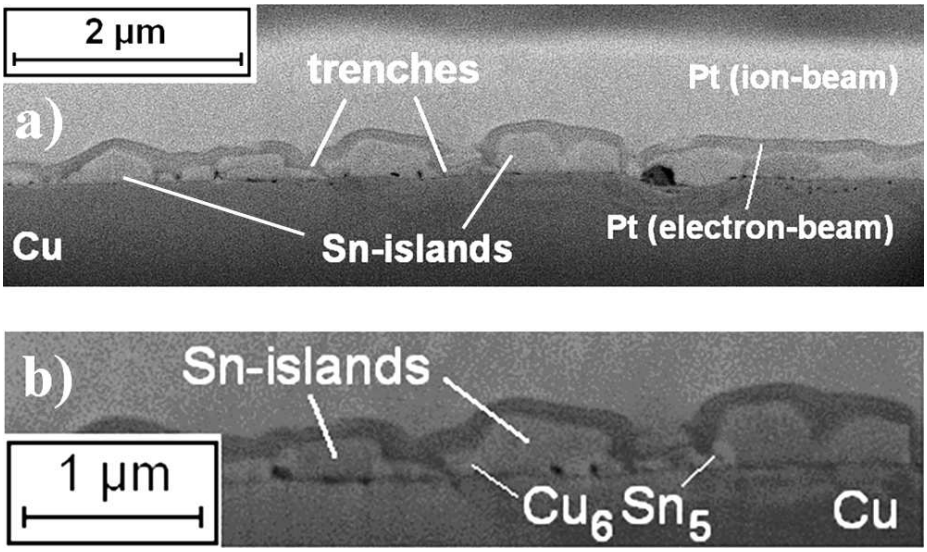

Figure 3.2: SEM images taken of cross-sections of a Cu/Sn specimen prepared by FIB machining one day after Sn deposition. The Pt capping deposit consists of two layers; the bright top one (low C content) was ion-beam deposited and the darker bottom one (high C content) was electron-beam deposited. a) The Sn coating represents a "network" of Sn islands (see also Fig. 3.1e) with trenches extending to the substrate between the islands. b) Already one day after Sn deposition formation of Cu_6Sn_5 (bright grains) was observed at the Cu/Sn interface.

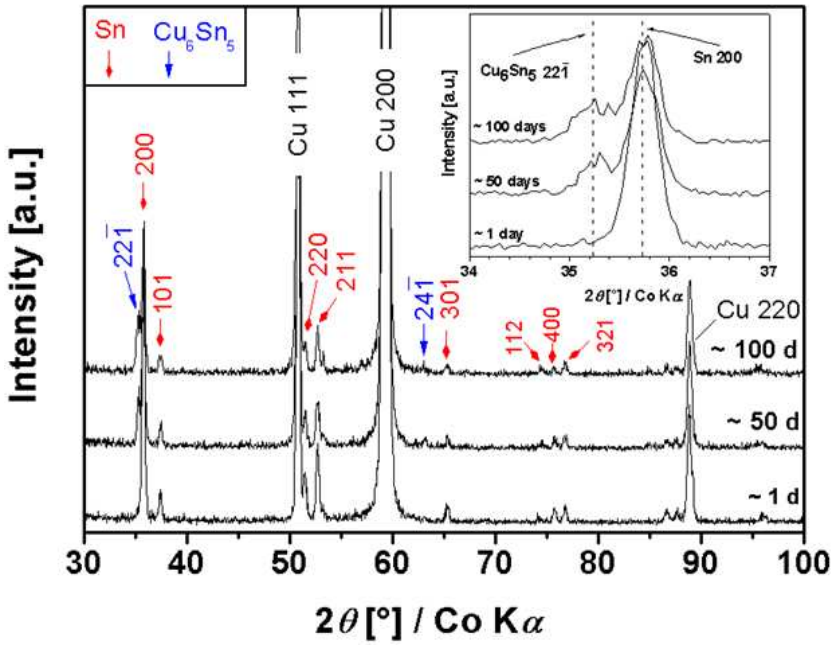

Figure 3.3: Diffraction patterns of the Sn coating (layer thickness of about 350 nm), sputter-deposited onto a Cu substrate, taken at different times upon ageing at room temperature. The inset shown in the upper right corner reveals the emergence of the diffraction signal of the 22$\bar{1}$ diffraction line of the Cu_6Sn_5 phase as function of ageing time at room temperature.

A cross-section through a Sn whisker (and its nucleation site) grown on a Cu/Sn specimen was prepared by FIB machining after about 50 days of room temperature ageing (see Fig. 3.4c). The whisker originated from a "Sn" island, which consisted (in this cross-sectional view) of one Sn grain and one Cu_6Sn_5 grain (see inset in Fig. 3.4c). Apparently, Cu_6Sn_5 had formed upon room temperature ageing thereby replacing (partly) a Sn grain of the Sn island. The whisker grown is separated from the underlying Sn island by a grain boundary, i.e. the whisker is not a direct continuation of a Sn grain.

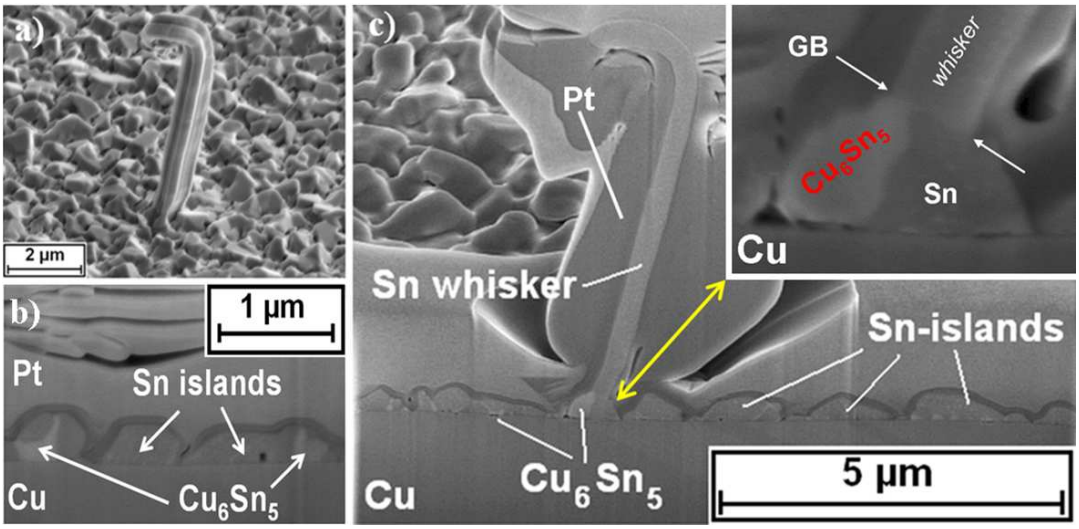

Figure 3.4: SEM micrograph (tilt-view) of the surface of the Sn layer; the Sn whisker shown was selected for FIB cross-sectional investigation. The SEM and FIB investigations were performed after about 50 days of room temperature ageing. **b)** SEM micrograph of a FIB cross-section taken at a distance of roughly 1-2 μm from the whisker, i.e. before conducting the FIB cut through the Sn whisker as shown in c). **c)** SEM micrographs of a FIB cross-section through the Sn whisker shown in a). The region of the whisker-nucleation site, on top of a Sn island (indicated with the yellow arrow), is shown magnified in the upper right corner. The "Sn" island consists (in this cross-sectional view) of one Sn grain and one Cu_6Sn_5 (relatively bright) grain. The whisker is separated from the underlying Sn island by a grain boundary (GB) indicated with arrows in the upper right inset, i.e. the whisker is not a direct continuation of a Sn grain.

3.3.2. Whisker growth and Sn transport

After an ageing time at room temperature of about 50 days, whiskers with diameters of about 1 μm (see e.g. Fig. 3.1a) and with lengths up to 100 μm were observed frequently (see Fig. 3.1b). The material flow of Sn from the Sn layer to the

whisker was assessed quantitatively by a mass balance approach. The whisker is conceived as a cylinder of a mass $m_W = \delta\pi r_w^2 h_w$, with δ as the Sn density of 7.31 g/cm^3, r_w as the whisker radius of 0.5 μm and h_w as the variable whisker length. The Sn inlands (out of which the whisker grew) are conceived as cones with mass $m_I = \delta 1/3\pi r_i^2 h_i$, with r_i as island radius of 0.5 μm and h_i as the island height of 0.35 μm. Then the total amount of Sn island material consumed upon whisker growth can be calculated as a function of whisker length (see Fig. 3.5).

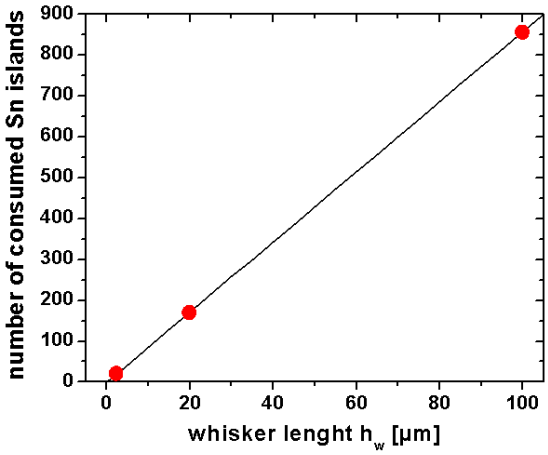

Figure 3.5: Mass balance approach in order to asses the material flow of Sn from the Sn layer to the whisker in dependence on the whisker length (see text for further details). The red dots correspond to the lengths of the whiskers shown in Fig. 3.6.

Evidently, the Sn material contained in one whisker (length of 1 µm and more) requires transport of an amount of Sn from the layer to the whisker (widely) surpassing the amount of Sn in one island of the Sn layer, out of which the whisker grew. This is illustrated by Fig. 3.6, where three whiskers with lengths of 3, 20 and 100 µm are shown. The dotted area in these figures indicates the areas of the Sn layer comprising an amount of Sn equal to that contained in the whisker concerned. This result, whisker growth by incorporation of an amount of Sn in the whisker much larger than contained in one Sn island, provides direct evidence for the occurrence of lateral transport of Sn over (enormous) distances, even much larger than the size of the areas indicated (as the areas indicated obviously did not provide all Sn in the whisker concerned). This occurrence of long-range lateral transport of Sn was already suggested about 40 years ago on the basis of top-view SEM investigations of closed Sn films showing Sn whiskers, because material depletion around the whisker root (e.g. by a local depression of the Sn surface) was not observed [4]. This suggestion was derived for a

Sn layer after ageing of several years at room temperature. The present results indicate that also for much shorter ageing times at room temperature, a material-depletion zone around a whisker root does not occur (was never observed in this work).

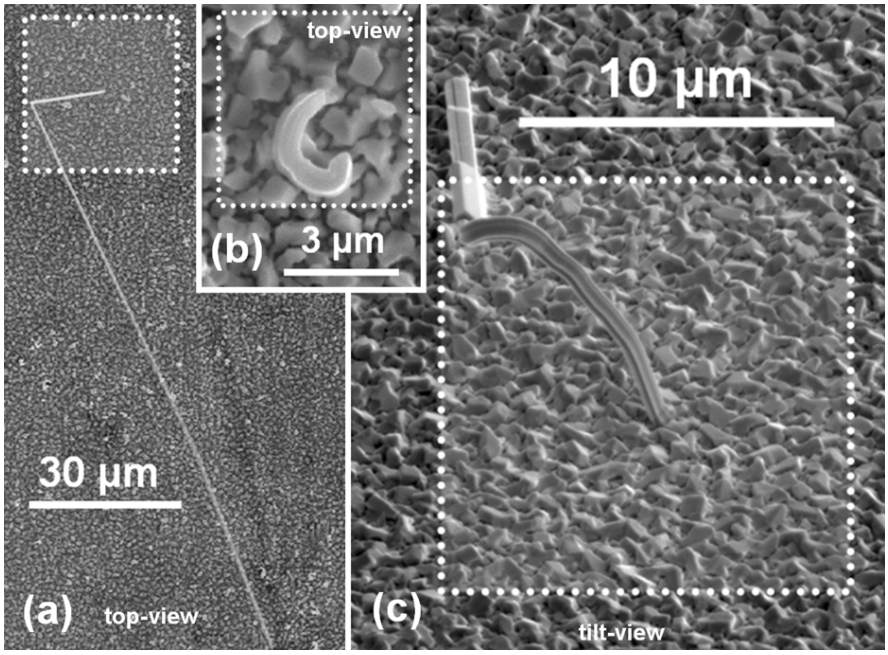

Figure 3.6: SEM micrographs of three Sn whiskers with lengths of 100 μm **(a)**, 3 μm **(b)** and 20 μm **(c)** after about 50 days of ageing at room temperature. The dotted areas indicate the areas of the Sn layer comprising an amount of Sn equal to that contained in the whisker concerned. This area of Sn was calculated from the number of Sn islands consumed according to Fig. 3.5.

The above conclusion is compatible with results of tracer diffusion experiments applying a system composed of a Sn^{120} layer deposited on a Sn^{118} layer with a "special" geometry. It could be shown that long-range Sn diffusion in the direction parallel to the substrate indeed can occur during ageing at room temperature (a Sn migration distance of about 3000 μm after about 300 days of room temperature ageing was determined) [45].

3.3.3. Residual macrostress evolution

The residual macrostress parallel to the Cu/Sn interface of the Sn coating sputter-deposited on Cu is shown in Fig. 3.7 as function of ageing time at room temperature. A compressive stress of about -18 MPa was observed shortly (~ 20 h) after Sn deposition. As one diffraction stress measurement took about 20 h (due to the low diffracted intensity caused by the small layer thickness), the initially (i.e. directly

after Sn deposition) present state of stress could not be determined experimentally employing diffraction stress analysis. Because (i) the Sn deposition was performed at a temperature in the range 50-80°C (corresponding to a homologous temperature in the range 0.64 – 0.71 for Sn) and (ii) the coefficient of linear thermal expansion of Sn (~ 22 x 10^{-6} K^{-1}) [46] exceeds that of Cu (~ 16.5 x 10^{-6} K^{-1}) [46], an initially tensile thermally induced stress of about 10-23 MPa♦ is expected after Sn deposition upon cooling to room temperature (~ 25°C). Intrinsic (growth) stresses arising during Sn deposition may occur as well (generation of intrinsic stresses due to island coalescence and grain growth (associated with grain-boundary area reduction)) [47, 48], but in view of the comparatively high homologous temperature of Sn during specimen preparation (cf. above) recovery processes likely operate during Sn layer growth, thereby relieving intrinsic growth stresses. Hence, the initial state of stress (after cooling to room temperature) is governed by the thermally induced stress and thus is of *tensile* nature. It then follows that already within the first 20 h of ageing at room temperature a *compressive* stress component of (at least) about -18 MPa had developed.

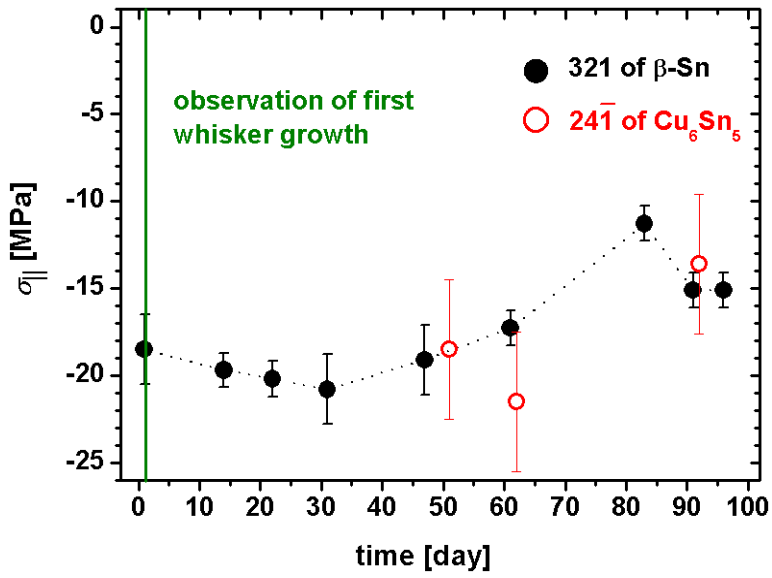

Figure 3.7: Residual macrostress parallel to the Cu/Sn interface of the Sn coating with a thickness of about 350 nm sputter-deposited on Cu (filled dots) as well as of the intermetallic compound Cu_6Sn_5 (open dots) as function of ageing time at room temperature, recorded using the 321 reflection of β-Sn and the 24$\bar{1}$ reflection of Cu_6Sn_5, respectively. The time of the first observation of whisker growth (~ 1 day) has been marked with the green vertical line.

♦ This consideration makes the occurrence of plastic deformation during cooling likely.

After layer deposition and during subsequent ageing Cu and Sn react to form Cu_6Sn_5 (only) at the Sn side of the Cu/Sn interface. The ongoing Cu_6Sn_5 formation extending from the Cu/Sn interface into the Sn layer is accompanied by a specific volume increase and due to the constraint imposed by the (rigid) substrate, residual compressive stress parallel to the Cu/Sn interface develops in the Sn layer.

Until an ageing time of 50 days at room temperature no further significant compressive stress build-up occurred (see Fig. 3.7), although the source for potential compressive stress generation, i.e. Cu_6Sn_6 growth from the Cu/Sn interface, was still operating. The occurrence of this stress plateau value of about -20 MPa coincided with the occurrence of whisker formation. It is thus suggested that whisker formation acts as stress-relief mechanism. Note, that indeed, the yield limit of Sn (for uniaxial loading) is about 10-15 MPa for polycrystalline, isotropic bulk Sn [42, 49].[#]

Once the yield limit has been exceeded, further generation of compressive stress is balanced by plastic strain accommodation, involving in the present case whisker growth. As long as this balance of stress generation and stress relief exists, whisker formation continues (this is compatible with the line of reasoning in Ref. [27]). Note that the evolution of microstructure, state of stress of and associated whisker growth on the island-type Sn coating on Cu does not differ from that reported for closed Sn films [19, 33, 34].

Upon continued long-time ageing (i.e. beyond 50 days) at room temperature the compressive stress in the Sn layer decreases (see Fig. 3.7) and thus whisker growth comes to a halt (as confirmed in separate experiments). This can be understood as follows: The build-up of compressive stress, by the formation of Cu_6Sn_5 in the Sn layer at the Cu/Sn interface, leads to the development of a negative nature of the stress gradient in the direction of increasing layer depth [36]. Such a stress gradient is relieved by transport of Sn atoms to the surface. Hence, continued growth of Cu_6Sn_5 can be associated with continued whisker growth, as stress-relief mechanism. However, once the growth rate of Cu_6Sn_5 at the Cu/Sn interface decreases (upon continued, long-time ageing; this holds for example for diffusion-controlled parabolic

[#] The yield limit can vary in dependence on grain size [50]. The polycrystalline island-type Sn microstructure with island dimensions of the order of 1 x 1 x 0.35 μm^3 exhibits a “high” grain-boundary density which can explain the observed strengthening of the Sn coating, as exhibited by the apparent increase of the yield limit up to about 20 MPa.

product-phase growth), the compressive stress in the Sn layer drops, and thus the whisker-growth rate decreases and eventually becomes nil.

The residual stress of the intermetallic compound Cu_6Sn_5 forming at the Cu/Sn interface was measured at three different times of ageing at room temperature. The residual stress in Cu_6Sn_5 is nearly the same as that of the Sn layer (see Fig. 3.7). This validates the above proposed mechanism for stress development, i.e. Cu_6Sn_5 formation at the Sn side of the Cu/Sn interface which is accompanied by a specific (molar) volume increase: a macroscopic in-plane volume misfit at the layer/substrate interface is induced, and as a consequence, the same compressive mechanical stress is generated in both Sn and Cu_6Sn_5, in order to comply with the constraint imposed by the (rigid) substrate.

To verify the governing role of the Cu_6Sn_5 formation for the generation of compressive stress in the Sn layer and thus the associated whisker formation, a Sn layer was sputter-deposited onto a pure Si substrate (see section 3.2.1) using the same sputter-deposition conditions as for the preparation of sputter-deposited Sn layer on the Cu substrate. After Sn deposition these Si/Sn specimens were aged at room temperature and SEM and diffraction stress analyses of the Sn deposit were performed similarly as for the Cu/Sn specimens. The inital microstructure of the Si layer of the Si/Sn specimen did not deviate significantly from that of the Sn layer of the Cu/Sn specimen. No intermetallic compound formation and no compressive stress development did occur upon ageing at room temperature.[*] Thus, in agreement with the above interpretation, whiskers did not form, indeed, on these Si/Sn specimens.

At this place it should be noted that very recently it has been shown experimentally by the group of the present authors that the presence of compressive mechanical stress by itself is not a sufficient condition for whiskering: A negative

[*] Diffraction stress analysis performed after three days and after 100 days of ageing at room temperature revealed the same, small tensile stress (~3.4±1 MPa) parallel to the Cu/Sn interface of the Sn layer of the Si/Sn specimen. Because (i) Sn deposition on Si was performed at a temperature in the range of 50-80°C and (ii) the coefficient of linear thermal expansion of Sn (~ 22 x 10-6 K-1)[46] exceeds that of Si (~ 2.7 x 10-6 K-1)[46], an initially, tensile thermally induced stress would occur in the Sn layer of a value exceeding by far the yield limit of Sn. The observed constant, small tensile stress of about 3.4±1 MPa indicates that thermal stress relaxation by means of plastic deformation had occurred during cooling after layer deposition. Consequently, no compressive stress (and no distinct stress gradient) had developed in the Sn coating.

nature of *out-of-plane residual stress-depth gradients* [36] in the direction from the Sn surface towards the Cu/Sn interface (cf. above discussion) in combination with a local negative nature of *in-plane residual stress gradients* [37] around the root of growing Sn whiskers are prerequisites for whiskering. Hence, even in the presence of tensile stress parallel to the surface, a negative nature of the stress gradients can induce plastic accommodation, involving whiskering, as observed.

The emergence of such stress gradients due to intermetallic compound formation, at the Sn/Cu interface and along the Sn grain boundaries, before whiskering, is supported by finite element simulations [51].

3.3.4. Composition-depth profile of a Sn whisker

It has been reported, on the basis of results from sputter-depth profiling in combination with AES analysis, that Sn whiskers growing from (electrodeposited) Sn layers on Cu-based substrates contain Cu impurities [52, 53]. These investigations were performed on Sn whiskers which were *not* isolated prior to analysis from the Sn layer and for this reason the following discussion of such data is relevant: Sputter treatment of a whisker which is in contact with the Sn layer affects a significantly larger area than only the whisker area, i.e. material from the whisker as well as from the near-surface regions of the surrounding Sn layer are removed during sputtering. During sputtering, re-deposition of the sputtered material on both the surface of the whisker and the surface of the Sn layer occurs. Thus Cu, originating from Cu_6Sn_5 in the (original) Sn layer, can occur as contaminant of the Sn whisker.

To avoid such complications, in the present work a whisker was isolated, prior to such analysis, from the Sn layer by means of a dedicated FIB-cutting treatment (described in section 3.2.2; see Fig. 3.8). Further, in case of whisker growth from high-purity (6N) sputter-deposited Sn layers on pure Cu substrates a possible incorporation of (and effects of) complex organic and inorganic impurities into the whisker during growth (as might happen in case of electrodeposited Sn layers) can be excluded.

AES analysis performed on the surface of the Sn whisker (see section 3.2.4) detected carbon as an impurity (due to atmospheric contamination) and revealed the presence of a Sn oxide layer with a thickness of several nanometres; no other elements were detected in the near-surface region of the Sn whisker. Two representative AES (differentiated) spectra taken from two different sputter depths (~ 60 and ~ 180 nm),

measured perpendicular to the length axis of the whisker, are shown in Fig. 3.9. For both sputter depths only Auger signals of Si (92 eV), Ar (210 eV) and Sn (420 eV) could be detected, i.e. Auger signals of Cu (920 eV) were not observed. The Auger signal of Si (92 eV) is a measurement artefact according to the processes described above, i.e. during sputter-depth profiling Si from the substrate was removed and subsequently re-deposited on the surface of the Sn whisker. The Auger signal of Ar (210 eV) is ascribed to Ar atoms which were incorporated in the Sn whisker during sputtering.

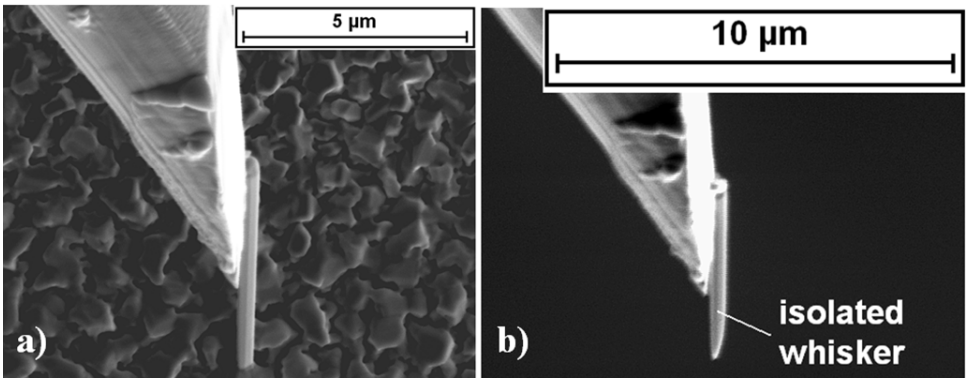

Figure 3.8: SEM images of two working stages of the dedicated FIB-cutting treatment (see section 3.2.2) which was applied in order to isolate a Sn whisker from the Sn coating. **a)** The Sn whisker is fixed to the tungsten needle (used as micro-manipulator) by Pt deposition at the contact point. Next the whisker is isolated from the Sn coating by cutting through the whisker root using the ion beam. **b)** The Sn whisker attached to the micro-manipulator is subsequently transferred onto a Si substrate.

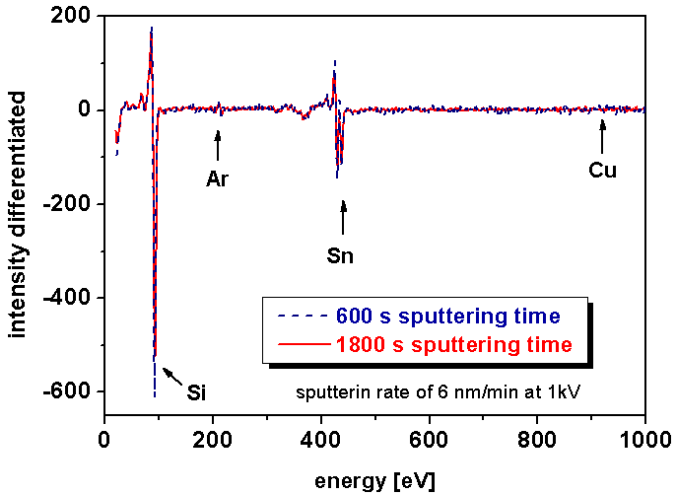

Figure 3.9: Auger electron spectra (differentiated) of the Sn whisker shown in Fig. 3.8 taken from two different sputter depths; ~ 60 nm (i.e. for the first sputtering time of 600 s) and ~ 180

nm (i.e. for a total sputtering time of 1800 s). Prior to analysis the Sn whisker was isolated from the Sn coating and transferred onto a Si substrate (cf. Fig. 3.8). The Auger signals of Si and Ar are due to measurement artefacts (see text).

From the present results it can be concluded that Sn whiskers growing from the Sn layer on top of a Cu substrate are composed of pure Sn, covered with an oxide layer on their surface, and thus do not contain Cu, as previously claimed [52, 53].

3.4. Conclusions

- The growth of the intermetallic compound Cu_6Sn_5 in the Sn layer on top of a Cu substrate (at the Cu/Sn interface, along Sn grain boundaries and in the volume of Sn), at room temperature, leads to compressive stress build-up in the Sn layer, in particular in the depth range where Cu_6Sn_5 forms. A negative stress *gradient* in the direction of increasing layer depth develops, which is a driving force for the transport of Sn atoms to the surface.
- At a certain stage of ageing a stationary state of stress is realized, implying that further stress build-up by continued Cu_6Sn_5 formation is compensated by stress relief. This stress-relief process involves Sn whisker formation on top of the Sn layer, which indeed sets in at the moment that a stationary state of stress is established.
- If, during ageing at room temperature, no intermetallic phase forms at the (Sn) layer / substrate interface, no (compressive) stress component is generated in the Sn layer close to the layer/substrate interface and thus no negative stress gradient occurs. Hence, whisker formation does not take place (as demonstrated in this work by experiments on Sn (layer) / Si (substrate) specimens).
- Long-range (i.e. over distances exceeding by far the in-plane dimension of one Sn island of the order 1 x 1 μm^2) lateral (parallel to the Cu/Sn interface) Sn diffusion is associated with whisker formation.
- The Sn whiskers are composed of *pure* Sn (apart from the presence of a thin naturally occurring surface oxide layer); previous claims of the presence (and role) of Cu in the whiskers are unjustified.

Acknowledgment

The authors would like to thank Dr E. Bischoff (Max Planck Institute for Metals Research) for assistance with the SEM investigations, Dipl.-Ing. B. Siegle and Dr L.P.H. Jeurgens (Max Planck Institute for Metals Research) for performing the AES measurements and Mrs. U. Eigenthaler (Max Planck Institute for Metals Research) for performing the experiments by focused ion beam microscopy.

References

[1] Arnold S. M. (1966). *Plating* **53**, 96.

[2] Directive 2002/95/EC of the European Parliament and of the Council of 27 January 2003 on the restriction of the use of certain hazardous substances in electrical and electronic equipment (2003). *Official Journal of the European Union* **L37**, 19.

[3] Compton K. G., Mendizza A. & Arnold S. M. (1951). *Corrosion* **7**, 327.

[4] Key P. L. (1970). *in Proc. of the 20th Electronic Components Conference*, 155.

[5] Galyon G. T. (2005). *IEEE Trans. Electron. Packag. Manuf.* **28**, 94.

[6] Ellis W. C., Gibbons D. F. & Treuting R. C. (1958). *In Growth and Perfection of Crystals* edited by Doremus, R. H., Roberts, B. W. and Turnbull, D. (Wiley, New York, 1958), pp. 102-120.

[7] Glazunova V. K. & Kudryavtsev N. T. (1963). *Russ. J. Appl. Chem.***36**, 543.

[8] Furuta N. & Hamamura K. (1969). *Jpn. J. Appl. Phys.* **9**, 1404.

[9] Fisher R. M., Darken L. S. & Carroll K. G. (1954). *Acta Metall.* **2**, 368.

[10] Herring C. & Galt J. K. (1952). *Phys. Rev.* **85**, 1060.

[11] LeBret J. B. & Norton M. G. (2003). *J. Mater. Res.* **18**, 585.

[12] Koonce S. E. & Arnold S. M. (1953). *J. Appl. Phys.; Letters to the Editor* **24**, 365.

[13] Eshelby J. D. (1953). *Phys. Rev.* **91**, 755.

[14] Frank F. C. (1953). *Philos. Mag.* **44**, 854.

[15] Hasiguti R. R. (1955). *Acta Metall.* **3**, 200.

[16] Franks J. (1958). *Acta Metall.* **6**, 103.

[17] Lindborg U. (1976). *Acta Metall.* **24**, 181.

[18] Tu K. N. (1994). *Phys. Rev. B* **49**, 2030.

[19] Lee B. Z. & Lee D. N. (1998). *Acta Mater.* **46**, 3701.

[20] Tu K. N., Chen C. & Wu A. T. (2007). *J. Mater. Sci. - Mater. Electron* **18**, 269.

[21] Boettinger W. J., Johnson C. E., Bendersky L. A., Moon K.-W., Williams M. E. & Stafford G. R. (2005). *Acta Mater.* **53**, 5033.

[22] Smetana J. (2007). *IEEE Trans. Electron. Packag. Manuf.* **30**, 11.

[23] Kakeshita T., Shimizu K., Kawanaka R. & Hasegawa T. (1982). *J. Mater. Sci.* **17**, 2560.

[24] Boguslavsky I. & Bush P. (2003). *Proceedings APEX Conference*, pp. S12.

[25] Osenbach J. W. (2009). *J. Appl. Phys.* **106**, 094903.

[26] Hutchinson B., Oliver J., Nylen M. & Hagström J. (2004). *Mater. Sci. Forum* **467-470**, 465.

[27] Buchovecky E. J., Du N. & Bower A. F. (2009). *Appl. Phys. Lett.* **94**, 191904.

[28] Buchovecky E. J., Jadhav N., Bower A. F. & Chason E. (2009). *J. Electron. Mater.* **38**, 2676.

[29] Tu K. N. (1973). *Acta Metall.* **21**, 347.

[30] Dyson B. F., Anthony T. R. & Turnbull D. (1967). *J. Appl. Phys.* **38**, 3408.

[31] Kumar K. S., Reinbold L., Bower A. F. & Chason E. (2008). *J. Mater. Res.* **23**, 2916.

[32] Reinbold L., Jadhav N., Chason E. & Kumar K. S. (2009). *J. Mater. Res.* **24**, 3583.

[33] Chason E., Jadhav N., Chan W. L., Reinbold L. & Kumar K. S. (2008). *Appl. Phys. Lett.* **92**, 171901.

[34] Sobiech M., Welzel U., Schuster R., Mittemeijer E. J., Hügel W., Seekamp A. & Müller V. (2007). *in Proc. of the 57th Electronic Components and Technology Conference in Reno, USA*, 192.

[35] Choi W. J., Lee T. Y., Tu K. N., Tamura N., Celestre S., MacDowell A. A., Bong Y. Y. & Nguyen L. (2003). *Acta Mater.* **51**, 6253.

[36] Sobiech M., Welzel U., Mittemeijer E. J., Hügel W. & Seekamp A. (2008). *Appl. Phys. Lett.* **93**, 011906.

[37] Sobiech M., Wohlschlögel M., Welzel U., Mittemeijer E. J., Hügel W., Seekamp A., Liu W. & Ice G. E. (2009). *Appl. Phys. Lett.* **94**, 221901.

[38] Pinsky D. A. (2008). *Microelectronics Reliability* **48**, 675.

[39] Leoni M., Welzel U. & Scardi P. (2004). *J. Res. Natl. Inst. Stand. Technol.* **109**, 27.

[40] Welzel U., Ligot J., Lamparter P., Vermeulen A. C. & Mittemeijer E. J. (2005). *J. Appl. Crystallogr.* **38**, 1.

[41] Welzel U. & Mittemeijer E. J. (2003). *J. Appl. Phys.* **93**, 9001.

[42] Gale W. F. (2004). *Smithells Metals Reference Book*. London: Butterworths.

[43] Ghosh G. & Asta M. (2005). *J. Mater. Res.* **20**, 3102.

[44] Zhang W., Egli A., Schwager F. & Brown N. (2005). *IEEE Trans. Electron. Packag. Manuf.* **28**, 85.

[45] Woodrow T. A. (2006). *Proccedings of SMTA International Conference in Rosemont, USA*, 1.

[46] Touloukian Y. S., Kirby R. K., Taylor R. K. & Desai P. D. (1975). *Thermal expansion - metallic elements and alloys*. New York: Plenum

[47] Floro J. A., Chason E., Cammarata R. C. & Srolovitz D. J. (2002). *MRS Bull.* **27**, 19.

[48] Tello J. S., Bower A. F., Chason E. & Sheldon B. W. (2007). *Phys. Rev. Lett.* **98**, 216104

[49] Taylor L. (1990). *Metals Handbook, Properties and Selection: Nonferrous Alloys and Special-Purpose Materials*. Metals Park, Ohio American Society for Metals

[50] Arzt E. (1998). *Acta Mater.* **46**, 5611.

[51] Sobiech M., Wohlschlögel M., Welzel U., Mittemeijer E. J., Hügel W., Seekamp A., Garza M., Koyuncu M., Liu W. & Ice G. E. (2009). *Presentation at the 3rd International Symposium on Tin Whiskers in Denmark.*

[52] Kawanaka R., Fujiwara K., Nango S. & Hasegawa T. (1983). *Jpn. J. Appl. Phys.* **22**, 917.

[53] Xu C., Fan C., Vysotskaya A., Abys J., Zhang Y., Hopkins L. & Stevie F. (2001). *Proceedings of the AESF SUR/FIN Conference*.

4. Phase formation at the Sn/Cu interface during room temperature ageing: Microstructural evolution, whiskering and interface thermodynamics

M. Sobiech, C. Krüger, U. Welzel, J. Y. Wang, E. J. Mittemeijer and W. Hügel

Abstract

The room temperature evolution of intermetallic phase formation in the system pure Sn (polycrystalline coating with a thickness of several microns) on pure Cu (polycrystalline bulk substrate) was investigated in detail by means of focused ion beam and transmission electron microscopy and X-ray diffraction. The experimental results were interpreted in terms of interface thermodynamics and interdiffusion kinetics. On this basis spontaneous Sn whiskering on the surface of the Sn coating as a consequence of intermetallic phase (Cu_6Sn_5) formation along Sn grain boundaries intersecting the Sn/Cu interface could be discussed and a treatment to mitigate spontaneous Sn whiskering could be proposed.

4.1. Introduction

Pure Sn and Sn-based alloys deposited on electronic components (e.g. composed of Cu) are frequently employed for soldering and protection. However, since nearly 60 years it is well known that Sn coatings are very prone to the formation of filamentary Sn whiskers [1, 2] which can potentially cause short-circuit failure of the electronic equipment during operation. Hence, the history of Sn whiskers is also a history of enormous financial damage including breakdowns of satellites, computer centers and military and medical devices [2]. Unfortunately, reliable whisker mitigation treatments are still lacking and thus this issue is of, in particular recent, great technological and scientific interest.

Sn whiskers are needle-like single crystals [3] which grow spontaneously on the surface of Sn coated Cu substrates during ageing at room temperature [4-7] through continuous addition of material to their base [8]. Even though the growth mechanism of a Sn whisker [5, 9-18] still remains to be revealed, the "driving force" for Sn whisker growth could be related to the build-up of residual mechanical stresses in the Sn coating [5, 6, 15, 16, 18-24] and thus whisker growth serves as s stress relief mechanism [5, 13, 15-20]. After Sn deposition on a Cu substrate, upon subsequent ageing at room temperature, Cu diffuses rapidly by an interstitial mechanism into the Sn coating [6, 25, 26] and the formation of the intermetallic phase Cu_6Sn_5 takes place on the Sn side of the Sn/Cu interface [5, 6, 19, 20, 27, 28]. Continued growth of Cu_6Sn_5 on the Sn side occurs along the Cu_6Sn_5/Sn interface by a continuous supply of Cu atoms, which takes place via Cu diffusion through Cu_6Sn_5 grain boundaries and interstitially in Sn [27]. Very recently it was shown experimentally that the growth of the intermetallic phase Cu_6Sn_5 along Sn grain boundaries intersecting the Sn/Cu interface induces in-plane residual compressive stresses, in combination with residual stress *gradients* (in out-of-plane [22] and in-plane [23] directions) in the Sn coating, which act as driving forces for the transport of Sn atoms to the whisker nucleation site and thus control whisker growth.

Even though the above described interrelation of intermetallic phase formation and spontaneous Sn whiskering in the system Sn on Cu during ageing at room temperature has been recognized as a crucial parameter controlling whisker growth [5, 6, 20], a rigorous explanation of the observed intermetallic phase formation along

grain boundaries in the Sn coatings, as compared to such phase formation along the Sn/Cu interface (and, possibly, along Cu grain boundaries), lacks. The present work aims to present a coherent understanding of intermetallic phase formation in the system (polycrystalline) Sn on (polycrystalline) Cu during ageing at room temperature by interpreting experimental results in terms of interface thermodynamics and interdiffusion kinetics. As a result a route to avoid whiskering can be proposed.

4.2. Experimental

Polycrystalline Sn thin films with a thickness of about 3 µm (for X-ray diffraction phases analysis (see below) Sn thin films with a thickness of about 1 µm were used, in order to enhance the (relative) contribution to the diffraction pattern of the intermetallic phase growing at the film/substrate interface) were electrodeposited onto pure Cu substrates (commercial leadframe material) using an industrial electrolyte by employing a laboratory electro-deposition setup (for further details see Ref. [21]). Directly after Sn deposition, the surface of the specimens was rinsed with methanol and subsequently the specimens were dried and aged at room temperature conditions (i.e., storage at ~ 25 °C / 25 – 50 % relative humidity). The surfaces of the Sn thin films were regularly checked during the initial ageing stage for the onset of Sn whisker growth using a scanning electron microscope (SEM). The SEM was also used for local chemical analysis by conventional energy dispersive X-ray analysis.

After different ageing times at room temperature the Sn thin films of separate specimens were stripped off selectively using an etching solution of 92 vol.% methanol, 5 vol.% HNO_3 and 3 vol.% HCl [29] in order to investigate the evolution of the growth morphology of the intermetallic phase at the Sn/Cu interface.

X-ray diffraction phase analysis employing the conventional ($\theta/2\theta$) diffraction geometry (with a step size of 0.02° 2θ and a counting time of 1 s per step) was performed using a Bruker TXS D8 Discover (parallel-beam) diffractometer with Cu Kα radiation (emerging from a micro-focus Cu X-ray anode operating at 50 kV / 20 mA) and an energy dispersive detector.

In order to prepare and investigate cross-sections of the Sn layer, the Sn/Cu interface and the Sn whiskers, for different room temperature ageing times, a dual-beam FEI Nova NanoLab 600 apparatus was employed, which allows cutting the specimens with a focused Ga-ion beam (FIB) and imaging subsequently the prepared

cross-section by means of either a focused ion beam or a focused electron beam in scanning mode. The FIB apparatus was also used for preparing thin (~50-60 nm) cross-sectional lamellae suitable for transmission electron microscopy (TEM) analysis. The TEM investigations were conducted employing a Philips CM 200 microscope which was operated at 200 kV.

4.3. Thermodynamic calculations

In the following, thermodynamic expressions for the Gibbs energies of interfaces crucial to this paper are presented in summarized fashion. For a detailed treatment of the concerned interface thermodynamics the reader is referred to the original publications [30, 31].

4.3.1. Gibbs surface energy of a single-component crystalline phase

The Gibbs surface energy of a single-component crystalline phase <*A*>, $G^S_{<A>}$, can be expressed as:

$$G^S_{<A>} = H^S_{<A>} - TS^S_{<A>} \quad (1)$$

where $H^S_{<A>}$ is the surface enthalpy, T is the temperature, and $S^S_{<A>}$ is the surface entropy. The Gibbs surface energy per mole of surface atoms (e.g. $G^S_{<A>}$ in J/mol) is connected to the surface energy per unit area (e.g. $\gamma^S_{<A>}$ in J/m^2) by the contact surface area $O_{<A>}$ per mole surface atoms according to [32]:

$$\gamma^S_{<A>} = \frac{G^S_{<A>}}{O_{<A>}} \quad (2)$$

with $O_{<A>} = f^{vapour}_{<A>} C V^{2/3}_{<A>}$

where $f^{vapour}_{<A>} (= 0.35)$ is a geometrical factor, $C = 5.42 N^{1/3}_{\mathrm{Av}} = 4.5\times10^8$ mol$^{1/3}$ (with N_{Av} as Avogadro`s number) is a constant and $V_{<A>}$ is the molar volume.

4.3.2. Gibbs surface energy of a binary crystalline phase

The Gibbs surface energy of a binary crystalline phase <*AB*> (in this work being either a crystalline solid solution or a crystalline (intermetallic) compounds with

an ordered structure), $G^{S}_{<AB>}$, can be obtained by considering the energy increase upon fracturing and thus creating a new surface [30]:

$$G^{S}_{<AB>} = c_{<A>} G^{S}_{<A>} + c_{<B>} G^{S}_{<B>} - f^{vapour}_{<i>} \Delta H_{<AB>} \quad (3)$$

where $c_{<i>}$ is the atomic fraction of the component *i* in <*AB*>, $f^{vapour}_{<i>} = f^{vapour}_{<A>} = f^{vapour}_{<B>} = 0.35$, and $\Delta H_{<AB>}$ is the enthalpy of formation of the binary crystalline phase. In the case of a crystalline solid solution the phenomenon of surface segregation (leading to deviation of the surface composition from the bulk composition) has to be taken into account upon calculation of $G^{S}_{<AB>}$, as described in Ref. [30].

The surface energy of a binary crystalline phase <*AB*> can be calculated from

$$\gamma^{S}_{<AB>} = \frac{G^{S}_{<AB>}}{f^{vapour}_{<i>} C V^{2/3}_{<AB>}} \quad (4)$$

with $V_{<AB>}$ as the molar volume of the binary crystalline phase <*AB*>.

4.3.3. Gibbs energy of the interface between two single-component crystalline phases

The Gibbs energy of the interface between two single-component crystalline phases <*A*> and <*B*>, $G^{I}_{<A>/<B>}$, comprises the contributions of the elastic (misfit) energy and the chemical interaction:

$$G^{I}_{<A>/<B>} = G^{I,elastic}_{<A>/<B>} + G^{I,chemical}_{<A>/<B>} \quad (5)$$

(i) The Gibbs interfacial elastic energy $G^{I,elastic}_{<A>/<B>}$ can be related to the energy of a high-angle grain boundary in pure metals, which is about a third of the averaged Gibbs surface energies for both metals, as shown by empirical estimations [33]:

$$G^{I,elastic}_{<A>/<B>} = \frac{1}{3}\left(\frac{G^{S}_{<A>} + G^{S}_{<B>}}{2}\right) \quad (6)$$

As a particular case, the energy of a high-angle grain boundary in <*A*>, *i.e.* an <*A*>/<*A*> interface, $G^{GB}_{<A>}$, is assessed by [34]:

$$G^{GB}_{<A>} = G^{I}_{<A>/<A>} = \frac{1}{3} G^{S}_{<A>} \quad (7)$$

(ii) The Gibbs interfacial chemical energy $G^{I,chemical}_{<A>/<B>}$ can be described by means of the corresponding enthalpy and entropy terms:

$$G^{I,chemical}_{<A>/<B>} = H^{I,chemical}_{<A>/<B>} - TS^{I,chemical}_{<A>/<B>} \quad (8)$$

which can be rewritten as follows:

$$G^{I,chemical}_{<A>/<B>} = \frac{f^{vapour}_{<i>}(\Delta\overline{H}^{0}_{<A> \text{ in } <B>} + \Delta\overline{H}^{0}_{<B> \text{ in } <A>})}{2} - T * f^{vacuum}_{<i>} 3R \ln \frac{\prod_i \theta_i^{0.5}}{\sum_i 0.5\theta_i + \Delta\theta_{\text{interface}}} \quad (9)$$

with $f^{vapour}_{<i>} = f^{vapour}_{<A>} = f^{vapour}_{<B>} = 0.35$, $\Delta\overline{H}^{0}_{<A> \text{ in } <B>}$ and $\Delta\overline{H}^{0}_{<B> \text{ in } <A>}$ as partial enthalpies of dissolution of A (B) atoms in <*B*> (<*A*>) at infinite dilution (the values of $\Delta\overline{H}^{0}_{<A> \text{ in } <B>}$ and $\Delta\overline{H}^{0}_{<B> \text{ in } <A>}$ can be obtained experimentally, e.g. see Ref. [35], or from the thermodynamic models used for the calculation of a binary A-B phase diagram, see section 4.3.5), *R* is the gas constant, θ_i is the Debye temperature of phase <*i*> and $\Delta\theta_{\text{interface}} = 34.1\times10^{-3}(-\frac{\Delta H_{<AB>}}{R})$; see also Ref. [36]).

Finally, the grain boundary energy of a single-component crystalline phase <*A*>, $\gamma^{GB}_{<A>}$, and the interface energy between two single-component crystalline phases <*A*> and <*B*>, $\gamma^{I}_{<A>/<B>}$, can be calculated as follows:

$$\gamma^{GB}_{<A>} = \frac{1}{3}\gamma^{S}_{<A>} \quad (10)$$

$$\gamma^{I}_{<A>/<B>} = \frac{G^{I}_{<A>/<B>}}{f^{vapour}_{<i>} C\, \overline{V}^{2/3}_{<A>-<B>}} \quad (11)$$

with $\overline{V}_{<A>-<B>}$ as the average molar volume of the <*A*> and <*B*> phases.

4.3.4. Gibbs energy of the interface between a single-component crystalline phase and a binary crystalline phase

The Gibbs energy of the interface between a single-component crystalline phase <*A*> and a binary crystalline phase <*AB*> (in this work being either a crystalline solid solution or a crystalline (intermetallic) compound), $G^{I}_{<A>/<AB>}$, comprises the contributions of the elastic (misfit) energy and the chemical interaction, analogous to the Gibbs energy of the interface between two single-component crystalline phases $G^{I}_{<A>/<B>}$ (cf. Eq. 5):

$$G^{I}_{<A>/<AB>} = G^{I,elastic}_{<A>/<AB>} + G^{I,chemical}_{<A>/<AB>} \quad (12)$$

Accordingly, both terms can be expressed as:

$$G^{I,elastic}_{<A>/<AB>} = \frac{1}{3}\left(\frac{G^{S}_{<A>} + G^{S}_{<AB>}}{2}\right) \tag{13}$$

$$G^{I,chemical}_{<A>/<AB>} = H^{I,chemical}_{<A>/<AB>} - TS^{I,chemical}_{<A>/<AB>} \tag{14}$$

Further it follows for the chemical contribution:

$$G^{I,chemical}_{<A>/<AB>} = f^{vapour}_{<i>}\Delta\overline{H}^{0}_{<A> \text{ in } <AB>} - T * f^{vacuum}_{<i>}\Delta\overline{S}^{0}_{<A> \text{ in } <AB>} \tag{15}$$

with $f^{vapour}_{<i>} = f^{vapour}_{<A>} = f^{vapour}_{<B>} = 0.35$, $\Delta\overline{H}^{0}_{<A> \text{ in } <AB>}$ as the partial enthalpy of dissolution of A atoms in <*AB*> at finite dilution (at $c_{<B>} = c^{S}_{<B>}$) and $\Delta\overline{S}^{0}_{<A> \text{ in } <AB>}$ as the partial entropy of mixing (at $c_{<B>} = c^{S}_{<B>}$) (in the case of solid solutions the possible occurrence of surface segregation has to be taken into account, cf. section 4.3.2). Note that extra energy terms have to be incorporated if <*A*> and <*AB*> exhibit not the same crystal structure, in order to ensure the same reference state for all phases.

Finally, the energy of the interface between <*A*> and <*AB* > phases can be calculated from

$$\gamma^{I}_{<A>/<AB>} = \frac{G^{I}_{<A>/<AB>}}{f^{vapour}_{<i>} C\ \overline{V}^{2/3}_{<A>-<AB>}} \tag{16}$$

where $\overline{V}_{<A>-<AB>}$ stands for the average molar volume of the <*A*> and <*AB*> phases.

4.3.5. Thermodynamic data

According to the binary Sn-Cu "bulk" phase diagram (see for example Ref. [37]) and within the temperature range of interest, i.e. from 0 to 200 °C, *(i)* two intermetallic phases (η'-Cu_6Sn_5 and ε-Cu_3Sn) are stable and *(ii)* the solubility of Cu in Sn, and that of Sn in Cu, can be neglected. In the calculations the formation of crystalline solid solutions (with compositions of "Cu_6Sn_5" and "Cu_3Sn"), competing with the formation of the intermetallic compounds (η'-Cu_6Sn_5 and ε-Cu_3Sn), was also considered (for the solid solutions the possible occurrence of surface segregation was taken into account in the calculation of the surface/interface energies, cf. sections 4.3.2 and 4.3.4).

The thermodynamic parameters required for calculation of (interface) energy values according to the expressions presented in sections 4.3.1 – 4.3.4 were obtained from both experimental data (see Table 4.1) and from theoretical calculation (see

Table 4.2) by employing the quantitative thermodynamic models presented for the system Sn-Cu [38].

The Gibbs energies of formation of the intermetallic compounds Cu_6Sn_5 (η') and Cu_3Sn (ε) are expressed as:

$$\Delta G_{<Cu_6Sn_5>} = -7747.65 - 0.371T \text{ [J/mol]} \quad (17)$$

$$\Delta G_{<Cu_3Sn>} = -11318.4 + 3.1T \text{ [J/mol]} \quad (18)$$

with T in K.

The Gibbs energy of formation of a Cu-Sn solid solution phase with a face-centered cubic (fcc) structure is given as:

$$G_{<CuSn-sol>} = c_{Cu}G^0_{Cu} + c_{Sn}G^0_{Sn} + RT(c_{Cu}\ln c_{Cu} + c_{Sn}\ln c_{Sn}) + G^{ex}_{<CuSn-sol>} \text{ [J/mol]} \quad (19)$$

with the excess molar Gibbs energy, $G^{ex}_{<CuSn-sol>}$, given by

$$G^{ex}_{<CuSn-sol>} = c_{Cu}c_{Sn}[-33842.061 + 33.557T + (-1900 - 23.3425T)(c_{Cu} - c_{Sn}) - 1.0237T(c_{Cu} - c_{Sn})^2] \text{ [J/mol]} \quad (20)$$

with T in K.

In order to account for the body-centered tetragonal (bct) structure of Sn the Gibbs energy difference pertaining to the bct-fcc transformation can be accommodated using [39]:

$$\Delta G_{Sn(bct)\rightarrow Sn(fcc)} = \Delta G_{Sn(bct)} - \Delta G_{Sn(fcc)} = 4150 - 5.2T \text{ [J/mol]} \quad (21)$$

with T in K.

Table 4.1: Experimental data for some thermodynamic parameters for relevant phases in the system Sn-Cu taken from [40-42]. V = molar volume, C_{Cu} = atomic fraction of Cu, θ = Debye temperature and γ^s = surface energy.

	<Cu>	<Sn>	<Cu_6Sn_5-sol>	<Cu_3Sn-sol>	<Cu_6Sn_5>	<Cu_3Sn>
V_i (10^{-6} m^3/mol)	7.10 [40]	16.29 [40]	11.28 [40]	9.39 [40]	10.73 [40]	6.82 [40]
C_{Cu} (at.%)	100	0	0.545	0.750	0.545	0.750
θ_i (K)	343 [41]	200 [41]				
$\gamma^s_{<i>}$ (J/m^2)	$2.07-0.37\times10^{-3}T$ [42]	$0.88-1.92\times10^{-4}T$ [42]				

Table 4.2: Theoretical data for thermodynamic parameters for the relevant phases in the system Sn-Cu [38]. Note that the partial enthalpies and entropies of mixing of Cu and Sn in both considered solid solutions (Cu_6Sn_5-Sol and Cu_3Sn-Sol) hold for T=298 K.

$\Delta\bar{H}^0_{<Sn>in<Cu>}$	$\Delta\bar{H}^0_{<Cu>in<Sn>}$	$\Delta H_{<Sn(bct)>\rightarrow<Sn(fcc)>}$	$\Delta S_{<Sn(bct)>\rightarrow<Sn(fcc)>}$
-35742 J mol^{-1}	-27792 J mol^{-1}	4150 J mol^{-1}	5.2 J mol^{-1} K^{-1}
$\Delta H_{<Cu6Sn5>}$	$\Delta S_{<Cu6Sn5>}$	$\Delta H_{<Cu3Sn>}$	$\Delta S_{<Cu3Sn>}$
-7748 J mol^{-1}	0.37 J mol^{-1} K^{-1}	-11318 J mol^{-1}	-3.1 J mol^{-1} K^{-1}
$\Delta H_{<Cu6Sn5-Sol>}$	$\Delta S_{<Cu6Sn5-Sol>}$	$\Delta H_{<Cu3Sn-Sol>}$	$\Delta S_{<Cu3Sn-Sol>}$
-6546 J mol^{-1}	0.29 J mol^{-1} K^{-1}	-5486 J mol^{-1}	1.92 J mol^{-1} K^{-1}
$\Delta\bar{H}^0_{<Sn>in<Cu6Sn5>}$ $\Delta\bar{H}^0_{<Cu>in<Cu6Sn5>}$	$\Delta\bar{S}^0_{<Sn>in<Cu6Sn5>}$ $\Delta\bar{S}^0_{<Cu>in<Cu6Sn5>}$	$\Delta\bar{H}^0_{<Sn>in<Cu3Sn>}$ $\Delta\bar{H}^0_{<Cu>in<Cu3Sn>}$	$\Delta\bar{S}^0_{<Sn>in<Cu3Sn>}$ $\Delta\bar{S}^0_{<Cu>in<Cu3Sn>}$
≈ -7748 J mol^{-1}	≈ 0.37 J mol^{-1} K^{-1}	≈ -11318 J mol^{-1}	≈ -3.1 J mol^{-1} K^{-1}
$\Delta\bar{H}^{0;\ at\ 298K}_{<Sn>in<Cu6Sn5-Sol>}$	$\Delta\bar{S}^{0;\ at\ 298K}_{<Sn>in<Cu6Sn5-Sol>}$	$\Delta\bar{H}^{0;\ at\ 298K}_{<Sn>in<Cu3Sn-Sol>}$	$\Delta\bar{S}^{0;\ at\ 298K}_{<Sn>in<Cu3Sn-Sol>}$
3234 J mol^{-1}	3.9 J mol^{-1} K^{-1}	-1615 J mol^{-1}	-2.47 J mol^{-1} K^{-1}
$\Delta\bar{H}^{0;\ at\ 298K}_{<Cu>in<Cu6Sn5-Sol>}$	$\Delta\bar{S}^{0;\ at\ 298K}_{<Cu>in<Cu6Sn5-Sol>}$	$\Delta\bar{H}^{0;\ at\ 298K}_{<Cu>in<Cu3Sn-Sol>}$	$\Delta\bar{S}^{0;\ at\ 298K}_{<Cu>in<Cu3Sn-Sol>}$
-24129 J mol^{-1}	-15.5 J mol^{-1} K^{-1}	-13485 J mol^{-1}	-0.41 J mol^{-1} K^{-1}

4.3.6. Critical thickness for phase formation

For the system (polycrystalline) Sn layer on (polycrystalline) Cu substrate three potential sites for the formation of Cu_6Sn_5 and Cu_3Sn (both as intermetallic compound and as solid solution) were considered in the present study, as shown schematically in Fig. 4.1: **(a)** at a Cu grain boundary *<Cu>/<Cu>*, **(b)** at a Sn grain boundary *<Sn>/<Sn>* and **(c)** at the interface between Sn and Cu *<Cu>/<Sn>*. At each of these sites the formation of a new phase is associated with replacement of an interface (grain boundary) with two new interfaces, which can be accompanied with a decrease or an increase of total interfacial energy. If the total interface energy increases due to such phase formation (i.e. 2 x $\gamma_{<new\ interface>}$ - $\gamma_{<old\ interface>}$ > 0; this inequality holds for the cases considered here, see Fig. 4.7), a critical thickness h^{crit} (i.e. a critical width for the

"slabs" shown in Fig. 4.1) can be calculated which indicates the minimal thickness of the product phase <*CuSn-P*> needed to compensate the increase of total interface energy by the (bulk) energy released by <*CuSn-P*> formation. Beyond this critical thickness h^{crit}, <*CuSn-P*> formation is energetically favored. Thus, a comparison of the critical thickness values calculated for different <*CuSn-P*> phases forming at a specific site allows determination of the phase which thermodynamically will preferably form at this site.

Note that the equations given for h^{crit} in Fig. 4.1 imply that the Gibbs energy of formation for <*CuSn-P*> should be expressed as energies per unit volume, whereas the equations and data given in sections 4.3.1 – 4.3.5 refer to energies per mole; the molar volumes for the corresponding conversion have been given in Table 4.1.

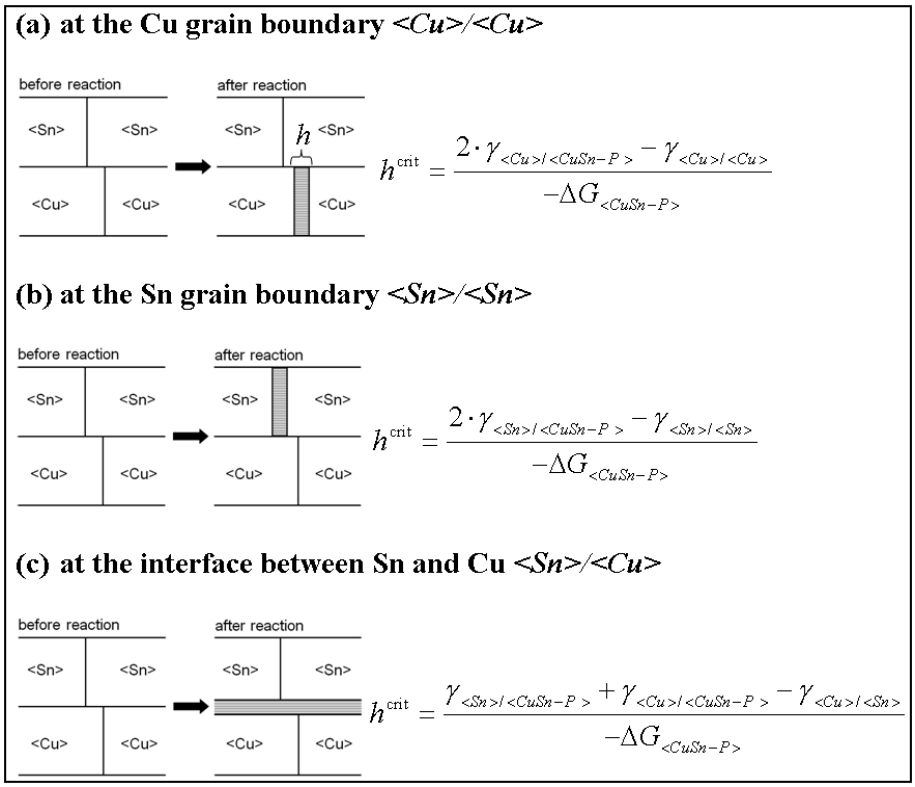

Figure 4.1: Different possible sites for CuSn-phase (<*CuSn-P*>; i.e. Cu_6Sn_5 and Cu_3Sn, as solid solution and as compound phase) formation in the system (polycrystalline) Sn on (polycrystalline) Cu; **(a)** at the Cu grain boundary <Cu>/<Cu>; **(b)** at the Sn grain boundary <Sn>/<Sn> and **(c)** at the interface between Sn and Cu <Cu>/<Sn>. The corresponding equations for the calculation of the critical thicknesses h^{crit}, beyond which the CuSn-phase considered is stable, have been plotted on the right-hand-side. Note that $\Delta G_{<CuSn-P>}$ in these equations should be expressed as energy per unit volume (see text).

4.4. Results and discussion

4.4.1. Microstructural investigation of Sn/Cu specimens

The microstructural evolution of polycrystalline Sn thin films ({321}-fiber texture, layer thickness of about 3 µm and in-plane grain sizes of 2-5 µm) with a columnar grain morphology electrodeposited on polycrystalline Cu substrates (see for further details Ref. [21]) was investigated in detail during ageing at room temperature (i.e. ~ 25°C) by employing FIB-based microscopy♣ (see Figs. 4.2-4.4). Additionally, detailed TEM analyses of the microstructure at and around a whisker nucleation site (see Fig. 4.5) and X-ray diffraction phase analyses (see Fig. 4.6) were conducted. Here, the focal point of interest was on the formation and growth of intermetallic phases during room temperature ageing.

♣ FIB machining of Sn on Cu systems induces artefacts in the Sn microstructure. During high-energetic Ga^+ ion beam cutting through the Sn on Cu system (e.g. in order to prepare cross-sections of the bilayer system), Cu atoms are removed from the substrate due to sputtering. Once the ion beam is switched off, Cu atoms from the gas phase react with the freshly prepared Sn surface, preferentially along Sn grain boundaries (as energetically preferred nucleation sites; see results of thermodynamic calculations performed in the present work and presented in section 4.4.4), and thus form Sn-Cu intermetallics [43]. Therefore cross-sectional FIB micrographs of Sn layers on Cu exhibit typically bright Sn grain boundaries (due to significant formation Sn-Cu intermetallics with a "line-like" morphology) as well as bright spots on the Sn grains due to the presence of fine Sn-Cu intermetallics, which had not formed under (undisturbed) ageing conditions. This could be shown unequivocally by preparing FIB cuts which did not extend to the Cu substrate, i.e. in such a case the Sn grain boundaries in the exposed section of the Sn layer were completely free of any Sn-Cu intermetallics.

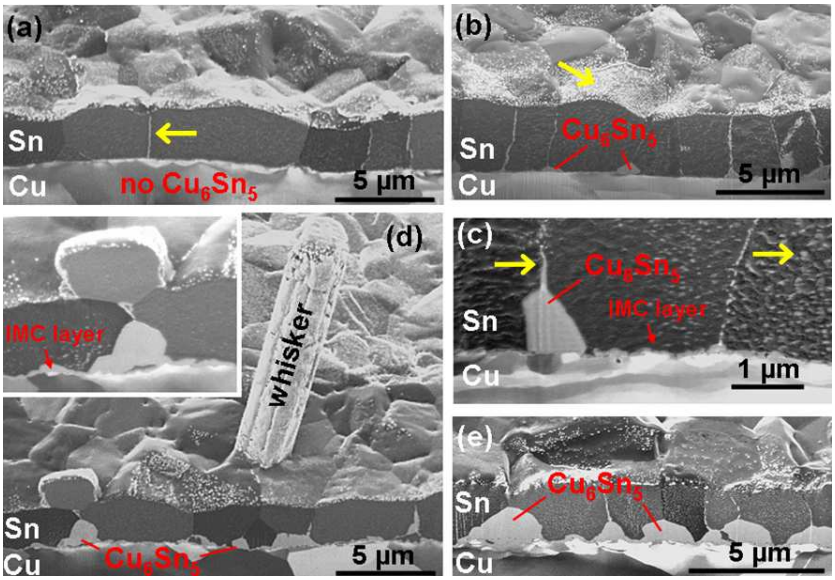

Figure 4.2: FIB cross-sectional micrographs of Sn/Cu specimens taken after different ageing times at room temperature: **(a)** Fresh (i.e. ~ 1 hour after Sn deposition); **(b)** ~ 5 days; **(c)** ~ 10 days; **(d)** ~ 30 days; **(e)** ~ 300 days. The intermetallic compound; Cu_6Sn_5 (IMC), formed during room temperature ageing, has been indicated in the figure. The bright phase decorating the Sn grain boundaries as well as the Sn surface (see arrows) represents IMC formed as artefact due to FIB-cutting (see footnote in section 4.4.1).

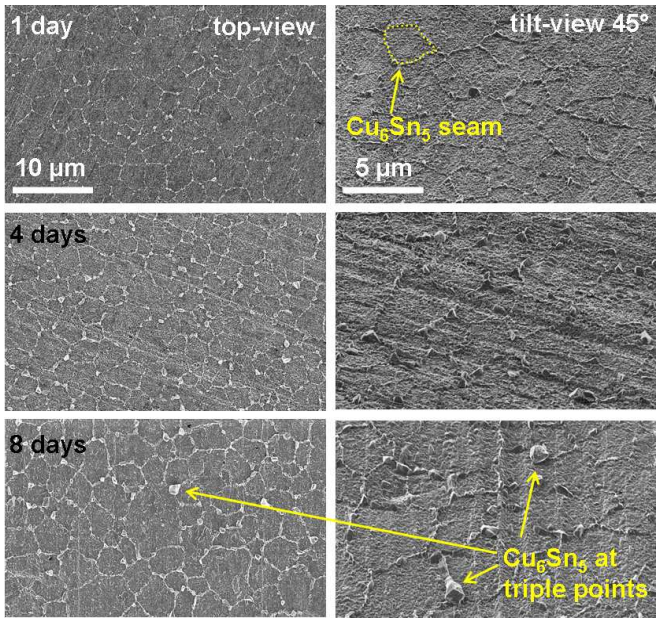

Figure 4.3: FIB micrographs taken after different ageing times at room temperature (in top- and tilt-view) from specimens where the Sn layer was stripped off selectively (cf. section 4.2). Thus the growth behavior of Cu_6Sn_5 at the Sn/Cu interface can be revealed: Cu_6Sn_5 forms preferentially along Sn grain boundaries, most pronouncedly at Sn grain boundary/interface triple junctions.

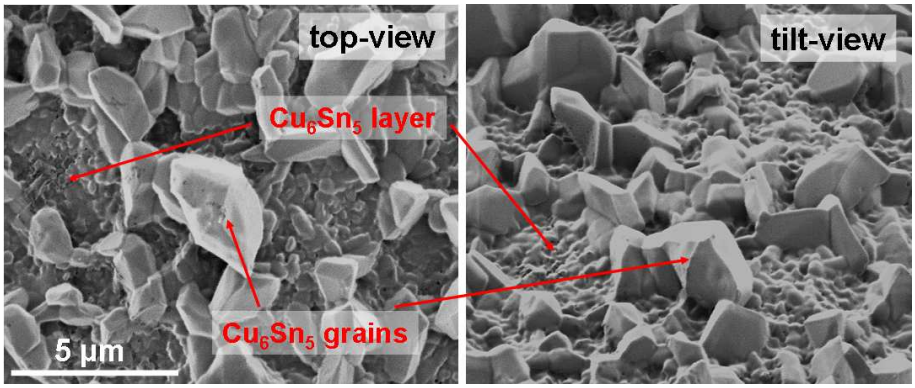

Figure 4.4: FIB micrographs (top- and tilt-view) taken from a specimen where the Sn coating was stripped off selectively after about 300 days of room temperature ageing (cf. section 4.2), showing the morphology of Cu_6Sn_5 formed at the Sn/Cu interface.

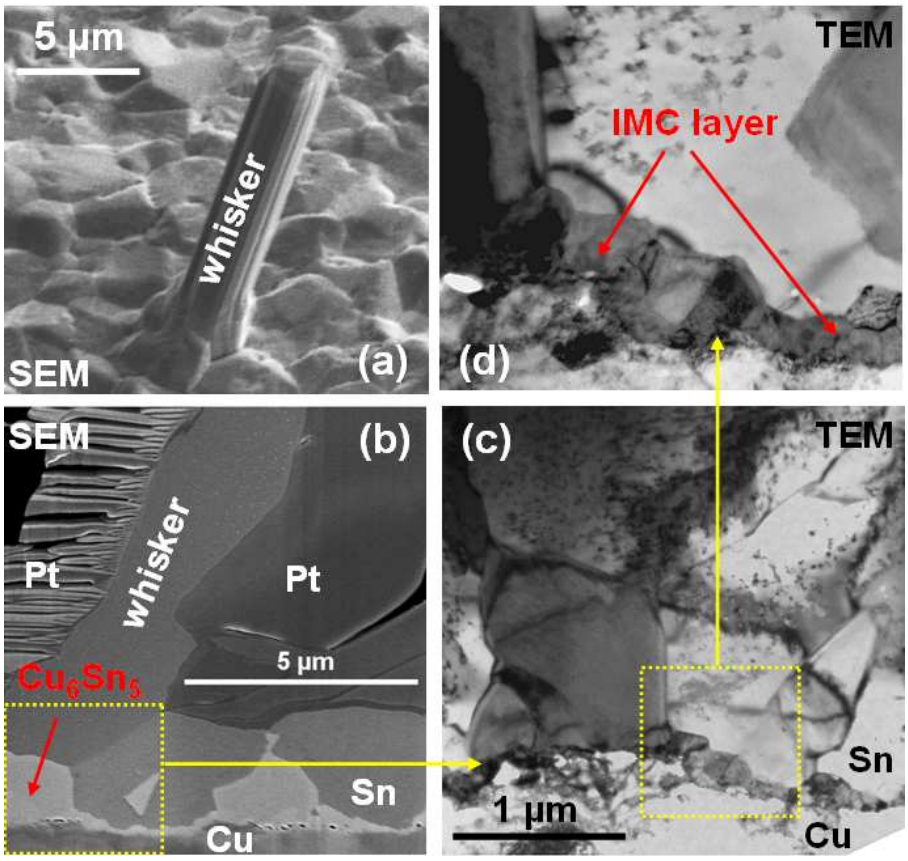

Figure 4.5: Side-view and cross-sectional micrographs of a Sn whisker of a Sn/Cu specimen taken after an ageing time of several weeks at room temperature. **(a)** SEM side-view. **(b)** SEM cross-sectional micrograph of the FIB-prepared lamella used for TEM analysis. The Pt-layer was deposited prior to FIB-milling in order to protect the specimen surface. **(c)** Bright field cross-sectional TEM micrograph taken from the region marked in yellow in Fig. 4.5b). **(d)** Bright field cross-sectional TEM micrograph, enhanced magnification of the region marked in yellow in Fig. 4.5c.

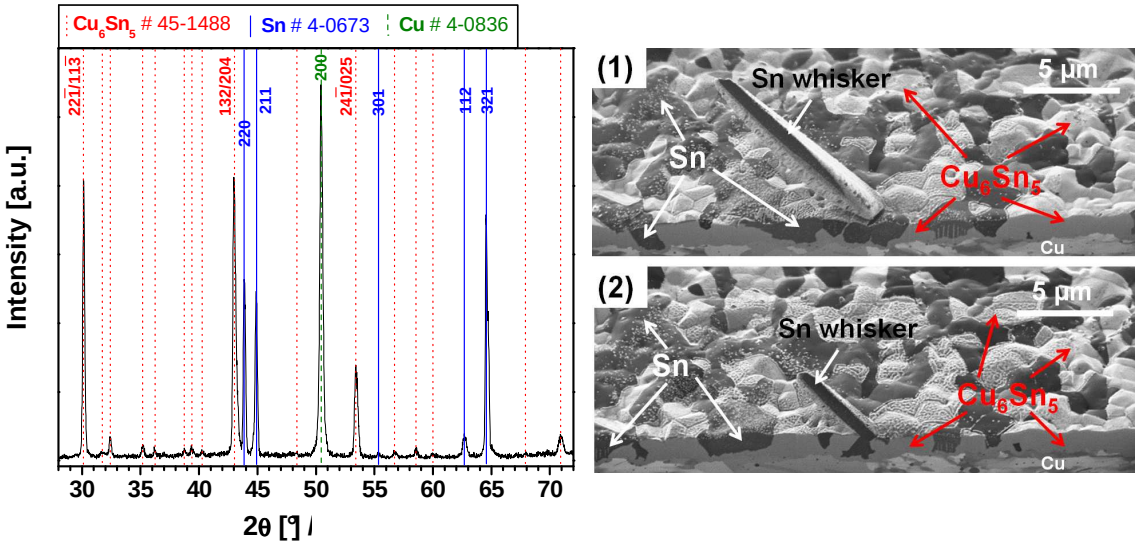

Figure 4.6: left: X-ray diffraction pattern (Cu Kα radiation) of a Sn thin film (thickness of about 1 µm) electrodeposited on Cu, recorded after an ageing time at room temperature of about 2 years. Apart from diffraction lines belonging to Sn and Cu, the presence of diffraction lines of *only* Cu_6Sn_5 is detectable (the three most intensive reflections of Cu_6Sn_5 have been indexed in the figure). The PDF-files employed for phase analysis have been indicated on top of the figure. right: FIB-cross sectional micrographs, taken shortly after diffraction analysis, through the Sn thin film aged for about 2 years: Cu_6Sn_5 had penetrated through the whole Sn layer of thickness of about 1 µm (see isolated remnants of Sn).

The experimental findings lead to the following picture of the microstructural development during room temperature ageing:

(1) Directly after Sn deposition, i.e. after an ageing time of roughly 1 hour, no significant intermetallic phase formation has taken place (see Fig. 4.2a). It was reported on the basis of atomic force [28] and transmission electron microscopy [20] analyses, that already 1 hour ageing after Sn deposition suffices to generate very fine-grained intermetallic particles at the Sn/Cu interface. At this ageing time, i.e. before the onset of significant intermetallic phase growth, the Sn/Cu specimen is still free of hillocks and whiskers.

(2) Upon continued ageing at room temperature, a significant amount of the intermetallic phase Cu_6Sn_5 (see Fig. 4.6; also verified by energy dispersive X-ray analyses (data not shown)) forms on the Sn side of the Sn/Cu interface, which phase extends *only* into the Sn (i.e. no intermetallic phase formation occurred on the Cu side). These findings, which agree with the results reported in Ref. [20], were

confirmed by time-resolved focused ion beam and X-ray diffraction phase analyses performed in this work for ageing periods up to two years (see Fig. 4.6)[≈].

(3) Initially, Cu_6Sn_5 formation occurs predominantly at the intersections of the Sn grain boundaries with the Sn/Cu interface (see Figs. 4.2 and 4.3). Upon continued ageing Cu_6Sn_5 growth proceeds significantly into the Sn coating along the Sn grain boundaries accompanied by lateral (i.e. in directions parallel to the Sn/Cu interface) growth (see Figs. 4.2-4.4). Pronounced Cu_6Sn_5 growth takes place particularly at triple junctions of Sn grain boundaries (see Fig. 4.3). As evident from the bright-field TEM micrograph shown in Fig. 4.5c, Cu_6Sn_5 forming along Sn grain boundaries grows as a single crystal (see also the idiomorphic surface morphology of Cu_6Sn_5 in tilt-view, Fig. 4.4).

The Sn-layer penetrating growth morphology of Cu_6Sn_5 is responsible for the development of residual compressive stress parallel to the Sn/Cu interface, in the Sn coating [21], and roughly four days after Sn deposition (for the investigated Sn/Cu specimens) whisker formation on the surface of the Sn coating occurs.

(4) Upon prolonged ageing at room temperature, Cu_6Sn_5 formation commenced also on the Sn side of the Sn/Cu interface, i.e. on the faces of the Sn grains adjacent to the Sn/Cu interface (see Fig. 4.2c), but with an extent (i.e. penetration of the Sn grains) much less than for the Cu_6Sn_5 formation along the Sn grain boundaries, as described above. This Cu_6Sn_5 layer is composed of fine-grained, rather columnar Cu_6Sn_5 grains (see Figs. 4.4 and 4.5d).

(5) The location of a whisker root at the surface of the Sn layer always coincided with particularly pronounced Cu_6Sn_5 formation at the Sn/Cu interface at the same lateral positions (see Figs. 4.2d and 4.5b).

(6) Apart from the formation of Cu_6Sn_5 in the Sn layer and the growth of Sn whiskers out of the Sn layer, the Sn microstructure remained unchanged during ageing.

4.4.2. Interface thermodynamic calculations for the system Sn on Cu

By employing the treatment for interface thermodynamics described in sections 4.3.1 – 4.3.5, the interface energies of all relevant material combinations (i.e. *<Cu>/<Cu>*, *<Sn>/<Sn>*, *<Sn>/<Cu>*, *<Cu>/<CuSn-P>* and *<Sn>/<CuSn-P>*)

[≈] For this purpose specimens with a Sn layer thickness of only about 1 µm were employed in order to obtained pronounced diffraction information of the growing intermetallic phase.

were calculated for the temperature range 0 – 200 °C (see Fig. 4.7). It follows that CuSn-phase formation at the interfaces is counteracted by the associated formation of new interfaces (i.e. $2 \cdot \gamma_{<Me>/<CuSn-P>} - \gamma_{<Me>/<Me>} > 0$) and as a consequence a critical thickness for CuSn-phase formation can be calculated (see section 4.3.6). The corresponding results will be discussed next.

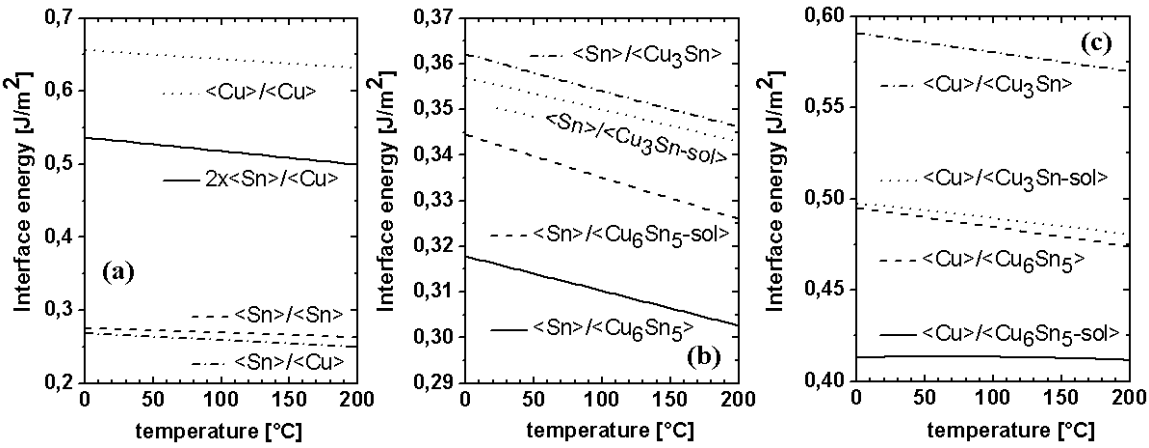

Figure 4.7: Interface energies for all relevant material combinations as function of temperature: **a)** interfaces between the pure metals <*Sn*> and <*Cu*>; **b)** interfaces between <*Sn*> and the CuSn phases Cu_3Sn and Cu_6Sn_5 (as solid solution and as compound) and **c)** interfaces between <*Cu*> and the CuSn phases Cu_3Sn and Cu_6Sn_5 (as solid solution and as compound).

4.4.3. Kinetic constraints for the formation of Cu_3Sn vs. Cu_6Sn_5

The calculated critical thicknesses h^{crit} for the formation of Cu_6Sn_5 and Cu_3Sn (either as solid solution or as compound) at a <*Cu*> grain boundary, a <*Sn*> grain boundary, and the <*Sn*>/<*Cu*> interface are shown as function of temperature in Figs. 4.8a-c).

As a general, first, result it follows that from a thermodynamic point of view formation of Cu_3Sn is favored over formation of Cu_6Sn_5, no matter which site (grain boundary or interface) for phase formation is considered. However, the experimental results (see section 4.4.1) indicate that during ageing at room temperature *only* Cu_6Sn_5 formation is observed. This discrepancy has a simple kinetic background: *(i)* at each position at the <*Sn*> side, upon inward diffusion of Cu, the stoichiometric composition needed for Cu_6Sn_5 formation will always be reached prior to the stoichiometric

composition compatible with the formation of Cu_3Sn, and *(ii)* formation of Cu_3Sn at the <*Cu*> side is impossible at room temperature because diffusion of Sn in Cu at room temperature is negligible [6, 25, 27]. Therefore, in the following discussion, only the critical thicknesses for the formation of Cu_6Sn_5 at different sites in the microstructure at the <*Sn*> side will be considered.

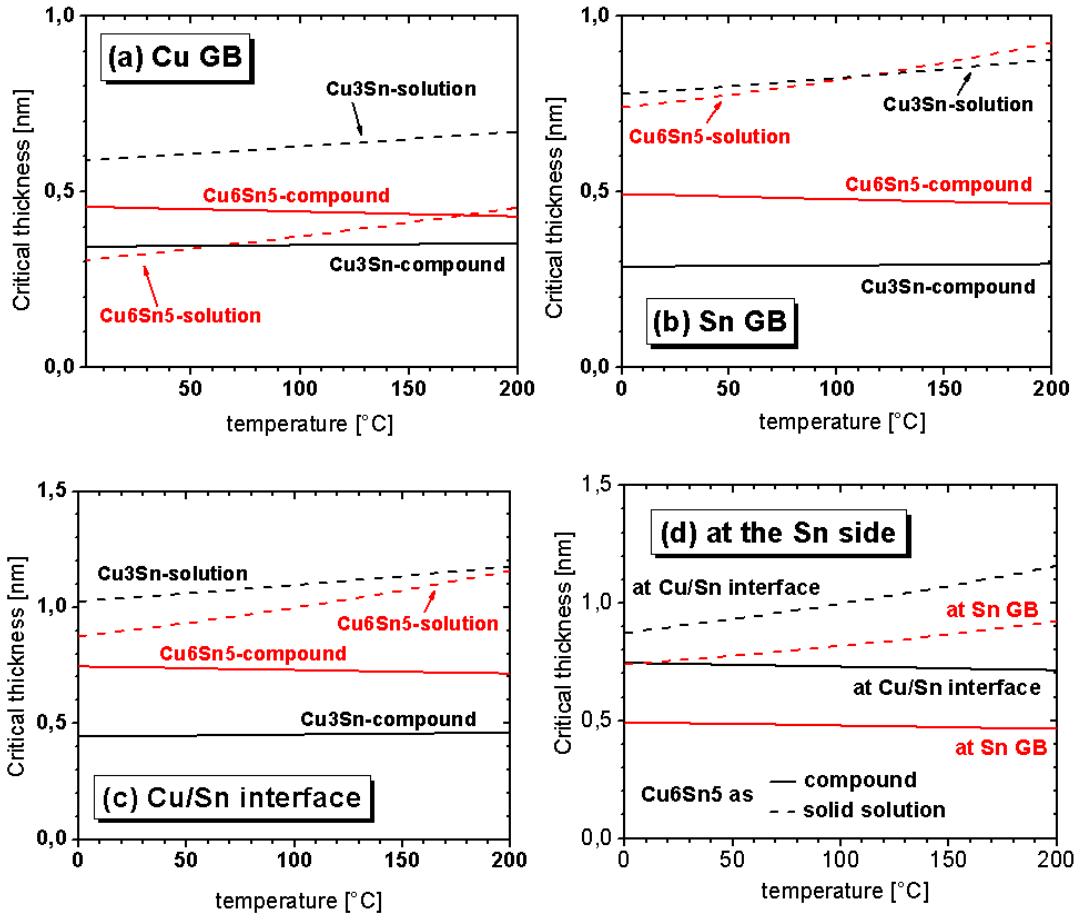

Figure 4.8: Critical thicknesses for CuSn-phase (i.e. Cu_6Sn_5 and Cu_3Sn, either as solid solution or as compound) formation at **(a)** a <*Cu*> grain boundary; **(b)** a <*Sn*> grain boundary and **(c)** the interface between <*Sn*> and <*Cu*>. In **(d)** the critical thicknesses for formation of Cu_6Sn_5 at the <*Sn*> side of the <*Sn*>/<*Cu*> interface are shown; this figure is a summary of the results shown in (b) and (c).

4.4.4 Critical thicknesses for formation of Cu_6Sn_5 at the Sn side of the Sn/Cu interface

The comparison of the critical thicknesses for nucleation of Cu_6Sn_5 at each possible nucleation site at the <*Sn*> side (see Fig. 4.8d) reveals that Cu_6Sn_5 formation as (ordered) compound is energetically preferred compared to its (disordered) solid solution state, i.e. Cu_6Sn_5 intermetallic compound formation will occur directly without passing a (metastable) solid solution state.

The critical thickness for formation of Cu_6Sn_5 as intermetallic compound at room temperature is lowest at <*Sn*> grain boundaries (~ 0.5 nm), followed by the <*Sn*>/<*Cu*> interface (~ 0.75 nm). Hence, Cu_6Sn_5 intermetallic compound formation along <*Sn*> grain boundaries is thermodynamically most preferred. This prediction is in very good agreement with the experimental observations (see section 4.4.1), which showed that Cu_6Sn_5 compound formation indeed occurs initially along <*Sn*> grain boundaries intersecting the <*Sn*>/<*Cu*> interface.

Upon continued ageing at room temperature, IMC formation does *not* proceed only along <*Sn*> grain boundaries until reaching the <*Sn*> layer surface. Diffusion of Cu in <*Sn*> grain boundaries is much faster that volume, bulk diffusion of Cu in Sn. This, together with the relatively low value for the critical thickness at this location, causes Cu_6Sn_5 to form first at <*Sn*> grain boundaries.[#] Formation of Cu_6Sn_5 at the <*Sn*>/<*Cu*> interface requires the transport of Cu by volume diffusion. This, together with the relatively large value for the critical thickness at this (thus less preferred) location, causes Cu_6Sn_5 to form at a later stage at the <*Sn*>/<*Cu*> interface (at the <*Sn*> side). Obviously, Cu enrichment by volume diffusion of Cu is most pronounced close to <*Sn*> grain boundaries intersecting the <*Sn*>/<*Cu*> interface (see Fig. 4.9): Cu arrives at this location by volume diffusion both from the substrate and from the <*Sn*> grain boundaries. Only after several days of ageing at room temperature Cu_6Sn_5 formation can also occur along the <*Sn*>/<*Cu*> interface remote from locations where <*Sn*> grain boundaries intersect the <*Sn*>/<*Cu*> interface.[♦] Thus the development of the irregular growth morphology of Cu_6Sn_5 can be understood.

[#] The increased diffusion of Cu along the <*Sn*> grain boundary intersecting the <*Sn/Cu*> interface governs the (morphology of the) formation and distribution of Cu_6Sn_5 in the Sn layer. This is compatible with observations that electrodeposited Sn layers containing co-deposited Cu exhibit significant, initial Cu_6Sn_5 formation *only* along <*Sn*> grain boundaries (i.e. in the form of "isolated" precipitates distributed over the <*Sn*> grain-boundaries), independent of the substrate material used (e.g. Cu [16], [44] or W [45]), as in this case the Sn layer itself serves as source for Cu atoms.

[♦] Heterogeneous nucleation of Cu_6Sn_5 and subsequent "island" coalescences lead to the formation of a polycrystalline, closed and rather planar layer of Cu_6Sn_5 at the <*Sn/Cu*> interface, as revealed by FIB and TEM analyses (see Figs. 4.2 and 4.5). This closed layer of Cu_6Sn_5 acts during further ageing at room temperature as diffusion barrier for Cu and thus further ("regular") growth of Cu_6Sn_5 proceeds significantly slower as compared to further ("irregular") growth of Cu_6Sn_5 along <*Sn*> grain boundaries intersecting the <*Sn/Cu*> interface, as observed.

Continued growth of the Cu_6Sn_5, originally formed at the <*Sn*> grain boundaries intersecting the <*Sn*>/<*Cu*> interface, could occur in particular in "diagonal" directions (see green arrows in Fig. 4.9), in order to minimize the total interface energy of the system upon grain growth.

The above discussion provides an explanation for the morphology and distribution of the developing Cu_6Sn_5 phase in the Sn layer as the outcome of both thermodynamic and kinetic arguments.

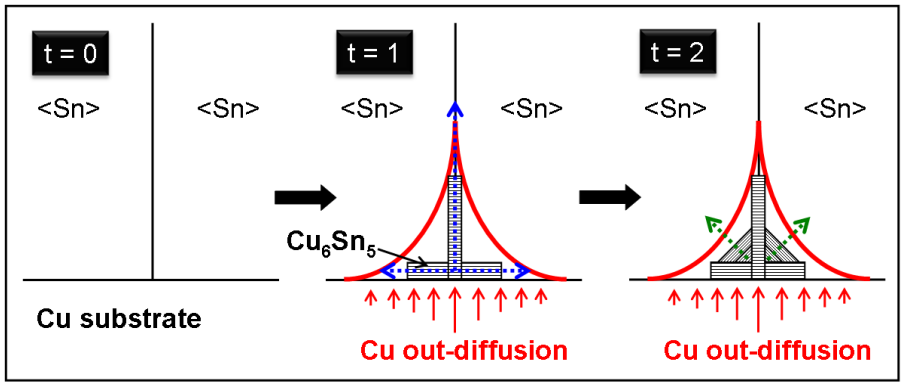

Figure 4.9: Schematic illustration of Cu diffusion and Cu_6Sn_5 formation processes during room temperature ageing (for successive ageing time steps t = 0, 1 and 2) at a <*Sn*> grain boundary intersecting the <*Sn*>/<*Cu*> interface, leading to the formation of Cu_6Sn_5 with an irregular growth morphology. The red, solid line illustrates a Cu iso-concentration profile in the Sn phase. The vertical blue arrow denotes grain-boundary diffusion of Cu along the <*Sn*> grain boundary: the horizontal blue arrows denote volume-diffusion of Cu originating from the <*Sn*> grain boundary (further see text).

4.5. Whisker mitigation by application of interface thermodynamics

The origin for Sn whisker formation in the system Sn on Cu has recently been ascribed to the development of stress *gradients*, parallel and perpendicular to the Sn/Cu interface, in the Sn layer as a consequence of the formation of Cu_6Sn_5 with an irregular growth morphology (see section 4.4.1) [22, 23]. On the basis of the treatment presented in this paper (see, in particular, section 4.4.4), the following whisker mitigation treatment can now be proposed.

During ageing at room temperature the occurrence of residual stress gradients, especially close to Sn grain boundaries, is caused by the laterally inhomogeneous development of Cu_6Sn_5, penetrating deeply into the Sn layer from the Sn/Cu interface, along Sn grain boundaries intersecting the Sn/Cu interface. Such gradients would not

develop such pronouncedly if a layer-like, planar growth of Cu_6Sn_5 along the entire Sn/Cu interface into the Sn layer would develop. In view of the results presented in section 4.4.4 (see Fig. 4.8) formation of planar Cu_6Sn_5 along the Sn/Cu interface could be achieved if the critical thickness for formation of Cu_6Sn_5 along the Sn/Cu interface becomes lower than that for formation of Cu_6Sn_5 along Sn grain boundaries, i.e. the layer/substrate interface energy must be increased and/or the Sn grain-boundary energy must be decreased. Moreover, a (laterally) closed, planar layer of Cu_6Sn_5 forming along the Sn/Cu interface acts as diffusion barrier for Cu from the substrate into the Sn coating which decelerates continued intermetallic phase formation in the Sn coating upon continued ageing at room temperature.

Incorporation of Pb into the Sn upon deposition on Cu changes, during subsequent ageing, the growth morphology of Cu_6Sn_5 to the desired, planar one [46], and indeed a Pb-content of even a few wt. % suffices to prevent effectively whisker formation [47]. It is very likely that the presence of Pb drastically reduces the Sn grain-boundary energy: wetting of Sn grain boundaries by Pb leads to Sn/Pb interfaces of energy about half of that of Sn/Sn interfaces (i.e. Sn grain boundaries) [48]. Hence, incorporation of Pb in the Sn layer implies application of interface thermodynamics to obstruct whisker formation.

4.6. Conclusions

- According to “bulk” thermodynamics, reaction in a Sn/Cu system can lead to the formation of the intermetallic compounds (IMC) Cu_3Sn and Cu_6Sn_5. Interface thermodynamics, recognizing the cost of IMC/Me interface formation, allows both the formation of Cu_3Sn and Cu_6Sn_5 at interfaces and grain boundaries, but favors the formation of Cu_3Sn at Sn grain boundaries, Cu grain boundaries and at the Sn/Cu interface.
- At room temperature significant diffusion of Cu into Sn can occur, but diffusion of Sn into Cu is negligible. As a consequence, Cu_3Sn formation does not occur initially. Instead, at the Sn side of the Sn/Cu system Cu_6Sn_5 formation (the Sn-rich IMC) occurs.
- Interface thermodynamics predicts that Cu_6Sn_5 formation occurs preferentially at the Sn grain boundaries intersecting the Sn/Cu interface, which agrees with the experimental observations.

- Cu_6Sn_5 formation along the Sn/Cu interface is thermodynamically possible but less favored (larger critical thickness than for Cu_6Sn_5 formation along Sn grain boundaries) and can only be realized by volume diffusion of Cu and therefore is observed only after prolonged ageing.
- The irregular growth morphology associated with the formation of Cu_6Sn_5 penetrating the Sn layer leads to pronounced lateral and vertical residual stress gradients in the Sn layer, especially close to Sn grain boundaries used for Cu_6Sn_5 formation, thereby driving whisker formation. It is proposed to apply the now available concept of interface thermodynamics to promote *planar growth* of closed Cu_6Sn_5 layers, i.e. to favor IMC formation at the Sn/Cu interface, for example by incorporation of a component in Sn that reduces the Sn grain-boundary energy. Pb is such a component.

Acknowledgment

The authors are much obliged to the company "*Hans Heimerdinger Oberflächentechnik*" in Pforzheim, Germany for specimen preparation. The authors would also like to thank Mrs Ulrike Eigenthaler (Max Planck Institute for Metals Research, Stuttgart) for preparing cross-sectional lamellae, by means of FIB, suitable for TEM analysis and Dr. Ewald Bischoff (Max Planck Institute for Metals Research, Stuttgart) for performing the TEM investigations.

References

[1] Compton K. G., Mendizza A. & Arnold S. M. (1951). *Corrosion* **7**, 327.

[2] Galyon G. T. (2005). *IEEE Trans. Electron. Packag. Manuf.* **28**, 94.

[3] Herring C. & Galt J. K. (1952). *Phys. Rev.* **85**, 1060.

[4] Britton S. C. (1974). *Trans. Inst. Metal Finish.* **52**, 95.

[5] Lee B. Z. & Lee D. N. (1998). *Acta Mater.* **46**, 3701.

[6] Tu K. N. (1973). *Acta Metall.* **21**, 347.

[7] Tu K. N. (1994). *Phys. Rev. B* **49**, 2030.

[8] Koonce S. E. & Arnold S. M. (1954). *J. Appl. Phys.* **25**, 134.

[9] Ellis W. C., Gibbons D. F. & Treuting R. C. (1958). *In Growth and Perfection of Crystals* edited by Doremus, R. H., Roberts, B. W. and Turnbull, D. (Wiley, New York, 1958), pp. 102-120.

[10] Furuta N. & Hamamura K. (1969). *Jpn. J. Appl. Phys.* **9**, 1404.

[11] Eshelby J. D. (1953). *Phys. Rev.* **91**, 755.

[12] Frank F. C. (1953). *Philos. Mag.* **44**, 854.

[13] Hasiguti R. R. (1955). *Acta Metall.* **3**, 200.

[14] Franks J. (1958). *Acta Metall.* **6**, 103.

[15] Lindborg U. (1976). *Acta Metall.* **24**, 181.

[16] Boettinger W. J., Johnson C. E., Bendersky L. A., Moon K.-W., Williams M. E. & Stafford G. R. (2005). *Acta Mater.* **53**, 5033.

[17] Buchovecky E. J., Du N. & Bower A. F. (2009). *Appl. Phys. Lett.* **94**, 191904.

[18] Tu K. N., Chen C. & Wu A. T. (2007). *J. Mater. Sci. - Mater. Electron* **18**, 269.

[19] Chason E., Jadhav N., Chan W. L., Reinbold L. & Kumar K. S. (2008). *Appl. Phys. Lett.* **92**, 171901.

[20] Kumar K. S., Reinbold L., Bower A. F. & Chason E. (2008). *J. Mater. Res.* **23**, 2916.

[21] Sobiech M., Welzel U., Schuster R., Mittemeijer E. J., Hügel W., Seekamp A. & Müller V. (2007). *in Proc. of the 57th Electronic Components and Technology Conference in Reno, USA*, 192.

[22] Sobiech M., Welzel U., Mittemeijer E. J., Hügel W. & Seekamp A. (2008). *Appl. Phys. Lett.* **93**, 011906.

[23] Sobiech M., Wohlschlögel M., Welzel U., Mittemeijer E. J., Hügel W., Seekamp A., Liu W. & Ice G. E. (2009). *Appl. Phys. Lett.* **94**, 221901.

[24] Choi W. J., Lee T. Y., Tu K. N., Tamura N., Celestre S., MacDowell A. A., Bong Y. Y. & Nguyen L. (2003). *Acta Mater.* **51**, 6253.

[25] Dyson B. F., Anthony T. R. & Turnbull D. (1967). *J. Appl. Phys.* **38**, 3408.

[26] Anthony T. R. & Turnbull D. (1966). *Appl. Phys. Lett.* **8**, 120.

[27] Tu K. N. & Thompson R. D. (1982). *Acta Metall.* **30**, 947.

[28] Zhang W., Egli A., Schwager F. & Brown N. (2005). *IEEE Trans. Electron. Packag. Manuf.* **28**, 85.

[29] Choi W. J., Jang S. Y., Kim J. H., Paik K. W. & Lee H. M. (2002). *J. Mater. Res.* **17**, 597.

[30] Sommer F., Singh R. N. & Mittemeijer E. J. (2009). *J. Alloys Compd.* **467**, 142.

[31] Jeurgens L. P. H., Wang Z. M. & Mittemeijer E. J. (2009). *International Journal of Materials Research* **100**, 1281.

[32] de Boer F. R., Boom R., Mattens W. C. M., Miedema A. R. & Niessen A. K. (1988). *North Holland, Amsterdam*.

[33] Miedema A. R. & De Boer F. R. (1979). *Z. Metallkd.* **70**, 14.

[34] Miedema A. R. & Boom R. (1978). *Z. Metallkd.* **69**, 183.

[35] Hultgren R., Desai P. D., Hawkins D. T., Gleiser M. & Kelley K. K. (1973). *Selected Values of the Thermodynamic Properties of Binary Alloys, Am. Soc. Met., Metals Park, OH,* .

[36] Sommer F., Singh R. N. & Witusiewicz V. (2001). *J. Alloys Compd.* **325**, 118.

[37] Li M., Du Z., Guo C. & Li C. (2009). *J. Alloys Compd.* **477**, 104.

[38] Liu X. J., Wang C. P., Ohnuma I., Kainuma R. & Ishida K. (2004). *Metall. Mater. Trans. A-Phys. Metall. Mater. Sci.* **35**, 1641.

[39] Dinsdale A. T. (1991). *Calphad* **15**, 317.

[40] Song J. Y., Tu J. & Lee T. Y. (2004). *Scripta Mater.* **51**, 167.

[41] Kittel C. (2005). *Introduction to solid state physics*. Hoboken, NY: Wiley.

[42] Wawra H. (1975). *Z. Metallkd.* **66**, 395.

[43] Osenbach J. W., DeLucca J. M., Potteiger B. D., Amin A., Shook R. L. & Baiocchi F. A. (2007). *IEEE Trans. Electron. Packag. Manuf.* **30**, 23.

[44] Sheng G. T. T., Hu C. F., Choi W. J., Tu K. N., Bong Y. Y. & Nguyen L. (2002). *J. Appl. Phys.* **92**, 64.

[45] Williams M. E., Moon K.-W., Boettinger W. J., Josell D. & Deal A. D. (2007). *J. Electron. Mater.* **36**, 214.

[46] Zhang W. & Schwager F. (2006). *J. Electrochem. Soc.* **153**, C337.

[47] Arnold S. M. (1966). *Plating* **53**, 96.

[48] Gupta D., Vieregge K. & Gust W. (1998). *Acta Metall.* **47**, 5.

5. Stress relaxation mechanisms of Sn and SnPb coatings electrodeposited on Cu: avoidance of whiskering

M. Sobiech, J. Teufel, U. Welzel, E. J. Mittemeijer and W. Hügel

Abstract

The interrelations of microstructural evolution, phase formation, residual stress development and whiskering behavior were investigated for the systems Sn coating on Cu and SnPb coating on Cu during ageing at room temperature. It was shown that the whisker-preventing effect of Pb-addition to pure Sn can be attributed to a Pb-induced change of the stress relaxation mechanism in the coating: Pure Sn coatings, with a columnar grain morphology, relax mechanical stress via localized, unidirectional grain growth from the surface of the coating (i.e. whisker formation occurs) whereas SnPb coatings, with an equiaxed grain morphology, relax mechanical stress via uniform grain coarsening without whisker formation. It can thus be suggested that tuning of the Sn grain morphology (i.e. establishing an equiaxed grain morphology) is a straightforward method of microstructural control to suppress whisker formation at room temperature. Experimental results obtained in this project validate this conclusion.

5.1. Introduction

The spontaneous formation [1] of single-crystalline [2-4] whiskers, during ageing at room temperature, on polycrystalline Sn thin films deposited on Cu can be understood as a response of the material to realize stress relaxation [1, 5-10]. The whiskering behavior (i.e. moment of whiskering, location of nucleation and kinetics of growth) for the system Sn on Cu can vary significantly, depending on the following parameters (see e.g. [1, 7, 11-16]):

i) Microstructure of the Sn coating: e.g. coating thickness, grain size, grain morphology, crystallographic texture and presence of (volume and grain boundary) impurities.

ii) Microstructure of the Cu substrate: e.g. grain size, grain morphology, crystallographic texture and presence of impurities.

iii) Source of stress generation: e.g. due to layer deposition (i.e. growth stress), thermally induced mismatch (e.g. by cooling after layer deposition), electromigration, external loading, oxidation/corrosion and formation of intermetallic phases upon ageing.

None of the whisker-growth models proposed until now [1, 5, 7, 17-24] is capable of explaining coherently and universally the wide scatter of observed whiskering behaviors. Very recently the process of spontaneous Sn whisker formation in the system Sn on Cu could be described as follows [25, 26]: After Sn deposition and during subsequent ageing at room temperature, Cu diffuses rapidly by an interstitial mechanism [8, 27] into the Sn coating, constituted of columnar grains, and formation of the intermetallic phase (IMC) Cu_6Sn_5 takes place only on the Sn side [10, 28], preferentially along Sn grain boundaries intersecting the Sn/Cu interface [5, 28, 29]. This irregular growth of Cu_6Sn_5 is accompanied by a volume expansion and, as a consequence, in-plane (i.e. orientated parallel to the Sn/Cu interface) residual compressive stresses, in particular at the depth of IMC formation, develop. As a result, residual stress *gradients* are generated in the Sn coating [25, 26]. These stress *gradients*, both in out-of-plane [25] and in-plane [26] directions, drive the transport of Sn atoms (thereby realizing stress relaxation) to the whisker nucleation site and thus control whisker growth.

Filamentary Sn whiskering on Sn finishes of electronic components can lead to whisker-induced short-circuit failures [11], which was already recognized in 1951 by Compton *et al.* [30] and today is the cause of great economic loss [31]. It was found empirically in the 1960s that SnPb coatings are much less prone to whiskering than pure Sn coatings [32]. In recent times environmental concerns about toxic substances in the electronic waste (e.g. Pb) initiated legislative directives for implementation of "green manufacturing", which forced the electronic industry to convert to Pb-free finish solutions [33]. As nowadays pure Sn is considered as the most suitable candidate to replace effectively and economically SnPb alloys, the Sn whisker phenomenon re-emerged as a serious reliability concern of modern interconnection systems and thus recently great scientific and practical interest emerged to arrive at fundamental understanding of whiskering [11].

Against the above background the purpose of the present work is *(i)* to determine the effect of Pb addition on the microstructure of pure Sn coatings in order to understand the whisker-mitigating effect of Pb (which has been controversially discussed in the literature [7, 9, 34, 35]) and *(ii)* to apply this knowledge to modify the microstructure of pure Sn coatings such that whisker formation does not occur.

5.2. Experimental procedures

5.2.1. Specimen preparation

Pure Sn and SnPb coatings, with thicknesses of about 3 and 7 µm (as determined by X-ray fluorescence and focused ion beam cross-sectional analyses), were electrodeposited onto both Cu (rolled, commercial leadframe material) and Fe substrates, using three different industrial electrolytes (on the basis of methansulfonic acid with organic additives and dissolved metal ions) by employing a laboratory-electrodeposition setup. After layer deposition all specimens were aged at room temperature without controlling the ambient atmosphere. Four different specimen types were prepared (see Tab. 1):

a) Columnar Sn on Cu (Sn/Cu-col)

b) Equiaxed Sn on Cu (Sn/Cu-equi)

c) SnPb on Cu (SnPb/Cu**)**

d) SnPb on Fe (SnPb/Fe)

In order to clearly distinguish in the following both types of pure Sn coatings, the respective description of the grain morphology (i.e. columnar or equiaxed) is used in the following. The above indicated abbreviated specimen notations are used in the figures and in Table 1.

Table 5.1: List of specimen types used in this work. Three different industrial Sn electrolytes (A-C; composed of *i)* metal ions, *ii)* organic additives and *iii)* methanesulfonic acid) were employed for specimen preparation. Prior to electroplating the substrates were cleaned (by ultrasonic (Mucasol©) and electrolytic (P1005, 5%) treatments) and surface activated (by pickling with Pictax©) in order to remove tarnish and oxide films.

specimen notation	*Sn/Cu-col*	*Sn/Cu-equi*	*Sn90Pb10/Cu* *Sn82Pb18/Cu*	*Sn80Pb20/Fe*
electrolyte type	A	B	C	C
initial grain morphology	columnar	equiaxed	equiaxed	equiaxed
bath temperature [°C]	40	30	40	40
current density [A/dm^2]	2	1	3	3
thickness [µm]	3	3	3 / 7	7
Pb-content	-	-	10 / 18 wt.%	20 wt.%

5.2.2. Microstructural analyses

Micrographs of the coating surface were obtained with a LEO 1450 VP scanning electron microscope (SEM), using an acceleration voltage of 15 kV and a beam current between 100 to 200 pA. The SEM was also employed for local (area of about one µm^2) energy dispersive X-ray (EDX) analyses as well as for local (area of some tens of µm^2) texture analyses by conventional electron backscatter diffraction (EBSD) using the additionally installed EBSD system (TSL, EDAX, Inc.) and the evaluation software OIM 4.5.

The grain morphologies of the coatings were investigated in top-view and cross-sectional view by employing a focused ion beam (FIB) microscope (FEI FIB 200 apparatus). The FIB was operated with an acceleration voltage of 30 kV and beam currents of 2700 pA (for cutting), 350 pA (for cleaning) and 11-70 pA (for imaging), respectively.

The (through-thickness averaged) residual stress evolution of each specimen was obtained by performing X-ray diffraction stress measurements without control of the penetration depth as a function of room temperature ageing employing a Philips (now: PANalytical) MRD Pro diffractometer. This diffractometer, equipped with an

Eulerian cradle (four-circle goniometer), was operated in parallel beam geometry (parallelization was realized by means of a polycapillary X-ray lens [36]) using Cu-Kα radiation (here the X-ray source was a conventional sealed Cu tube operated at 45 kV/ 40 mA) with an X-ray beam size of 4 x 4 mm^2, a parallel-foils collimator as secondary X-ray optics, a flat graphite monochromator in the diffracted beam and a proportional counter. X-ray diffraction texture analyses were conducted directly after specimen preparation as well as after prolonged ageing at room temperature. Qualitative X-ray diffraction phase analysis was performed after several ageing times within the 2θ-range of 20-90°, with a step size of 0.02° 2θ and a step time of 2 s, applying the conventional ($\theta/2\theta$) diffraction geometry.

The residual stress-depth distribution of each specimen was obtained by conducting X-ray diffraction stress measurements at selected, constant penetration depths [37] after an ageing time at room temperature of about 30 days employing a Bruker D8 Discover TXS diffractometer. This diffractometer, equipped with an Eulerian cradle, was operated in parallel beam geometry (parallelization was realized by means of a 2D-collimating X-ray mirror (Xenocs Fox 2D) [38]) using Cu-Kα radiation (here the X-ray source was a rotating micro-focus X-ray anode operated at 50 kV / 20 mA) with a X-ray beam size of 1 x 1 mm^2, a parallel-foils collimator as secondary X-ray optics and an energy-dispersive detector with a geometrical acceptance window of around 4 x 15 mm^2.

Based on direction- and position-dependent X-ray diffraction stress measurements in the specimen frame of reference, the mechanical macrostress state of the coatings was found to be planar, approximately rotationally symmetric and laterally inhomogeneous. The lateral inhomogeneity with respect to the state of stress was ascribed to the inhomogeneous formation of intrinsic growth stresses during electrodeposition. All stress measurements performed on the same specimen position were carried out along the same in-plane direction in the specimen frame of reference and thus the stress component, $\sigma_{\parallel}$ (= σ_{11} = σ_{22}; the stress parallel to the substrate), was determined. Mechanical stresses of the Sn coating were calculated from lattice strains measured employing the 301, 321 and 312 reflections on the basis of the $\sin^2\psi$-method [39]. The specimen was assumed to be macroscopically elastically *quasi-isotropic* and therefore the *hkl*-dependent diffraction (X-ray) elastic constants S^{hkl}_1 and $½S^{hkl}_2$ were derived from single-crystal data [40] using the Neerfeld-Hill model [39]. In order to

control the penetration depth (and thus the information depth) of the X-ray beam, a combined ω-χ-ϕ tilting (ω, χ and ϕ are instrumental angles describing the orientation of the specimen with respect to the laboratory frame of reference) of the specimen was applied. The complete strategy for X-ray diffraction stress measurements at fixed penetration depths is described in detail elsewhere [37].

5.3. Results

Starting immediately after specimen preparation the evolutions of the microstructure (i.e. the phase composition, the crystallographic texture, the grain morphology and the whiskering behavior) and the corresponding residual stress of each specimen type were traced during ageing at room temperature by means of X-ray diffraction and FIB-based investigations.

5.3.1. Phase and texture analyses

The X-ray diffraction patterns obtained for Sn and SnPb coatings on Cu shortly after (i.e. after a few hours) layer deposition are shown in Fig. 5.1. The diffraction lines of the Cu substrate have been marked in red.

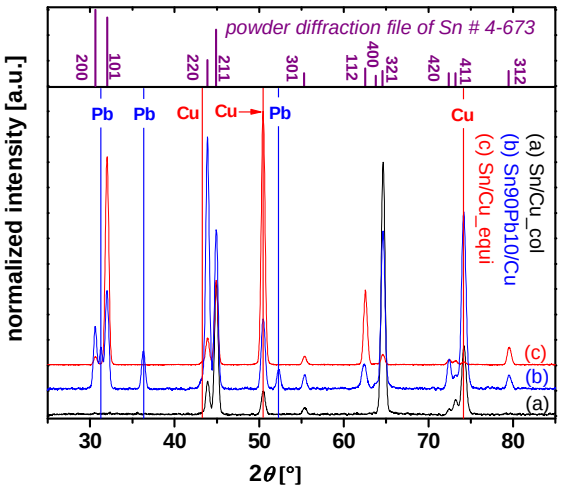

Figure 5.1: Diffraction patterns of the specimen types **(a)** Sn/Cu_col, **(b)** Sn90Pb10/Cu and **(c)** Sn/Cu_equi, with coating thicknesses of about 3 µm, taken directly after layer deposition. The diffraction lines of Cu and Pb have been marked in red and blue, respectively. Note that due to the rolling texture of the Cu substrate the 111 diffraction line is nearly not visible. The schematic powder diffraction pattern (according to the PDF file # 4-673) of Sn is shown on top. Directly after Sn deposition no intermetallic phase was observed by X-ray diffraction.

The diffraction pattern of the columnar Sn on Cu shows that the coating was composed of pure Sn exhibiting a pronounced {321}-fiber texture. The Sn90Pb10 coating on Cu exhibited two separate phases, Sn and Pb (occurrence of both phases was confirmed by FIB microscopy and local EDX analyses), as expected from the phase diagram [40], and showed a distinct {110}-fiber texture of the Sn phase. The equiaxed Sn coating on Cu showed a modest {101}-fiber texture. The crystallographic texture of each specimen was determined by global (i.e. irradiated area of several mm^2) X-ray diffraction and local (i.e. surface area of about several tens of μm^2) electron back scatter diffraction (both not shown here) measurements.

After several weeks of ageing at room temperature additional diffraction lines belonging to the intermetallic phase Cu_6Sn_5 appeared. This phase started to grow from the layer/substrate interface into Sn and SnPb coatings as the result of reaction between Sn and Cu (see section 5.3.2 and Fig. 5.2).

Continued X-ray diffraction investigation, performed up to an ageing time of about one year, revealed that the phase composition as well as the (global) crystallographic texture determined for each specimen type remained unchanged.

5.3.2. Grain morphology, intermetallic formation and whiskering behavior

The microstructure of the Sn and SnPb coatings on Cu was investigated by cross-sectional FIB micrographs after different ageing times at room temperature (see Fig. 5.2).#

[#] FIB machining of Sn (SnPb) on Cu systems induces artefacts in the Sn microstructure. During high-energetic Ga^+ ion beam cutting through the Sn (SnPb) on Cu system (e.g. in order to prepare cross-sections of the bilayer system), Cu atoms are removed from the substrate due to sputtering. Once the ion beam is switched off, Cu atoms from the gas phase react with the freshly prepared Sn surface, preferentially along Sn grain boundaries, and thus form Sn-Cu intermetallics [16]. Therefore, cross-sectional FIB micrographs of Sn layers on Cu exhibit typically bright Sn grain boundaries (due to significant formation Sn-Cu intermetallics with a "line-like" morphology) as well as bright spots on the Sn grains due to the presence of fine Sn-Cu intermetallics, which had not formed during (undisturbed) ageing conditions. This could be shown unequivocally by preparing FIB cuts which did not extended to the Cu substrate, i.e. in such a case the Sn grain boundaries in the exposed section of the Sn layer were completely free of any Sn-Cu intermetallics.

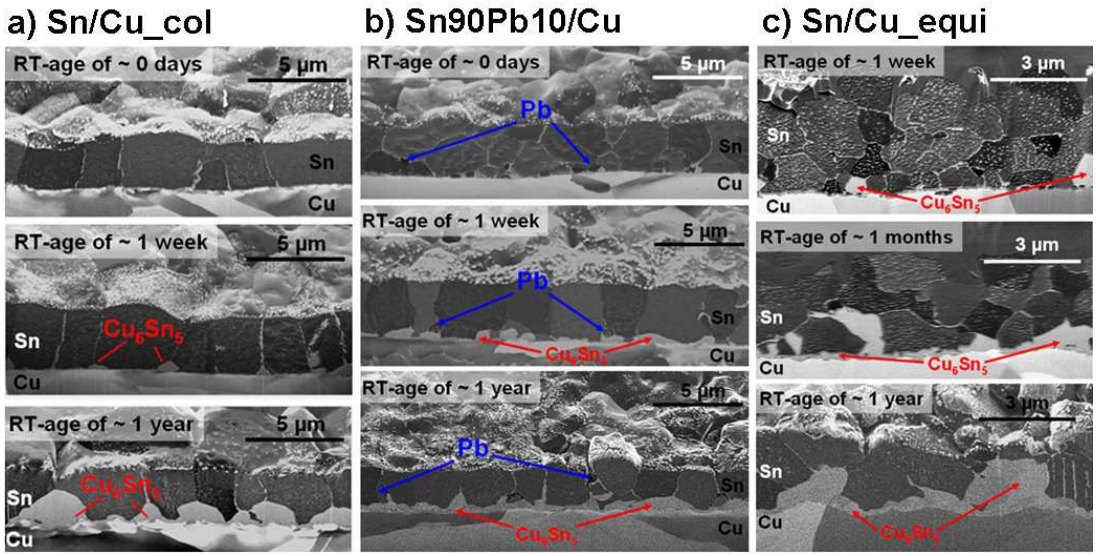

Figure 5.2: Microstructural evolution upon room temperature ageing of **a)** Sn/Cu_col, **b)** Sn90Pb10/Cu and **c)** Sn/Cu_equi specimens, with coating thicknesses of about 3 µm, as revealed in cross-sectional view by means of FIB microscopy.

The columnar Sn coating on Cu showed initially (i.e. after some hours of room temperature ageing) a columnar microstructure with in-plane grain sizes of about 2-5 µm. A few surface grains with inclined (with respect to the surface normal) grain boundaries were also present (see Fig. 5.3 on top).

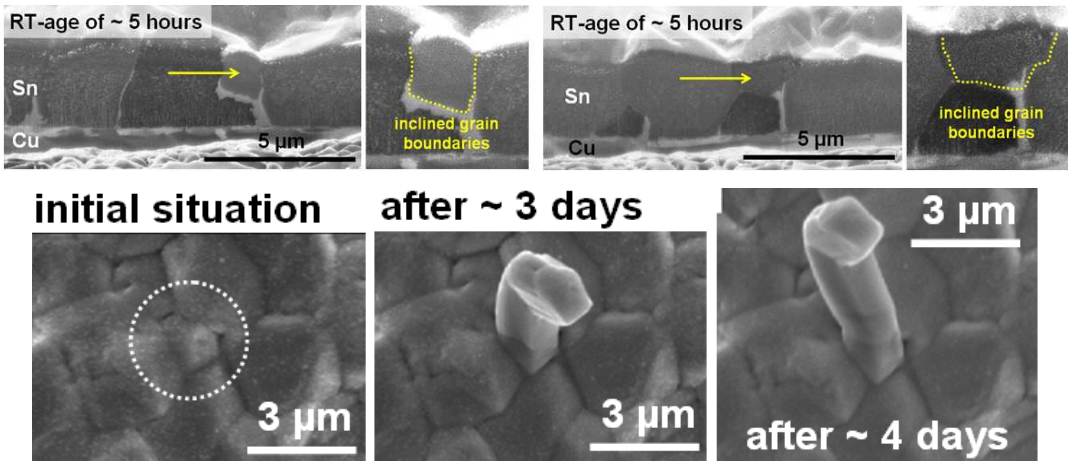

Figure 5.3: Top: Cross-sectional FIB micrographs of the specimen Sn/Cu_col showing the initial Sn grain morphology observed ~ 5 hours after Sn layer deposition. The arrows indicate surface grains with inclined (with respect to the surface normal) grain boundaries. Bottom: Top-view SEM micrographs of the same specimen showing the onset of whiskering upon ageing.

During continued ageing, lasting up to about one year, no significant changes of the Sn grain morphology occurred (note that the texture of the columnar Sn coating remained unchanged; see section 5.3.1). However, two striking microstructural changes could be observed during ongoing ageing:

(i) The intermetallic phase Cu_6Sn_5 formed preferentially along Sn grain boundaries intersecting the Sn/Cu interface and extended upon prolonged ageing significantly into the Sn coating, leading to an irregular growth morphology (see Fig. 5.2a).

(ii) Roughly 3-4 days after Sn deposition the first whiskers formed, initiating from pre-existing Sn grains (see bottom part of Fig. 5.3) on the surface of the Sn coating (see Fig. 5.4a) and kept on growing for the next weeks of ageing, some of them reaching lengths of several tens of micrometers. The root of the whiskers in the coating exhibited inclined (with respect to the surface normal) grain boundaries and at the location directly underneath the root, at the Sn/Cu interface, pronounced formation of Cu_6Sn_5 had occurred (see cross-sectional micrograph *(iii)* in Fig. 5.4a). The same microstructural observations were made at several whisker-nucleation sites.

The Sn90Pb10 coating on Cu exhibited initially an equiaxed Sn microstructure with in-plane grain sizes of about 1-3 µm. Small Pb inclusions with grain sizes of about 0.1-0.5 µm were present along Sn grain boundaries (proved by local EDX analyses); only a few Pb inclusions could also be observed in the bulk of Sn grains. During subsequent ageing the following striking microstructural changes occurred:

(i) Grain coarsening of both phases accompanied by a modification of the grain morphology from equiaxed to columnar took place. The in-plane Sn grain sizes increased to about 2-4 µm and the small Pb inclusions disappeared in favor of the development of larger Pb particles with in-plane grain sizes of about 0.5-1 µm forming exclusively along Sn grain boundaries (the presence of Pb in Sn and along Sn grain boundaries was also observed in Ref. [7], but for specimens with a significantly lower Pb-content of about 2 wt. % and only after an ageing time of about one month). Already after one week of ageing these microstructural modifications had been largely completed (compare the FIB micrographs in Fig. 5.2b taken after ageing times of one week and one year).

(ii) The growth morphology of the intermetallic phase Cu_6Sn_5 changed from initially "irregular" to rather "regular/planar" during prolonged ageing at room temperature (see the FIB micrographs in Fig. 5.2b taken after ageing times of one week and one year, respectively, and compare with Fig. 5.2a), which can also be concluded upon

inspection of the data presented in Refs. [34] and [35] where microstructural analyses were performed (only) after an prolonged ageing time at room temperature.

(iii) The Sn90Pb10 coating on Cu remained throughout the entire investigation period whisker-free. However, hillock formation occurred upon ageing at room temperature (see Fig. 5.4b), also reported in Ref. [35]. The precise onset time of hillock formation was not determined, but it was observed that hillock formation occurred not within the first week of ageing, i.e. hillock formation set in once the modification of the grain morphology from equiaxed to columnar had been completed. Furthermore, it was shown by top-view and cross-sectional EDX and FIB analyses that hillocks are "single crystals" composed of pure Sn, as holds for Sn whiskers (see Fig. 5.4). Hillocks, in contrast with whiskers, typically exhibit an aspect ratio smaller than one, i.e. their length (out-of-plane direction) is smaller than their diameter (the in-plane direction) and underneath the hillocks a grain-boundary arrangement occurs which is significantly different from that observed underneath a whisker root (compare the images (iii) in Figs. 5.4a and 5.4b; see also Ref. [41]).

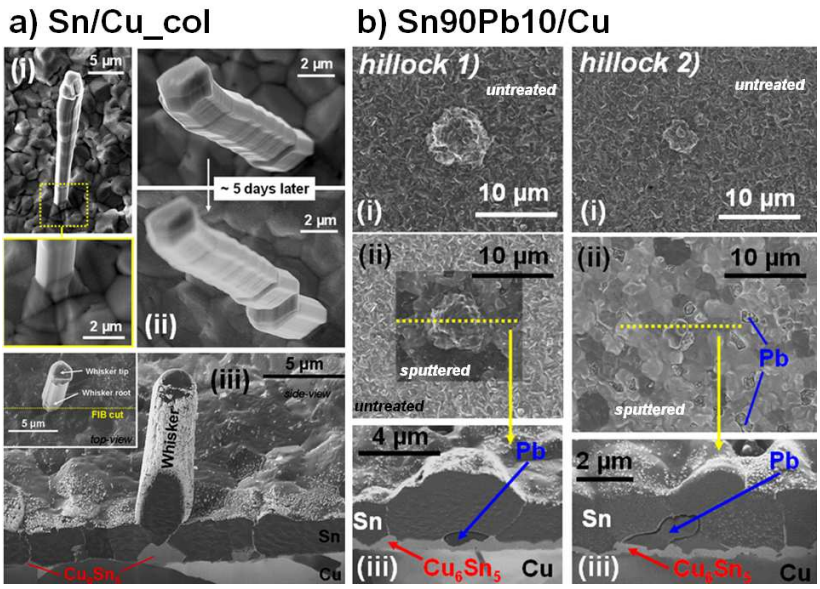

Figure 5.4: Surface structures (i.e. whiskers and hillocks) formed during ageing at room temperature on **a)** Sn/Cu_col and **b)** Sn90Pb10/Cu specimens, both with a coating thickness of about 3 µm. The FIB micrographs were taken after several days of ageing at room temperature. The top-view microstructure of the Sn90Pb10 coatings could only be visualized after sputtering away a fine-grained "surface layer": in b) the images *(i)* were taken before and images *(ii)* after extensive ion beam treatment of the same specimen position.

These findings on the microstructural evolution of SnPb coatings on Cu during room temperature ageing were extended by observations made for SnPb coatings on Cu and on Fe having either an increased Pb content (i.e. ~ 18-20 wt.%), or an increased layer thickness (i.e. ~ 7 µm), or both, (see Figs. 5.5-5.6). The following additional insights were thereby obtained:

(iv) With increased Pb addition the averaged grain size of the Sn and Pb phases in the coating decreased and an even more equiaxed grain morphology occurred (compare Figs. 5.5a and 5.5b, as well as Figs. 5.5c and 5.5d).

(v) With increased Pb addition and/or with increased coating thickness the ageing time needed for the transition of the grain morphology from equiaxed to columnar increased; the microstructure of the Sn82Pb18 coating on Cu with a layer thickness of ~ 7 µm was even after ageing times of about one year still partly equiaxed (see Fig. 5.5d).

(vi) The growth of the intermetallic phase Cu_6Sn_5 was found to be not significantly dependent on both the coating thickness and the Pb content, i.e. in all cases the growth morphology of Cu_6Sn_5 changed from initially "irregular" to "regular" upon ongoing ageing.

vii) Sn82Pb18 coatings on Cu were within the entire investigation period (whisker-and) hillock-free, independent of their layer thickness (i.e. for both layer thicknesses of 3 and 7 µm).

viii) Sn80Pb20 coatings on Fe were also hillock- and whisker-free within the investigation period, but contrary to Sn82Pb18 coatings on Cu, Sn80Pb20 coatings on Fe were free of interfacial intermetallic phases. These coatings remained also equiaxed for extended ageing times; significant grain coarsening occurred only within the first week of ageing at room temperature (see Fig. 5.6).

The equiaxed Sn coating on Cu exhibited "initially" an equiaxed Sn microstructure with in-plane grain sizes of about 0.5-2 µm (see Fig. 5.2c). During ageing lasting up to about one year grain growth occurred resulting in a rather coarse-grained, but still more or less equiaxed grain morphology with in-plane Sn grain sizes of about 2 µm. The intermetallic phase Cu_6Sn_5 forming at the Sn/Cu interface exhibited throughout the entire ageing period an irregular growth morphology, as observed for columnar Sn on Cu (compare Figs. 5.2c and 5.2a). In this case, however, Cu_6Sn_5 formation occurred preferentially by replacing, in a massive way, successively Sn grains, whereas in columnar Sn coatings on Cu the growth of Cu_6Sn_5 proceeded

preferentially along Sn grain boundaries intersecting the Sn/Cu interface. The equiaxed Sn coating on Cu was throughout the entire ageing time at room temperature of about one year whisker- and hillock-free.

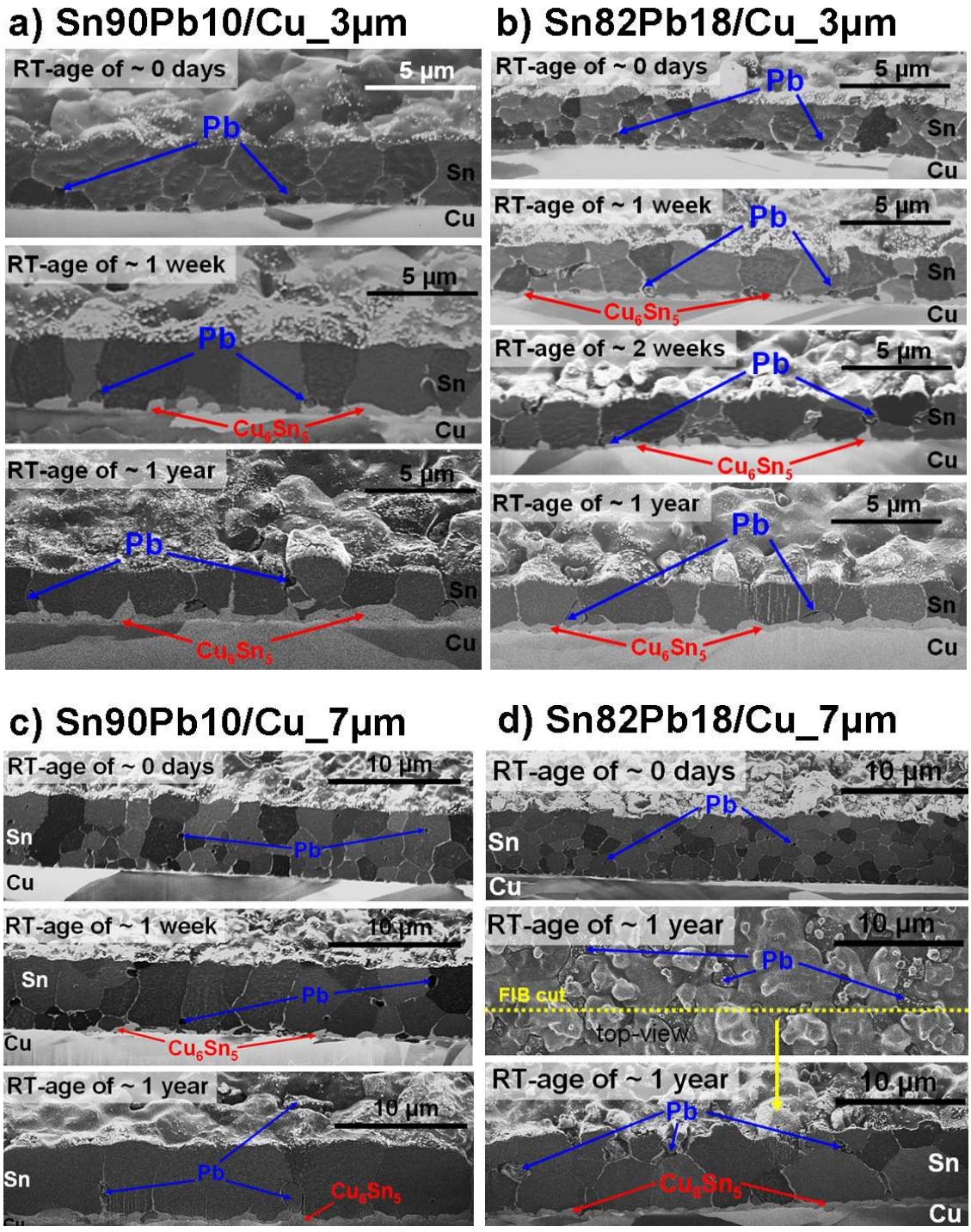

Figure 5.5: Microstructural evolution upon room temperature ageing observed by FIB microscopy of the specimens: **a)** Sn90Pb10/Cu with a coating thickness of ~ 3 µm (cf. Fig. 5.2b). **b)** Sn82Pb18/Cu with a coating thickness of ~ 3 µm. **c)** Sn90Pb10/Cu with a coating thickness of ~ 7 µm. **d)** Sn82Pb18/Cu with a coating thickness of ~ 7 µm.

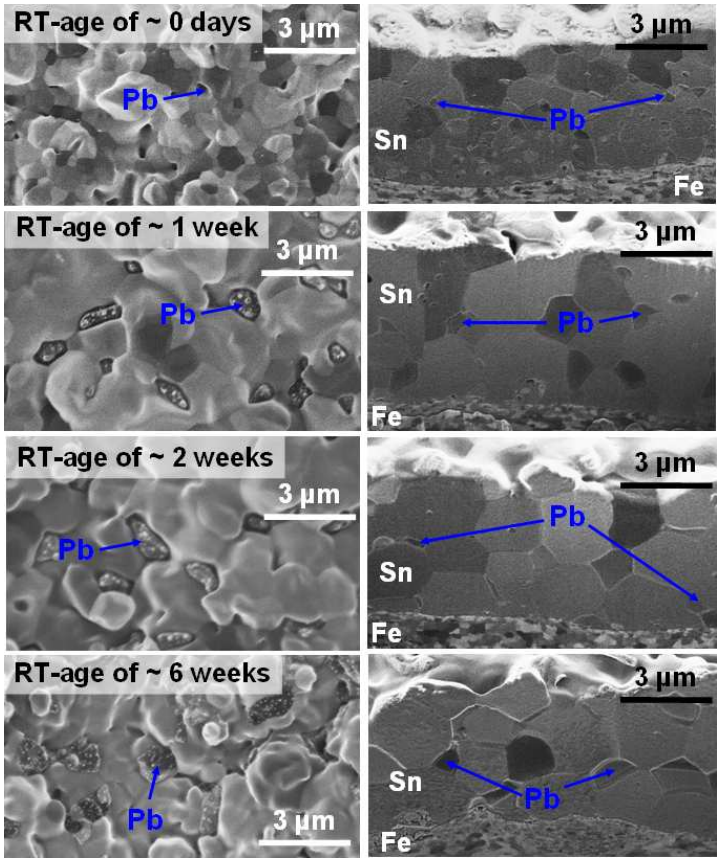

Figure 5.6: Microstructural evolution during room temperature ageing of a Sn80Pb20 coating (thickness of about 7 µm) electrodeposited on (pure) Fe as revealed by top- (left) and cross-sectional (right) FIB microscopy. Note that intermetallic phase formation did not occur.

5.3.3. Diffraction analysis of residual stress evolution

The residual stress of the columnar Sn coating on Cu (see Fig. 5.7a) changed, upon ageing at room temperature, from initially tensile (~ 2 MPa) to compressive and attained a more or less constant value of about -8 MPa after several days. The emergence of the first whiskers on the surface of the columnar Sn coating coincided with the residual stress reaching the plateau level of about -8 MPa, i.e. after an ageing time of about 3-4 days (see bottom part of Fig. 5.3 and Fig. 5.4a).

The residual stress evolutions of the Sn90Pb10 coating on Cu and the equiaxed Sn coating on Cu, upon ageing at room temperature, are very similar (see Figs. 5.7b and 5.7c), and differ pronouncedly from that observed for the columnar Sn coating on Cu (see Fig. 5.7a). For the Sn90Pb10 and equiaxed Sn coatings the residual stress changed with a much slower rate from tensile (1-2 MPa) to compressive and saturation of compressive stress occurred at a value of only about – (2-3) MPa which was achieved only after ageing times of about 20 days. Note that (*i)* both specimen types

did not show whiskering within the entire period of ageing time investigated (cf. section 5.3.2), but *(ii)* the Sn90Pb10 coating on Cu showed hillock formation, for ageing times exceeding one week, whereas the equiaxed Sn coating on Cu remained hillock-free (further investigated SnPb coatings on Cu (cf. with Tab. 1) revealed a qualitatively similar residual stress evolution as the Sn90Pb10 coating, apart for the coating Sn82Pb18 on Fe, which remained stress-free even after prolonged ageing times at room temperature, i.e. after several weeks) (see also Fig. 5.6).

The X-ray diffraction stress measurements discussed above were performed without control of the penetration depth of the X-rays and therefore, in view of the modest thickness of the Sn and Sn90Pb10 coatings, the obtained stress values represent through-thickness averaged residual stresses [42]. However, it was shown recently that pronounced (local) stress *gradients* [25, 26] can occur in the Sn coatings. Therefore, in this work X-ray diffraction stress measurements were also performed at different controlled penetration depths [37] in order to assess the stress gradients in the direction of increasing depth. As the stress-depth profile obtained by using X-ray diffraction represents the Laplace transformed stress-depth profile in real space [43, 44], an inverse Laplace transformation was performed here using an iterative procedure (see also as appropriate examples Refs. [45, 46]) in order to derive the real stress-depth distribution.

The near-surface stress-depth profiles in real space obtained for all specimen types after an ageing time at room temperature of about 30 days are shown in Fig. 5.7d. All stress-depth profiles show the occurrence of negative stress gradients in the direction of increasing depth. The most pronounced negative stress gradient is observed for the columnar Sn coating on Cu. The Sn90Pb10 coating on Cu and the equiaxed Sn coating on Cu exhibit negative stress gradients of about the same value, even tough their absolute stress values differ.

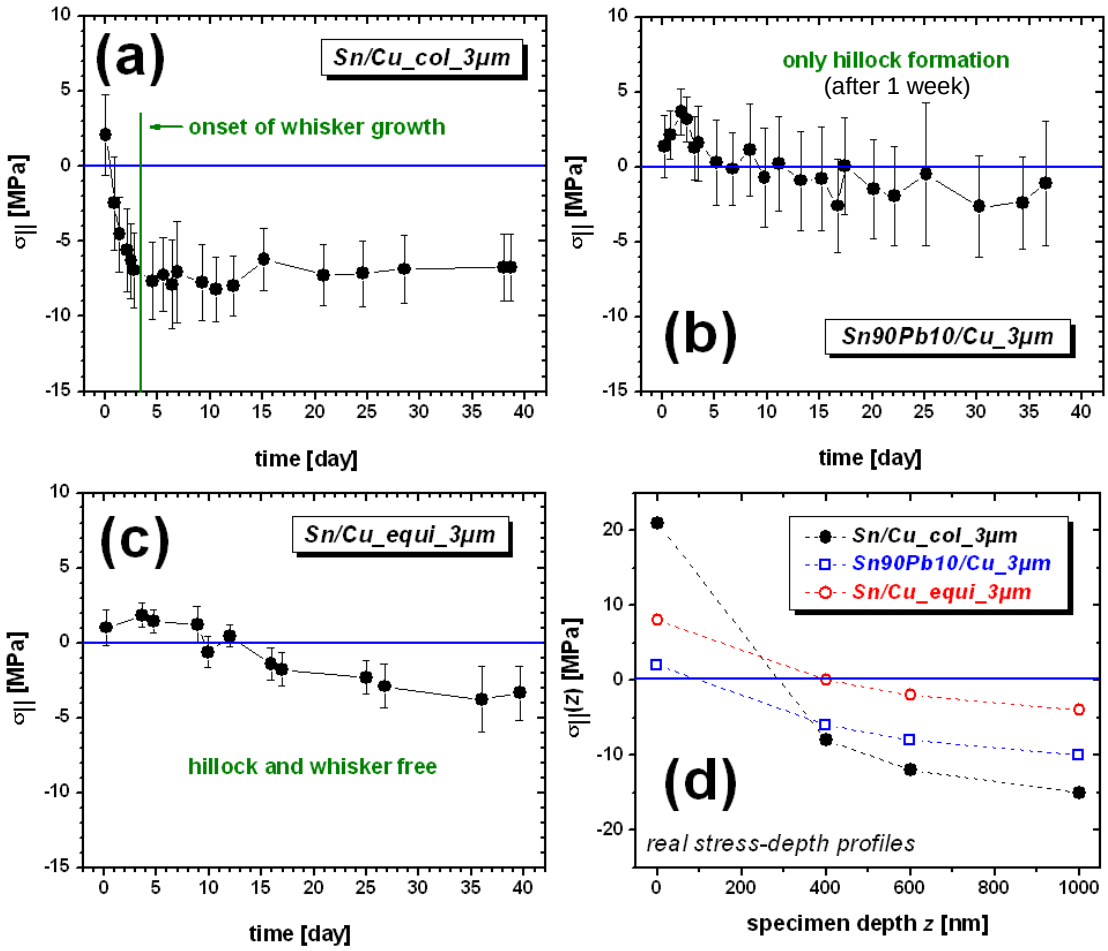

Figure 5.7: Residual through-thickness averaged stress of the Sn coatings (thickness of about 3 µm) of **a)** Sn/Cu_col, **b)** Sn90Pb10/Cu and **c)** Sn/Cu_equi specimens as a function of ageing time at room temperature. The 321 (for Sn/Cu_col), 301 (for Sn90Pb10/Cu) and 312 (Sn/Cu_equi) diffraction lines of Sn were employed for the stress analysis. **d)** Near-surface stress-depth profiles in real space derived for the three specimens after about 30 days of ageing at room temperature.

5.4. Discussion

The occurrence or absence of whiskering from Sn and SnPb coatings deposited on Cu will be discussed in the following in terms of the coating microstructure and its development upon ageing at room temperature, using the microstructural data presented in section 5.3.

5.4.1. Spontaneous whiskering of columnar Sn coatings on Cu at room temperature

The observed occurrence of spontaneous Sn whiskering of columnar Sn coatings on Cu is consistent with recent literature reports [1, 5, 9, 23, 25, 26, 29]. The formation of Cu_6Sn_5 along the grain boundaries of the columnar grains in the Sn coating, which intersect the Sn/Cu interface, leads to the development of residual compressive stress parallel to the Sn/Cu interface due to the constraints imposed by the (rigid) substrate upon increase of the specific volume associated with intermetallic phase formation at the Sn side of the Sn/Cu interface. Indeed, in SnPb coatings on Fe, which do not exhibit intermetallic compound formation during ageing at room temperature, no residual stress occurs (cf. with section 5.3.3 and Fig. 5.6). Roughly 3-4 days after Sn deposition the residual stress attains a constant plateau value of about -8 MPa (see Fig. 5.7a) and at the same time whiskering initiates (see Fig. 5.3 at bottom). During continued ageing whisker growth proceeds (with ~ 0.2 Å/s, as determined by time-resolved SEM observations on several whiskers), while the residual stress remains more or less unchanged, even though the source for compressive stress generation, i.e. Cu_6Sn_5 growth, as described above, still operates (see Fig. 5.2a). This can be understood as follows: Compressive stress development/increase due to Cu_6Sn_5 growth can continue until the yield limit of Sn is exceeded.[#] Volume misfit due to further growth of Cu_6Sn_5 then induces plastic deformation, evidently ultimately involving in the present case whisker growth, as a localized stress-relaxation mechanism. This balance of stress generation and stress relief controls the whiskering behavior: Indeed, once the growth of Cu_6Sn_5 came effectively to a halt due to slow-downed kinetics upon long-time ageing at room temperature, whisker growth also stopped (as observed in the present experiments).

The near-surface stress-depth profile in real space obtained for the columnar Sn coating on Cu after an ageing time of about 30 days (i.e. during active whisker growth as demonstrated in the present work by SEM investigation) reveals the presence of a pronounced (negative) stress-depth gradient (see Fig. 5.7d). This is compatible with the penetration of Cu_6Sn_5 into the Sn layer along Sn grain boundaries intersecting the

[#] The uniaxial yield limit is about 10-15 MPa for polycrystalline, isotropic bulk Sn [40]; note that the residual stress was measured by X-ray diffraction without controlling the penetration depth and thus the determined stresses represent through-thickness averaged values. The measured stress is thus lower than the maximum stress occurring in the coating

Sn/Cu interface: The compressive stress is generated particularly in the depth range where Cu_6Sn_5 formation proceeds. Consequently, a negative stress-depth gradient in the direction of increasing depth develops in the columnar Sn coating. Such a stress gradient drives (i.e. is relieved by) the transport of Sn atoms to the surface, i.e. the whisker roots. Note that is has been shown recently that lateral, in-plane negative stress gradients occur as well around the whisker-nucleation sites [26]. It is the negative nature of such stress gradients that drives whiskering. Consequently, whisker growth can occur even in the presence of tensile stress parallel to the surface, provided that a negative nature of the stress *gradients* prevails; see the measured near-surface stress-depth profile in the columnar Sn coating on Cu (Fig. 5.7d). The above discussion does not explain why stress relief by Sn transport leads to whiskering at only specific sites. This phenomenon is addressed next (see Fig. 5.8).

The Sn coating, deposited on a rigid substrate (as for example Cu), has a largely columnar grain morphology and is covered with a native Sn-oxide layer on top (the surface oxide forms immediately upon room temperature ageing and has a thickness of several nanometres [10, 29]). The grain boundaries, running from top to bottom, can be strongly pinned at the *(i)* the Sn/oxide interface and *(ii)* the Sn/Cu interface. Consequently, the Cu_6Sn_5-induced compressive stress cannot be relaxed by some mechanism requiring mobile grain boundaries in the coating. Instead it is suggested here that, in order that a whisker can nucleate and grow (causing stress relief), a specific grain-boundary arrangement must be present in the surface adjacent region of the coating: The grain-boundary arrangement at the whisker root (see cross-sectional micrograph *(iii)* in Fig. 5.4a) comprises inclined (with respect to the surface normal) grain boundaries, resembling the grain-boundary arrangement pertaining to some surface grains, as observed directly after layer deposition (see Fig. 5.3 on top). Once the appropriate stress gradients have developed, in particular by pronounced Cu_6Sn_5 formation underneath such surface grains, whisker formation can occur by growth from these already pre-existing surface grains (see Fig. 5.3 at bottom). Significant penetration of Cu_6Sn_5 into the Sn coating along Sn grain boundaries intersecting the Sn/Cu interface, directly underneath such a surface grain, constrained by a grain-boundary arrangement with inclined grain boundaries, leads, in particular at these locations to pronounced compressive stress, especially in in-plane directions in the bottom part of the Sn coating, whereas in the top part of the Sn coating tensile stress is present (cf. Fig. 5.7d). As a result, the stress-depth gradient is associated with a

vacancy concentration-depth gradient (a higher equilibrium vacancies concentration in the tensilely stressed part). This stress (vacancy-concentration) gradient induces mass transport of Sn, likely via grain boundaries (note that the homologous temperature of Sn at room temperature equals about 0.6). This suggests that whiskering can be discussed as a (local, see below) Coble-creep-like phenomenon, as follows:

Coble creep is (obviously) enhanced in (moderately) stressed, *finely* grained materials as the Sn coatings of this study (cf. Ref. [47]). To prevent porosity/void formation upon Coble creep in bulk materials, as the consequence of the change of grain shape by the diffusional mass transport (via grain boundaries), grain-boundary sliding occurs in the bulk materials (i.e. to avoid grain-boundary separation). For the largely columnar Sn coating considered here such grain-shape change does not occur globally but only locally: At locations in the surface adjacent region where a grain-boundary arrangement with inclined grain boundaries occurs, shear stresses act on such inclined grain boundaries (note the planar nature of the state of stress in the Sn coating). It is suggested that the shear stresses acting along the inclined grain boundaries in the surface adjacent part of the Sn coating realize, by establishing shear along these inclined grain boundaries, outward “growth”, i.e. in the “unconstrained” directions, of the surface grains constrained by these inclined grain boundaries. In fact this proposed mechanism involves an localized process of grain-boundary sliding (see Fig. 5.8). Thereby this *local* process of grain-boundary sliding allows local maintenance of Sn transport to the location of whisker nucleation and thereby establishes relaxation of the stress (and thereby vacancy concentration) gradients in the *entire* Sn coating.

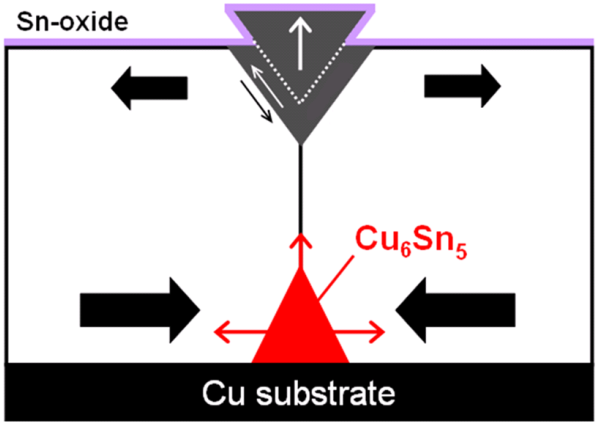

Figure 5.8 Schematic model of whisker formation in a columnar Sn coating on a Cu substrate (upon ageing at room temperature). Significant penetration of Cu_6Sn_5 into the Sn coating along

Sn grain boundaries, directly underneath a surface grain with inclined grain boundaries, leads in particular at these locations to pronounced stress-depth gradients; compressive stress prevails in the bottom part of the Sn coating whereas in the top part of the Sn coating tensile stress is present. This stress gradient (induces a vacancy-concentration gradient and) tends to realize mass transport of Sn form the bottom to the surface of the Sn layer along grain boundaries. At location where a surface grain with inclined grain boundaries is present, such mass transport can be realized on a more or less permanent basis, because shear stresses acting along inclined grain boundaries (as a consequence of the planar state of stress) can realize shear along these inclined grain boundaries leading to outward growth of such surface grains (i.e. whiskering).

5.4.2. Microstructural control of stress relaxation; the role of grain morphology

As compared to coatings with a largely columnar grain morphology (see the discussion in section 5.4.1), finely grain coatings with a high density of inclined (with respect to the surface normal) grain boundaries cDan realize accumulation of grain-shape change, due to diffusional transport induced by the acting stress (-depth) gradients, at many places by grain boundary sliding: Many grain-boundary segments inclined with respect to the surface-normal direction and thus subjected to shear stresses (as a consequence of the state of planar stress), occur in such coatings. Hence Coble-type creep can occur throughout the entire coating. This immediately provides an explanation for the observation that equiaxed coatings do not exhibit whiskering (instead a (marginal) rather uniform thickening of the coating occurs in the out-of-plane direction, as long as significant stress (-depth) gradients exist).

On this basis of the results obtained for the various cases, studied in this work, can be interpreted in a consistent way.

a) SnPb coatings on Cu

Adding of Pb to pure Sn modifies the initial microstructure from columnar to equiaxed (see Fig. 5.2b). The formation of an equiaxed microstructure is due to the simultaneous co-deposition of Sn and Pb: Pb islands formed on Sn grains inhibit upon further deposition the development of columnar Sn grains [48]. Thus, with increasing Pb-content, the Sn grain morphology becomes increasingly more equiaxed and finer.
The developing stress-depth gradients, due to Cu_6Sn_5 formation at the coating/layer interface, leads to diffusional transport of Sn along perpendicular and inclined

(segments of) grain boundaries, in combination with grain-boundary sliding at inclined grain boundaries (segments) leading to grain-shape change (see discussion in section 5.4.1 and at the begin of section 5.4.2). This stress relaxation and grain-shape change process is accompanied by grain coarsening (see Figs. 5.2 and 5.5): A driving force for grain-boundary density reduction always operates and ultimately, given sufficient grain-boundary mobility, an initially present equiaxed microstructure (in a thin film) will (always) be replaced by a columnar grain morphology, as observed (see Figs. 5.2 and 5.5).

In this context it is remarked that the presence of Pb in Sn (along grain boundaries) can bring about a significantly enhanced grain boundary mobility as compared to pure Sn.[+] Hillock formation, i.e. extended lateral growth of a Sn protrusion, instead of whisker formation, can thus be interpreted for in particular SnPb coatings of largely columnar grain morphology, as a consequence of local lateral movement of the few inclined grain boundaries, intersecting the surface, along which grain-boundary sliding, leading to outward transport of Sn, takes place (see Fig. 5.4b). This interpretation is supported by observations of hillock formation in Ref. [52].

Upon adding of Pb to pure Sn the growth morphology of Cu_6Sn_5 changes from initially “irregular” to “regular” (i.e. layer-like) during ageing at room temperature (compare Figs. 5.2b with 5.2a). Due to the precipitation of initially dissolved Pb at grain boundaries (the solubility of Pb in Sn at room temperature is nearly nil), their subsequent growth and the coarsening of the initially present Pb particles at these Sn grain boundaries, these boundaries are no longer available for (further) “irregular” Cu_6Sn_5 formation (see also Ref. [28]), and Cu_6Sn_5 formation along the coating/layer interface is promoted. This change in Cu_6Sn_5 growth morphology is associated with a

[+] Impurities can either enhance or reduce significantly the grain boundary mobility (GBM) of metals. As an example, Ga enhances [49] and Si reduces [50] the GBM of Al.

Additional experiments performed by the present authors showed that significant (in-plane) grain growth can occur, if a columnar SnPb coating on Cu is subjected to a heat treatment at 150°C for 1 h (called “post-bake” in industrial manufacturing [51]), whereas (in-plane) grain growth does *not* occur in columnar and equiaxed (pure, electrodeposited) Sn coatings on Cu applying the same heat treatment. Recently Boettinger *et al.* [7] indeed have shown experimentally by transmission electron microscopy investigations of Sn98Pb2 coatings that small Pb particles prevail along Sn grains boundaries.

less severe level of induced compressive stress, for the same amount of Cu_6Sn_5 formation, as observed (cf. Figs. 5.2 and 5.7).[#]

b) Equiaxed Sn coatings on Cu

In agreement with the discussion in section 5.4.1 and at the begin of section 5.4.2, the pure Sn coating on Cu with an equiaxed grain morphology does not show whisker formation, because grain-shape change by Coble-type creep can be accommodated at many places throughout the microstructure, in contrast with coatings exhibiting a largely columnar grain morphology.

Further, as compared to the SnPb coatings (cf. section 5.4.2a), a much lower grain-boundary mobility in pure Sn obstructs a transition of equiaxed to columnar grain morphology upon ageing at room temperature.

5.5. Avoidance of whisker formation by microstructural control

The whisker-mitigating effect of Pb addition to pure Sn coatings has been controversially discussed in the literature [7, 9, 34, 35]): It was claimed that the addition of Pb to pure Sn affects the growth morphology of Cu_6Sn_5 at the coating/layer interface [34], the crystallographic texture of the Sn coating [34], the grain morphology of the Sn coating [7, 34] and the residual stress evolution of the coating [7, 9, 34, 35]. A coherent understanding of the Pb-induced mechanism of whisker mitigation has not been presented until now.

This work shows that the effect of Pb regarding prevention of whiskering is due to the Pb-induced, equiaxed grain morphology of the SnPn coating. Indeed, a pure Sn coating of equiaxed grain morphology also does *not* show whisker formation (see Fig. 5.2c). This implies further that the effect of Pb on the Cu_6Sn_5 morphology ("regular/planar" instead of "irregular") is not of governing importance for mitigation of whisker formation (albeit a lower level of compressive stress and a less pronounced

[#] Both "irregular" and "regular" growth of Cu_6Sn_5 at the Sn side of the Sn/Cu interface is accompanied by the same specific volume increase, but irregular growth of Cu_6Sn_5 is much more effective in generating in-plane compressive stress due to its pronounced (inhomogeneous) in-plane expansion into the Sn. Regular (layer-like) growth of Cu_6Sn_5 orientated along the Sn/Cu interface exhibits a less pronounced (and rather homogenous) out-of-plane volume expansion into the Sn which is much less effective in generating in-plane compressive stress.

stress-depth gradient occur as a result of this effect; see section 5.4.2a). The same holds for the grain-boundary mobility enhancing effect of Pb, which leads to rapid grain growth leading to a transition of the grain morphology from equiaxed to columnar (see section 5.4.2a).

Pb acts "just" as an agent to bring about an equiaxed grain morphology in the Sn coating. As a general conclusion it is proposed to suppress spontaneous whiskering on Sn coatings by microstructural control, i.e. to bring about an equiaxed grain morphology. This can be done, e.g. by appropriate choice of the chemistry of the electrolyte, the substrate material and/or the deposition routine.

5.6. Conclusions

- Spontaneous whiskering on the surface of Sn coatings with a columnar grain morphology deposited on Cu is the outcome of a localized stress relaxation mechanism which runs as follows: *(i)* Formation of the intermetallic compound Cu_6Sn_5 in the coating at the interface with the substrate induces a negative stress-depth gradient (tensile → compressive) in the coating. *(ii)* The stress-depth gradient is associated with a vacancy-concentration depth gradient. Thereby mass transport is generated from the bottom to the upper part of the coating. Such mass transport in principle leads to a grain-shape change, which has to be accommodated: Coble-type creep. *(iii)* Grain-boundary sliding, as a natural mechanism to maintain the massive nature of the specimen upon Coble-type creep is only possible on a more or less permanent basis for the few surface grains, in the largely columnar coating, which are constrained by grain boundaries inclined with respect to the surface normal. Shear forces act only along inclined grain boundaries in the coating (planar state of stress). Thus whiskering is conceived as the outcome of local process of grain-boundary sliding allowing local maintenance of Sn transport to the location of whisker nucleation, thereby establishing relaxation of stress gradients in the entire coating. Hillock formation, instead of whisker formation, occurs in a largely columnar coating, if the inclined grain boundary segments have a relatively high mobility as holds for SnPb coatings.
- In finely grained (SnPb and pure Sn) coatings with an equiaxed grain morphology many (segments) of grain boundaries inclined with respect to the surface normal occur and thus are subjected to shear stress (due to the planar state of stress). Now

grain-shape change due to diffusional transport along grain boundaries, induced by the acting stress (-depth) gradients, can be accommodated at many places throughout the coating, i.e. globally, by grain-boundary sliding. The net morphological change is a (slight) increase of the coating thickness. Thus it is proposed to suppress spontaneous whiskering on Sn coatings by microstructural control, i.e. to bring about an equiaxed grain morphology.

- Side effects of the addition of Pb to the Sn coating are: *(i)* A lower level of residual compressive stress and thus a smaller stress-depth gradient, because occupation of the grain boundaries in the coating by Pb promotes Cu_6Sn_5 formation in a planar fashion along the interface. *(ii)* An increase of the mobility of the grain boundaries in the coating causing a transition from an initially equiaxed grain morphology to an ultimately columnar grain morphology.

Acknowledgment

The authors are much obliged to the company ‘Hans Heimerdinger Oberflächentechnik’ in Pforzheim (Germany) for specimen preparation.

References

[1] Tu K. N., Chen C. & Wu A. T. (2007). *J. Mater. Sci. - Mater. Electron* **18**, 269.

[2] Fisher R. M., Darken L. S. & Carroll K. G. (1954). *Acta Metall.* **2**, 368.

[3] Herring C. & Galt J. K. (1952). *Phys. Rev.* **85**, 1060.

[4] LeBret J. B. & Norton M. G. (2003). *J. Mater. Res.* **18**, 585.

[5] Lee B. Z. & Lee D. N. (1998). *Acta Mater.* **46**, 3701.

[6] Hasiguti R. R. (1955). *Acta Metall.* **3**, 200.

[7] Boettinger W. J., Johnson C. E., Bendersky L. A., Moon K.-W., Williams M. E. & Stafford G. R. (2005). *Acta Mater.* **53**, 5033.

[8] Tu K. N. (1973). *Acta Metall.* **21**, 347.

[9] Chason E., Jadhav N., Chan W. L., Reinbold L. & Kumar K. S. (2008). *Appl. Phys. Lett.* **92**, 171901.

[10] Kumar K. S., Reinbold L., Bower A. F. & Chason E. (2008). *J. Mater. Res.* **23**, 2916.

[11] Galyon G. T. (2005). *IEEE Trans. Electron. Packag. Manuf.* **28**, 94.

[12] Sheng G. T. T., Hu C. F., Choi W. J., Tu K. N., Bong Y. Y. & Nguyen L. (2002). *J. Appl. Phys.* **92**, 64.

[13] Fyre A., Galyon G. T. & Palmer L. (2007). *IEEE Trans. Electron. Packag. Manuf.* **30**, 2.

[14] Zhang W., Egli A., Schwager F. & Brown N. (2005). *IEEE Trans. Electron. Packag. Manuf.* **28**, 85.

[15] Williams M. E., Moon K.-W., Boettinger W. J., Josell D. & Deal A. D. (2007). *J. Electron. Mater.* **36**, 214.

[16] Osenbach J. W., DeLucca J. M., Potteiger B. D., Amin A., Shook R. L. & Baiocchi F. A. (2007). *IEEE Trans. Electron. Packag. Manuf.* **30**, 23.

[17] Ellis W. C., Gibbons D. F. & Treuting R. C. (1958). *In Growth and Perfection of Crystals* edited by Doremus, R. H., Roberts, B. W. and Turnbull, D. (Wiley, New York, 1958), pp. 102-120.

[18] Eshelby J. D. (1953). *Phys. Rev.* **91**, 755.

[19] Frank F. C. (1953). *Philos. Mag.* **44**, 854.

[20] Franks J. (1958). *Acta Metall.* **6**, 103.

[21] Furuta N. & Hamamura K. (1969). *Jpn. J. Appl. Phys.* **9**, 1404.

[22] Hutchinson B., Oliver J., Nylen M. & Hagström J. (2004). *Mater. Sci. Forum* **467-470**, 465.

[23] Buchovecky E. J., Du N. & Bower A. F. (2009). *Appl. Phys. Lett.* **94**, 191904.

[24] Osenbach J. W. (2009). *J. Appl. Phys.* **106**, 094903.

[25] Sobiech M., Welzel U., Mittemeijer E. J., Hügel W. & Seekamp A. (2008). *Appl. Phys. Lett.* **93**, 011906.

[26] Sobiech M., Wohlschlögel M., Welzel U., Mittemeijer E. J., Hügel W., Seekamp A., Liu W. & Ice G. E. (2009). *Appl. Phys. Lett.* **94**, 221901.

[27] Dyson B. F., Anthony T. R. & Turnbull D. (1967). *J. Appl. Phys.* **38**, 3408.

[28] Sobiech M., Krüger C., Welzel U., Wang J., Mittemeijer E. J. & Hügel W. (2010). *Acta Mater.*, in preparation.

[29] Sobiech M., Welzel U., Schuster R., Mittemeijer E. J., Hügel W., Seekamp A. & Müller V. (2007). *in Proc. of the 57th Electronic Components and Technology Conference in Reno, USA*, 192.

[30] Compton K. G., Mendizza A. & Arnold S. M. (1951). *Corrosion* **7**, 327.

[31] Brusse J. A., Ewell G. J. & Siplon J. P. (2002). *in Proc. of the 16th Passive Components Symposium, CARTS EUROPE*, 221.

[32] Arnold S. M. (1966). *Plating* **53**, 96.

[33] Directive 2002/95/EC of the European Parliament and of the Council of 27 January 2003 on the restriction of the use of certain hazardous substances in electrical and electronic equipment (2003). *Official Journal of the European Union* **L37**, 19.

[34] Zhang W. & Schwager F. (2006). *J. Electrochem. Soc.* **153**, C337.

[35] Murakami K., Okano M., Hino M., Takamizawa M. & Nakai K. (2008). *J. Japan Inst. Metals* **72**, 648.

[36] Leoni M., Welzel U. & Scardi P. (2004). *J. Res. Natl. Inst. Stand. Technol.* **109**, 27.

[37] Kumar A., Welzel U. & Mittemeijer E. J. (2006). *J. Appl. Crystallogr.* **39**, 633.

[38] Wohlschlögel M., Schülli T. U., Lantz B. & Welzel U. (2008). *J. Appl. Crystallogr.* **41**, 124.

[39] Welzel U., Ligot J., Lamparter P., Vermeulen A. C. & Mittemeijer E. J. (2005). *J. Appl. Crystallogr.* **38**, 1.

[40] Gale W. F. (2004). *Smithells Metals Reference Book*. London: Butterworths.

[41] Pedigo A. E., Handwerker C. A. & Blendell J. E. (2008). *Proceedings of the 57th Electronic Components and Technology Conference in Orlando, USA*, 1498.

[42] Delhez R., De Keijser T. H. & Mittemeijer E. J. (1987). *Surf. Eng.* **3**, 331.

[43] Dölle H. J. (1979). *J. Appl. Crystallogr.* **12**, 489.

[44] Behnken H. & Hauk V. (2000). *Mater. Sci. Eng. A* **300**, 41.

[45] Boulle A., Masson O., Guinebretiere R. & Dauger A. (2003). *J. Appl. Crystallogr.* **36**, 1424.

[46] Wohlschlögel M., Welzel U. & Mittemeijer E. J. (2009). *J. Mater. Res.* **24**, 1342.

[47] Courtney T. H. (2000). *Mechanical behaviour of materials*. Boston: McGraw-Hill.

[48] Petersson I. & Ahlberg E. (2000). *Journal of Electroanalytical Chemistry* **485**, 166.

[49] Molodov D. A., Czubayko U., Gottstein G., Shvindlerman L. S., Straumal B. & Gust W. (1995). *Philosophical Magazine Letters* **72**, 361.

[50] Zhang Y., Lu G. H., Zhang H., Wang T., Deng S. H. & Hu X. L. (2007). *2006 Beijing International Materials Week* **546** 829.

[51] Dittes M., Oberndorff P. & Petit L. (2003). *in Proc. of the 53rd ECTC Conference in New Orleans, USA* 822.

[52] Jadhav N., Buchovecky E. J., Chason E. & Bower A. F. (2010). *JOM* **62**, 30.

6. Driving force for Sn-whisker growth in the system Cu-Sn

M. Sobiech, U. Welzel, E.J. Mittemeijer ,W. Hügel and A. Seekamp

Abstract

The evolution of residual stress gradients in Sn thin films on Cu-substrates upon ageing at ambient temperature has been investigated, for specimens which do exhibit and which do *not* exhibit Sn-whisker growth, by performing X-ray diffraction stress measurements at constant penetration depths. Comparison of the measured near-surface stress-depth profiles for both types of specimens, as function of ageing time at ambient temperature, showed that a significant negative stress gradient from the surface towards the Sn/Cu-interface is decisive for Sn-whisker growth in the system Cu-Sn.

6.1. Introduction

Since more than 50 years it is well known that pure Sn thin films deposited on Cu are very prone to formation of single-crystalline [1, 2] Sn-whiskers exhibiting growth rates of around 1 Å/s [3-5] and up to 10000 Å/s in the presence of externally applied mechanical stresses [2]. Sn-whiskers grow through continuous addition of material to their base (i.e. the part of a Sn-whisker once 'extruded' from the Sn layer remains morphologically unchanged during further growth) [6] and their growth morphologies exhibit a great diversity (see Fig. 6.1). The diameters of Sn-whiskers are about 1-10 µm, while their length can reach values up to several millimetres [7]. Nowadays pure Sn is the material of choice for use as surface finish of leadframe materials in microelectronic devices. However, the uncontrolled filamentary Sn-whisker growth can cause short-circuit failure by bridging fine-pitched (~ 200 µm) leadframe legs of modern microchip packages and therefore Sn-whiskering is of great concern for high-reliability applications.

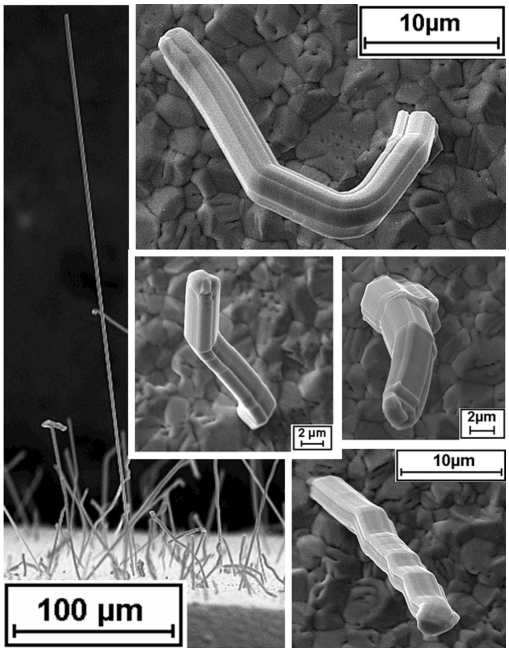

Figure 6.1: Scanning electron microscopy images of several Sn-whiskers showing different growth morphologies.

Several models have been proposed for the mechanism of Sn-whisker growth on Cu [3, 5, 8-15], but none of these is able to explain the moment of whiskering and all observed phenomena. After Sn deposition and during subsequent ageing at ambient

temperature, Cu diffuses into the Sn thin film [16, 17] and the formation of the intermetallic compound Cu_6Sn_5 takes place at the Cu/Sn-interface [17], preferentially along the Sn grain boundaries intersecting the Cu/Sn interface [13, 14]. The Cu_6Sn_5 formation is accompanied by a volume expansion and as a consequence, residual compressive stresses can be generated in the Sn thin films. Such compressive stresses have been conceived as driving the formation of Sn-whiskers on the Sn surface [14, 18] and whisker growth can thus be regarded as a stress relief phenomenon [10, 12, 14, 17]. It has been speculated that negative stress gradients either in the direction from the Sn surface towards the intermetallic compound region near the interface with the substrate [13-15, 17, 19] or parallel to the surface of the Sn layer in the direction from the whisker root towards the whisker surroundings, would drive the transport of Sn atoms to the whisker root and thus realize Sn-whisker growth [15, 20]. Sound experimental evidence for any of these hypotheses lacks until now.

6.2. Experimental

Sn thin films with a thickness of about 4 µm were electrodeposited on pure Cu-substrates (commercial leadframe material) using industrial electrolytes. The Sn grain morphology is columnar with in-plane grain sizes of 2-5 µm. The layer has a {321}-fibre texture (for further details concerning specimen preparation see Ref. [18]). One group of specimens was aged directly after Sn deposition at ambient temperature (called 'as-deposited' in the following) and the other group of specimens was first annealed, within 24 h after Sn deposition, at 150°C for 1 hour using a conventional furnace (this treatment is called 'post-bake' in the following) and then subsequently aged at ambient temperature. The 'post-bake' treatment is applied in industrial manufacturing as a mitigation treatment regarding whisker formation [21, 22].

Micrographs of the Sn layer surface were obtained with a LEO 1450 VP scanning electron microscope, using an acceleration voltage of 15 kV and a beam current between 100 to 200 pA. The cross sectional grain morphologies of the Sn layers were investigated by focused ion beam (FIB) imaging using a NOVO 600 NanoLab workstation.

X-ray diffraction stress measurements at constant penetration depths were performed employing a Bruker TXS D8 Discover diffractometer operating in parallel beam geometry (parallelization was realized by means of a 2D-collimating X-ray

mirror (Xenocs Fox 2D), see Ref. [23]) with a X-ray beam size of 0.8 x 0.8 mm2 and Cu-Kα radiation emerging from the point focus (100 x 100 µm2 under take off angle of 6°) of a rotating micro-focus X-ray anode working at 50 kV / 20 mA. The specimen was mounted on an Eulerian cradle which allowed tilting and rotating the specimen as required for depth-dependent X-ray diffraction stress measurements according to the method developed in Ref. [24]. The diffracted beam was passed through a parallel-plate collimator used as secondary optics and was subsequently recorded by an energy-dispersive detector with a geometrical acceptance window of around 1 x 1 cm2.

Based on direction and position dependent X-ray diffraction stress measurements in the specimen frame of reference, the mechanical macrostress state of the Sn thin films was found to be planar, approximately rotationally symmetric and laterally inhomogeneous. The lateral inhomogeneity with respect to the state of stress is ascribed to the inhomogeneous formation of intrinsic growth stresses during electrodeposition. All stress measurements performed on the same specimen position were carried out along the same in-plane direction in the specimen frame of reference and thus only one component, □‖ (stress parallel to the Sn layer surface), of the stress tensor will be reported. Mechanical stresses were calculated from lattice strains measured employing the 321 reflection on the basis of the sin2ψ-method [25]. The specimen was assumed to be macroscopically elastically quasi-isotropic and therefore the hkl-dependent diffraction (X-ray) elastic constants Shkl1 and ½Shkl2 were derived from single-crystal data [26] using the Neerfeld-Hill model [25]. In order to control the penetration depth (and thus the information depth) of the X-ray beam, a combined ω-χ-ϕ tilting (ω, χ and ϕ are instrumental angles describing the orientation of the specimen with respect to the laboratory frame of reference) of the specimen was applied. The complete strategy for X-ray diffraction stress measurements at fixed penetration depths has been described in detail elsewhere [24].

6.3. Results and Discussion

The through-thickness averaged (see below) residual macrostress evolutions of 'as-deposited' and 'post-baked' specimens as a function of ageing at ambient temperature were investigated using the side-inclination method without controlling the penetration depth of the X-ray beam during the stress measurement [18]. The residual stresses of the 'as-deposited' specimen changed after about 2 days from

initially tensile (~ 10 MPa) to compressive. Sn-whisker formation occurred about 10 days after Sn deposition when the compressive stress had reached a plateau value of around - 8 MPa. The residual stresses of the 'post-baked' specimen (initial state of stress of about 10 MPa) decreased but remained tensile up to an ageing time of about 30 days and apparently had reached a plateau value of about 2-4 MPa (in agreement with results reported in Ref. [14]). The next stress data for the 'post-baked' specimen was collected around 210 days after Sn deposition and a compressive stress of about -8 MPa was found. Yet, throughout the entire observation period, no whisker formation could be detected (additional long-term observations revealed that 'post-baked' specimens did not exhibit whisker growth for time periods up to, at least, three years). The above result indicates that specimens subjected to a 'post-bake' treatment can develop compressive stresses upon long-time ageing at ambient temperature. Hence, the presence of compressive mechanical stress is by itself not a sufficient condition for whisker formation.

The 'post-bake' treatment does neither affect the crystallographic texture of the Sn layer nor the Sn-oxide thickness on the Sn surface (see for further details Ref. [18]). Two important microstructural differences of 'as-deposited' and 'post-baked' specimens were observed: First, after 'post-bake' treatment the intermetallic compound at the Cu/Sn-interface consists of two phases (Cu_6Sn_5 and Cu_3Sn, see Fig. 6.2. Cu_3Sn formation occurs only at temperatures exceeding 60°C [17]). Secondly, the morphology of the intermetallic compound at the Cu/Sn-interface was more regular and more planar in the specimen subjected to the 'post-bake' treatment. An initially flat intermetallic compound layer, consisting of Cu_6Sn_5 and Cu_3Sn, formed during 'post-bake' treatment (see Fig. 6.2, dotted line). Upon subsequent long-time ageing at ambient temperature further growth of the intermetallic compound Cu_6Sn_5 occurs along the Sn grain boundaries (see Fig. 6.2, solid line) and at this stage the character of the stress for the 'post-baked' specimen changed from tensile to compressive. The comparatively thick 'post-bake'-induced intermetallic compound layer acts as a diffusion barrier for Cu and decelerates therefore additional Cu_6Sn_5 growth, and thereby compressive stress development, during ambient temperature ageing [22].

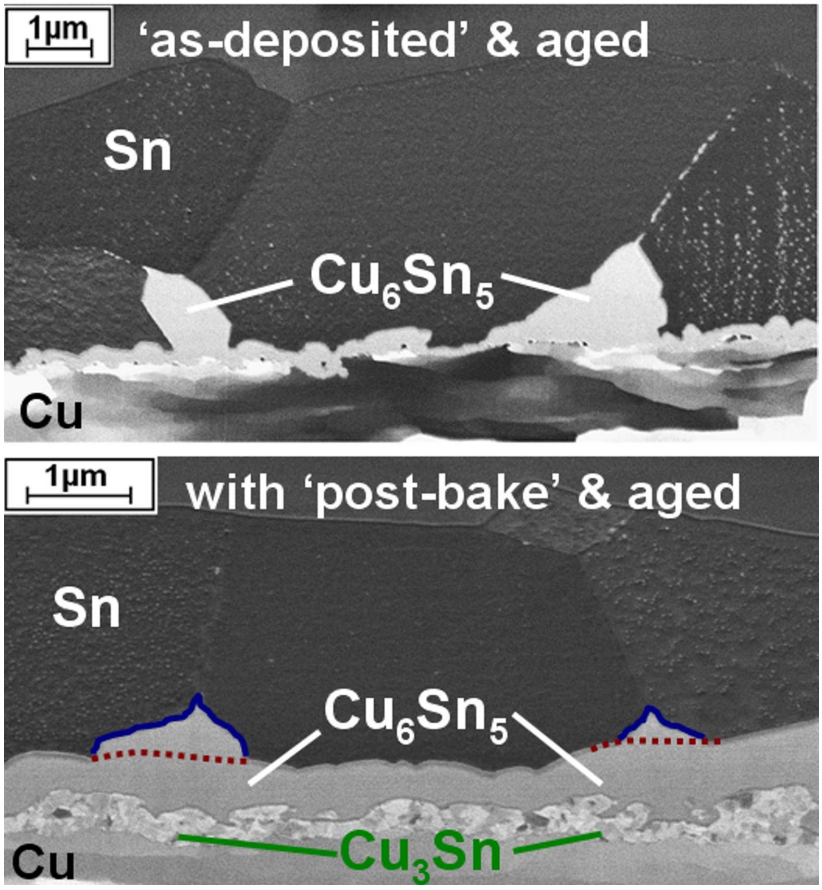

Figure 6.2: FIB-cross sectional micrographs of 'as-deposited' and 'post-baked' specimens taken about 8 months after Sn deposition. The 'as-deposited' specimen (see image on top) exhibits a very irregular Cu_6Sn_5 formation along the Sn grain boundaries starting at the Cu/Sn-interface. The dotted line (see image at bottom) indicates the rather flat intermetallic compound layer present directly after 'post-bake' treatment. Upon long-time ageing at ambient temperature of the 'post-baked' specimen further modest growth of Cu_6Sn_5 (see solid line in image at bottom) occurred along the Sn grain boundaries.

The X-ray diffraction stress measurements discussed above and as reported in the literature, all have been performed without control of the penetration depth of the X-rays and, in view of the modest thickness of the Sn layers, therefore the stress values derived on that basis have to be considered as through-thickness averaged residual stresses. In order to assess stress gradients in the direction of increasing depth, X-ray diffraction stress measurements at different controlled penetration depths τ were conducted in this work using the method developed in Ref. [24]. A measured stress-depth profile using X-ray diffraction represents the Laplace transformed stress-depth profile in real space [27]. In order to derive the stress-depth profile in real space an

inverse Laplace transformation has been developed and performed here using an iterative procedure (an analytical approach is not possible [28]).

The near-surface stress-depth profiles in real space as obtained upon ageing at ambient temperature for 'as-deposited' and 'post-baked' specimens after one day (before whisker formation for the 'as-deposited' specimen) and after about 8 months (during whisker growth for the 'as-deposited' specimen) are shown in Fig. 6.3. The stress-depth profiles for both types of specimens after ageing at ambient temperature for one day show that negligible stress gradients were present in the near-surface regions. After about 8 months of ageing at ambient temperature the stress-depth profile taken for the 'as-deposited' specimen reveals a significant negative stress gradient near the surface of the Sn layer, whereas no stress gradient is observed for the 'post-baked' specimen.

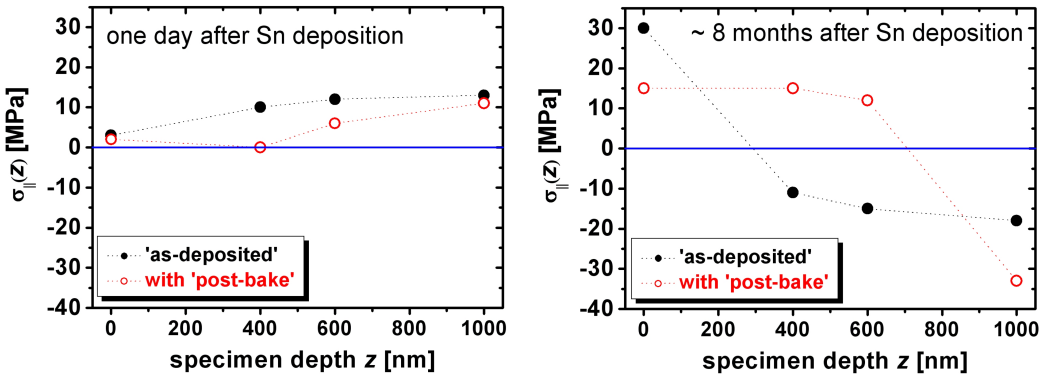

Figure 6.3: Near-surface stress-depth profiles in real space derived from the as measured stress-depth profiles in Laplace space, for 'as-deposited' and 'post-baked' specimens for ageing times at ambient temperature of one day (i.e. before the onset of whisker formation for the 'as-deposited' specimen) and of about 8 months (i.e. during whisker growth for the 'as-deposited' specimen).

Based on the microstructural characteristics visible in the FIB-cross sectional micrographs of these specimens (see Fig. 6.2), the evolution of the residual stress gradients observed for both types of specimens can be understood as follows. The 'as-deposited' specimen reveals a very irregular Cu_6Sn_5 formation at the Cu/Sn-interface characterized by deep penetration of Cu_6Sn_5 along the Sn grain boundaries of the Sn layer. Recognizing the specific volume increase associated with Cu_6Sn_5 formation, the stress in the Sn layer, in particular at the depths where Cu_6Sn_5 had formed along the Sn grain boundaries, must become compressive as lateral expansion of the Sn grain

boundaries in the depth range concerned is constrained by the adjacent Sn grains. In case of the 'post-baked' specimen, only after long-time ageing at ambient temperature Cu_6Sn_5 formation along the Sn grain boundaries occurred (see Fig. 6.2, solid line). However, the penetration of Cu_6Sn_5 along the Sn grain boundaries is very much less than for the 'as-deposited' specimen. Hence, considering the mechanism for compressive stress generation as discussed above for the 'as-deposited' Sn layer, the generation of compressive stresses in the 'post-baked' specimen occurs to a much lesser extent and, in particular, is concentrated in a depth range much closer to the Cu/Sn-interface than for the 'as-deposited' specimen.

6.4. Conclusions

The following conclusion can be drawn for the investigated Cu-Sn specimens (for time scales of the order of the investigation period that is up to, at least, several years): The development of a negative stress gradient in the direction from the surface of the Sn layer to the intermetallic compound region near the interface with the substrate is decisive for Sn-whisker growth. Due to such a stress gradient transport to the surface of Sn atoms perpendicular to the surface/interface is promoted and thus whisker growth serves as a stress-relief mechanism. Note that a prerequisite for this mechanism of whisker formation is the presence of a negative stress gradient, but that it is not required that the stress at the Sn surface is compressive. Indeed, this work has shown that even a tensile stress at the Sn surface in combination with a negative stress gradient leads to whisker formation. Thus the 'post-bake' treatment is successful in mitigating whisker formation not because a compressive stress is avoided (in fact upon long-time ageing at ambient temperature a compressive stress does occur), but because a negligible stress gradient occurs in the near-surface region of the Sn thin film.

Acknowledgment

The authors would like to thank M. Wohlschlögel (Max Planck Institute for Metals Research, Stuttgart, Germany) for assistance during experimentation and for constructive discussions concerning data evaluation.

References

[1] Herring C. & Galt J. K. (1952). *Phys. Rev.* **85**, 1060.

[2] Fisher R. M., Darken L. S. & Carroll K. G. (1954). *Acta Metall.* **2**, 368.

[3] Ellis W. C., Gibbons D. F. & Treuting R. C. (1958). *In Growth and Perfection of Crystals* edited by Doremus, R. H., Roberts, B. W. and Turnbull, D. (Wiley, New York, 1958), pp. 102-120.

[4] Glazunova V. K. & Kudryavtsev N. T. (1963). *Russ. J. Appl. Chem.Russ. J. Appl. Chem.* **36**, 543.

[5] Furuta N. & Hamamura K. (1969). *Jpn. J. Appl. Phys.* **9**, 1404.

[6] Koonce S. E. & Arnold S. M. (1954). *J. Appl. Phys.* **25**, 134.

[7] Key P. L. (1970). *in Proc. of the 20th Electronic Components Conference*, 155.

[8] Eshelby J. D. (1953). *Phys. Rev.* **91**, 755.

[9] Frank F. C. (1953). *Philos. Mag.* **44**, 854.

[10] Hasiguti R. R. (1955). *Acta Metall.* **3**, 200.

[11] Franks J. (1958). *Acta Metall.* **6**, 103.

[12] Lindborg U. (1976). *Acta Metall.* **24**, 181.

[13] Tu K. N. (1994). *Phys. Rev. B* **49**, 2030.

[14] Lee B. Z. & Lee D. N. (1998). *Acta Mater.* **46**, 3701.

[15] Tu K. N., Chen C. & Wu A. T. (2007). *J. Mater. Sci. - Mater. Electron* **18**, 269.

[16] Dyson B. F., Anthony T. R. & Turnbull D. (1967). *J. Appl. Phys.* **38**, 3408.

[17] Tu K. N. (1973). *Acta Metall.* **21**, 347.

[18] Sobiech M., Welzel U., Schuster R., Mittemeijer E. J., Hügel W., Seekamp A. & Müller V. (2007). *in Proc. of the 57th Electronic Components and Technology Conference in Reno, USA*, 192.

[19] Galyon G. T., Xu C., Lal S., Notohardjono B. & Palmer L. (2005). *in Proc. of the 55th Electronic Components and Technology Conference in Lake Buena Vista, USA*, 421.

[20] Choi W. J., Lee T. Y., Tu K. N., Tamura N., Celestre S., MacDowell A. A., Bong Y. Y. & Nguyen L. (2003). *Acta Mater.* **51**, 6253.

[21] Dittes M., Oberndorff P. & Petit L. (2003). *in Proc. of the 53rd ECTC Conference in New Orleans, USA* 822.

[22] Osenbach J. W., Shook R. L., Vaccaro B. T., Potteiger B. D., Amin A. N., Hooghan K. N., Suratkar P. & Ruengsinsub P. (2005). *IEEE Trans. Electron. Packag. Manuf.* **28**, 36.

[23] Wohlschlögel M., Schülli T. U., Lantz B. & Welzel U. (2008). *J. Appl. Crystallogr.* **41**, 124.

[24] Kumar A., Welzel U. & Mittemeijer E. J. (2006). *J. Appl. Crystallogr.* **39**, 633.

[25] Welzel U., Ligot J., Lamparter P., Vermeulen A. C. & Mittemeijer E. J. (2005). *J. Appl. Crystallogr.* **38**, 1.

[26] Gale W. F. (2004). *Smithells Metals Reference Book*. London: Butterworths.

[27] Dölle H. J. (1979). *J. Appl. Crystallogr.* **12**, 489.

[28] Behnken H. & Hauk V. (2000). *Mater. Sci. Eng. A* **300**, 41.

7. Local, submicron, strain gradients as the cause of Sn whisker growth

M. Sobiech, M. Wohlschlögel, U. Welzel, E. J. Mittemeijer, W. Hügel, A. Seekamp, W. Liu and G. E. Ice

Abstract

It has been shown experimentally that local *in-plane residual strain gradients* occur around the root of spontaneously growing Sn whiskers on the surface of Sn coatings deposited on Cu. The strain distribution has been determined with synchrotron white beam micro Laue diffraction measurements. The observed *in-plane residual strain gradients* in combination with recently revealed *out-of-plane residual strain-depth gradients* [M. Sobiech, U. Welzel, E. J. Mittemeijer, W. Hügel, and A. Seekamp, Appl. Phys. Lett. **93**, 011906 (2008)] provide the driving forces for whisker growth.

7.1. Introduction

The mechanisms of spontaneous formation and growth of Sn whiskers from surfaces of Sn coatings deposited on Cu represent a controversially discussed phenomenon since more than 50 years [1, 2]. As nowadays the system Sn-Cu will usually be applied for interconnection of electronic systems, filamentary Sn whiskering on Sn coated leadframe legs of modern microelectronic devices constitutes an issue of great technological relevance, because whisker-induced short-circuit failures have resulted in enormous costs including failures of satellites, military and medical devices [1].

Sn whiskers are 'nearly' perfect single crystal filamentary structures [3, 4] (see Fig. 7.1) with diameters of ~ 1-10 µm and with lengths up to several millimetres. Whiskers grow through continuous addition of material to their base [5] with growth rates of around 0.1 nm/s [6] and up to 1000 nm/s in the presence of externally applied mechanical stresses [4]. Despite of 50 years of study, no proposed model to date is capable of explaining all key features of whisker growth behavior on Sn thin films deposited on Cu [2, 6-13] (e.g. moment of whiskering, location of nucleation sites, kinetics of growth and development of specific surface morphologies).

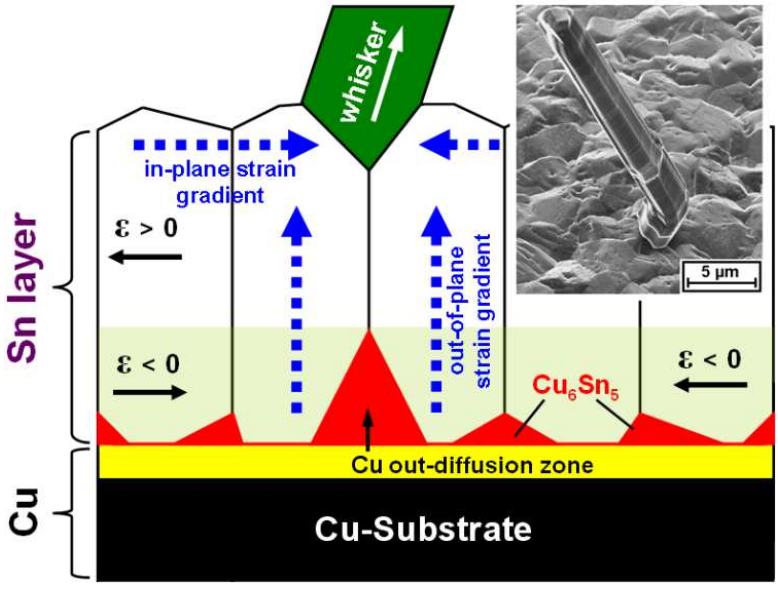

Figure 7.1: Schematic model, on the basis of the results of the present work, of the whisker-formation process in Sn thin films deposited on Cu substrates upon ageing at room temperature. The focused ion beam micrograph illustrates the growth morphology of a Sn whisker.

The driving force for whisker growth has been attributed by the majority of researchers to a build-up of mechanical compressive strains in the Sn coating during and/or after layer production and thus whisker growth can be regarded as a strain relief phenomenon [2, 7-9, 13-16]. Compressive strains in the Sn coating develop upon ageing at room temperature due to intermetallic phase formation at the Cu/Sn interface: After Sn deposition and during subsequent ageing at room temperature, Cu diffuses into the Sn thin film [14, 17] leading to the formation of the intermetallic compound Cu_6Sn_5 [14], preferentially along the Sn grain boundaries intersecting the Cu/Sn interface [2, 8, 18]. The Cu_6Sn_5 formation is accompanied by a volume expansion and as a consequence, residual compressive strains parallel to the surface can be generated in the Sn thin film [2, 8, 18]. It has been speculated that negative strain gradients either in the direction from the Sn surface toward the intermetallic compound region near the interface with the substrate [1, 2, 8, 14, 18] (i.e., the strain becomes less compressive toward the Sn surface) or parallel to the surface of the Sn layer in the direction from the whisker root toward the whisker surroundings (i.e., the strain becomes less compressive toward the whisker root), drive the transport of Sn atoms to the whisker root and thus control Sn whisker growth [2, 19]. However, conclusive experimental evidence for the presence or absence of strain gradients has remained elusive.

Only very recently, experimental evidence has been presented which indicates that compressive strains are not a prerequisite for whisker formation, but that, instead, the strain *gradient* in the direction from the surface of the Sn layer to the intermetallic compound region must be negative [20]. Thus whisker growth can occur in the presence of a tensile strain in the surface region of the Sn layer.

A previous attempt to assess the residual strain distribution around a Sn whisker using the white beam Laue diffraction technique [19] suffered from low experimental accuracy for strain detection. Moreover, the present work demonstrates that it is of paramount importance to conduct strain characterization around the whisker *during its ongoing growth*, because otherwise the locally acting driving force(s) are likely absent. In this letter we discuss the role of *in-plane residual strain gradients* determined experimentally around the root of growing Sn whiskers in combination with recently revealed *out-of-plane residual strain-depth gradients* [20] (see section above) as driving forces for whisker growth.

In the present work Sn thin films with a thickness of about 3 µm were electrodeposited onto pure Cu substrates (commercial leadframe material) using an industrial electrolyte by employing a laboratory electro-deposition setup. The Sn layer has a {321}-fiber texture and a columnar Sn grain morphology with in-plane grain sizes of 2-5 µm (for further details see Ref. [18]). Directly after Sn deposition the surface of the specimens was rinsed with methanol and subsequently the specimens were dried and aged at room temperature (i.e. storage at ~ 22°C/ 25-50% relative humidity without controlling the ambient atmosphere). The first whiskers were observed roughly 4 days after Sn deposition.

7.2. Experimental

In order to experimentally determine the strain distribution around growing Sn whiskers, high-resolution white beam micro Laue diffraction measurements were performed at the synchrotron beamline 34ID-E [21] at the Advanced Photon Source (APS) of the Argonne National Laboratory (Argonne, Illinois, USA). The region around the root of growing Sn whiskers covering an area of ~ 20 x 20 μm^2 was step-scanned (with steps of 0.5 µm steps using an x-y translation stage) with a polychromatic (8-24 keV) focused x-ray beam of ~ 0.3 x 0.3 μm^2. Since the size of the Sn grains is larger than the focused x-ray beam, a single crystal micro-diffraction Laue pattern was recorded for each probed specimen position. In combination with a high-precision CCD area detector for data collection, two dimensional (i.e. the diffraction data recorded at each probed specimen position contain information from all positions along the penetration depth through the film thickness of around 3 µm) residual strain measurements were performed on the basis of white beam Laue diffraction. By using computer-automated peak search routines the angular positions of the Bragg reflections were determined and by employing pattern-recognition software the diffraction pattern could be indexed with respect to reference patterns [22]. The crystallographic orientation and the (deviatoric) strain tensor components were derived directly from the indexed Laue diffraction patterns. The accuracy of this method depends strongly on the experimental setup and on the resolution of the CCD detector used for the measurement. In the present study the diagonal (deviatoric) strain tensor components could be determined with an accuracy of about 0.01% strain.

7.3. Results and Discussion

After ageing the specimen at room temperature for around 40 days, two dimensional micro-diffraction measurements were made around the root of growing Sn whiskers. The crystallographic orientation map and the corresponding diagonal (deviatoric) strain tensor components measured at each probed position in the vicinity of a whisker root (see Fig. 7.3) are shown in Fig. 7.2. Also shown are the radially averaged values of these strain tensor components around the whisker root. Off-diagonal components are not shown due to significantly higher strain uncertainty.

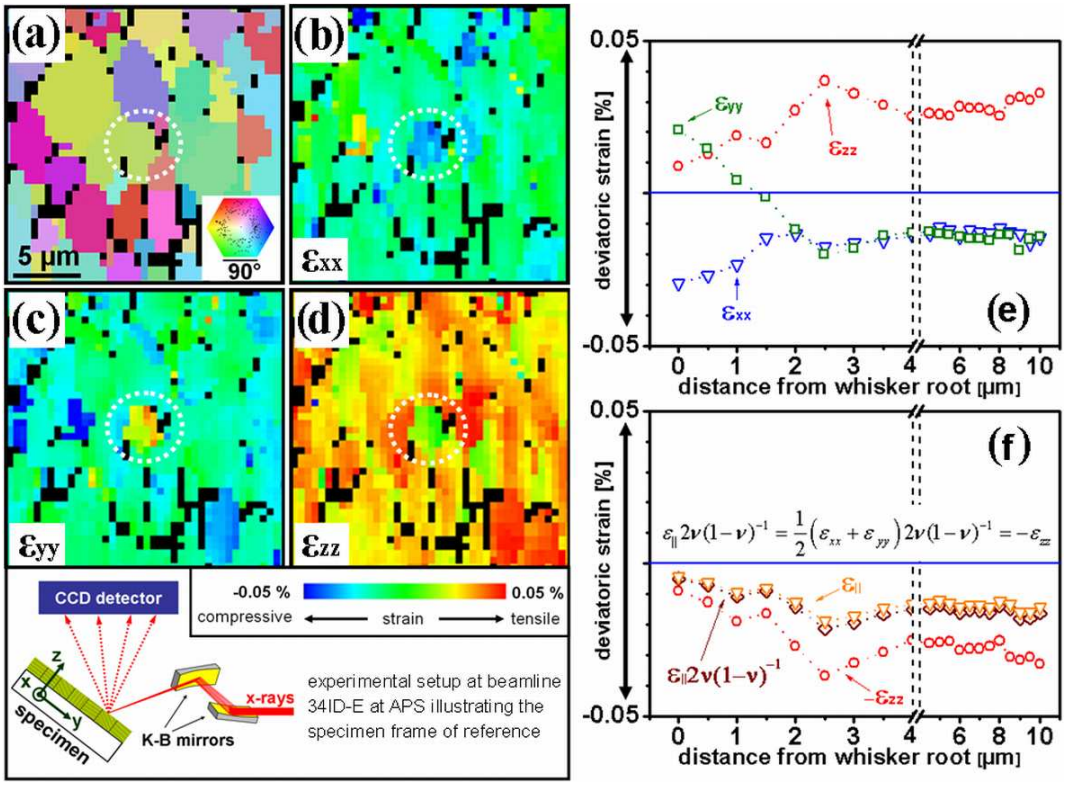

Figure 7.2: Two dimensional micro-diffraction (area of ~ 20 x 20 µm^2) data taken around the root (white dotted circle) of a growing Sn whisker. The regions colored black correspond to not indexed data points. a) The orientation image displays the corresponding (RGB) color-coded crystallographic orientations of the [001] axis of the Sn grains with respect to the [001] pole (which has the white color-code). b)-d) Color-coded diagonal (deviatoric) strain tensor components εxx, ε_{yy} and ε_{zz} (see the illustration of the beamline setup and indication of the specimen frame of reference at the bottom of the figure). The scale bar displays the color-coded deviatoric strains. e) Radially, in the plane of the surface, averaged values of all diagonal (deviatoric) strain tensor components (ε_{xx}, ε_{yy} and ε_{zz}) as function of the distance from the whisker root. f) Radially averaged in-plane strain ε|| as function of the distance from the whisker root in comparison with the radially averaged values of $\varepsilon_{\parallel} 2\nu(1-\nu)^{-1}$ and $-\varepsilon_{zz}$.

The in-plane strain tensor components ε_{xx} and ε_{yy} can be used to calculate the (averaged) in-plane (parallel to the specimen surface) strain $\varepsilon_{\parallel}$ ($\varepsilon_{\parallel} = ½ (\varepsilon_{xx} + \varepsilon_{yy})$; see Figs. 7.2e, f). The diagonal (deviatoric) strain tensor component ε_{zz} (strain component normal to the specimen surface) can also be used to assess the (averaged) in-plane strain due to mechanical equilibrium conditions by taking the (isotropic) Poisson's ratio of Sn ($\nu = 0.36$; in this work the isotropic Poisson's ratio of Sn has been calculated from single crystal elastic constants [23] by adopting the elastic grain interaction model of Eshelby-Kröner [24]) into account. The radial averaging of the strains over differently orientated (mechanically anisotropic, tetragonal) Sn grains justifies the use of the isotropic Poisson's ratio. As here an in-plane state of stress has to be considered the following relations hold for the corresponding strain: $\varepsilon_{\parallel} 2\nu(1-\nu)^{-1} = ½ (\varepsilon_{xx} + \varepsilon_{yy}) 2\nu(1-\nu)^{-1} = -\varepsilon_{zz}$. The comparison of the thus calculated values for $\varepsilon_{\parallel} 2\nu(1-\nu)^{-1}$ with the measured values for the (averaged) in-plane strain $-\varepsilon_{zz}$ clearly confirms data consistency (see Fig. 7.2f).

The residual (out-of-plane) strain ε_{zz} is less tensile at the whisker nucleation site than in the surroundings of the whisker root (see Figs. 7.2d, e), i.e. the in-plane strain, $\varepsilon_{\parallel}$ (see Fig. 7.2f), is less compressive at the whisker root than in the whisker surroundings (note: because deviatoric strain components have been determined, the nature (absolute value) of the strain is unknown). It must be emphasized that this finding was confirmed by performing measurements for several (i.e. five) growing Sn whiskers (time-resolved scanning electron microscopy (SEM) investigations allowed to prove their ongoing growth behavior), whereas whisker-free specimens upon the same room temperature ageing conditions did *not* exhibit either in-plane nor out-of-plane residual strain gradients (whisker-free specimens were produced by applying a post-plating annealing treatment of 150°C for 1 h [18], called 'post-bake' in industrial manufacturing). Hence, *negative in-plane (radially averaged) residual strain gradients* occur in the direction from the whisker root toward the whisker surroundings (see Fig. 7.2f), i.e. the strains are more tensile / less compressive at the whisker root.

After ageing of about 50 days at room temperature the whisker pertaining to the results shown in Fig. 7.2 showed a length of about 40 µm and a diameter of about 3 µm (see Fig. 7.3a). Close inspections of the whisker tip during its growth showed that the surface morphology did not change with time, which is compatible with whisker growth by pushing up from the base [5]. In order to reveal the microstructure at the whisker root and near the Cu/Sn interface underneath the Sn whisker, FIB cross-

sections in steps of around 1.2 µm parallel to the surface, progressing toward the whisker root, were prepared sequentially after the last SEM investigation (see Fig. 7.3b). Evidently, the Cu_6Sn_5 formation at the Cu/Sn interface occurs preferentially along the grain boundaries of the columnar grains constituting the Sn layer. The development of Cu_6Sn_5 along Sn grain boundaries is particularly pronounced underneath the whisker root (see Fig. 7.3b, image 3). This finding was confirmed by cross-sectional FIB investigations performed on many more Sn whiskers and whisker surroundings.

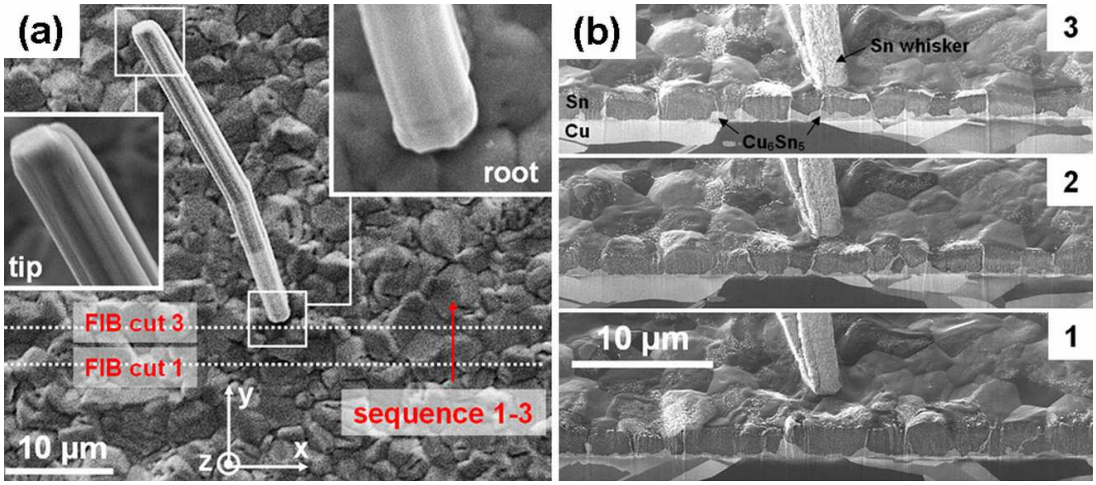

Figure 7.3: a) SEM micrographs of the Sn whisker and its surroundings, pertaining to the results shown in Fig. 7.2. The white dotted lines illustrate the approximate locations of b) the sequence of cross-sectional FIB micrographs with respect to the specimen frame of reference (cf. Fig. 7.2).

The measured residual strain distribution and the observed microstructure around the whisker root lead to the following proposal for the mechanism of whisker formation (see also Fig. 7.1): The deep penetration of Cu_6Sn_5 along the Sn grain boundaries at the Cu/Sn interface induces in-plane compressive (macro) strains in the Sn layer, particularly in the depth range where Cu_6Sn_5 formation along the Sn grain boundaries proceeds. Due to mechanical equilibrium conditions in-plane tensile (macro) strains then occur in the Sn layer close to the surface; most pronouncedly at those surface locations where penetration of Cu_6Sn_5 along Sn grain boundaries is most distinctive, as underneath a whisker. As a consequence, both negative out-of-plane residual strain gradients, in the direction from the surface of the Sn layer to the Cu/Sn interface (for specific experimental evidence, see Ref. [20]) and negative in-plane residual strain gradients in the direction from the whisker-nucleation site toward the

whisker surroundings (see Fig. 7.2) occur. These out-of-plane and in-plane negative strain gradients provide a driving force for the transport of Sn atoms to the whisker nucleation site, as strain-relief mechanism, and thus lead to Sn whisker growth.

Whiskers do not form at every location at the surface corresponding with a pronounced Cu_6Sn_5 formation underneath, as follows from the cross-sectional FIB micrographs shown in Fig. 7.3. This may be related to the crystallographically anisotropic nature of (self) diffusion in Sn: the precise crystallographic orientation of the Sn grains around and above the location with pronounced Cu_6Sn_5 formation co-determines the rate of Sn transport from the strained surroundings to the potential whisker-nucleation site.

7.4. Conclusions

In this work it was shown experimentally by employing high-resolution synchrotron white beam micro Laue diffraction that *negative in-plane residual strain gradients* occur around the root of a growing Sn whisker. These *negative* in-plane residual strain gradients in combination with *negative* out-of-plane residual strain-depth gradients [20] are the cause of transport of Sn atoms to the whisker root, as a strain-relief mechanism. Compressive strain is not a prerequisite for whisker formation. Instead, the nature of the three dimensional strain *gradients* around a potential whisker-nucleation site is decisive for whisker formation.

Acknowledgment

The authors are much obliged to the company ‘Hans Heimerdinger Oberflächentechnik’ in Pforzheim (Germany) for specimen preparation. Use of the Advanced Photon Source was supported by the Office of Basic Energy Sciences, U.S. Department of Energy, under Contract No. DE-AC02-06CH11357. G.E.I. was supported by the Division of Material Sciences and Engineering, Office of Basic Energy Sciences, U.S. Department of Energy.

References

[1] Galyon G. T. (2005). IEEE Trans. Electron. Packag. Manuf. **28**, 94.

[2] Tu K. N., Chen C. & Wu A. T. (2007). J. Mater. Sci. - Mater. Electron **18**, 269.

[3] Herring C. & Galt J. K. (1952). Phys. Rev. **85**, 1060.

[4] Fisher R. M., Darken L. S. & Carroll K. G. (1954). Acta Metall. **2**, 368.

[5] Koonce S. E. & Arnold S. M. (1953). J. Appl. Phys.; Lett. to the Editor **24**, 365.

[6] Ellis W. C., Gibbons D. F. & Treuting R. C. (1958). In Growth and Perfection of Crystals edited by Doremus, R. H., Roberts, B. W. and Turnbull, D. (Wiley, New York, 1958), pp. 102-120.

[7] Lindborg U. (1976). Acta Metall. **24**, 181.

[8] Lee B. Z. & Lee D. N. (1998). Acta Mater. **46**, 3701.

[9] Hasiguti R. R. (1955). Acta Metall. **3**, 200.

[10] Franks J. (1958). Acta Metall. **6**, 103.

[11] Frank F. C. (1953). Philos. Mag. **44**, 854.

[12] Eshelby J. D. (1953). Phys. Rev. **91**, 755.

[13] Boettinger W. J., Johnson C. E., Bendersky L. A., Moon K.-W., Williams M. E. & Stafford G. R. (2005). Acta Mater. **53**, 5033.

[14] Tu K. N. (1973). Acta Metall. **21**, 347.

[15] Chason E., Jadhav N., Chan W. L., Reinbold L. & Kumar K. S. (2008). Appl. Phys. Lett. **92**, 171901.

[16] Kumar K. S., Reinbold L., Bower A. F. & Chason E. (2008). J. Mater. Res. **23**, 2916.

[17] Dyson B. F., Anthony T. R. & Turnbull D. (1967). J. Appl. Phys. **38**, 3408.

[18] Sobiech M., Welzel U., Schuster R., Mittemeijer E. J., Hügel W., Seekamp A. & Müller V. (2007). in Proc. of the 57th Electronic Components and Technology Conference in Reno, USA, 192.

[19] Choi W. J., Lee T. Y., Tu K. N., Tamura N., Celestre S., MacDowell A. A., Bong Y. Y. & Nguyen L. (2003). Acta Mater. **51**, 6253.

[20] Sobiech M., Welzel U., Mittemeijer E. J., Hügel W. & Seekamp A. (2008). Appl. Phys. Lett. **93**, 011906.

[21] Ice G. E., Larson B. C., Tischler J. Z., Liu W. & Yang W. (2005). Mater. Sci. Eng. A **399**, 43.

[22] Chung J.-S. & Ice G. E. (1999). J. Appl. Phys. **86**, 5249.

[23] Gale W. F. (2004). Smithells Metals Reference Book. London: Butterworths.

[24] Welzel U., Ligot J., Lamparter P., Vermeulen A. C. & Mittemeijer E. J. (2005). J. Appl. Crystallogr. **38**, 1.

8. Summary

The system Sn on Cu will usually be applied for interconnection of modern electronic systems (see e.g. Refs. [14-15] in chapter 1), i.e. for mechanical, thermal and electrical "integration" of electronic components (e.g. composed of Cu) on rigid substrates (i.e. printed circuit boards) by (e.g. Sn) solder-joint technology. Nowadays Sn is the material of choice for this purpose because the up to now commonly and successfully used SnPb alloys for soldering and coating applications are prohibited by law since 1st July 2006 due to environmental concerns (Pb-free and "green" legislation). However, it is well known since nearly 60 years that pure Sn thin films deposited on Cu substrates are very prone to spontaneous formation of needle-like Sn single-crystals, called whiskers, during ageing at room temperature (see e.g. Refs. [2-3] in chapter 1). Such filamentary Sn whiskers exhibiting growth rates of about 1 Å/sec constitute an issue of great technological relevance for Sn coated leadframe legs of modern microelectronic devices because whisker-induced short-circuit failures of various electronic devices have resulted in enormous financial damage including breakdowns of satellites, computer centres and military and medical devices (see Fig. 8.1) (see Refs. [2] and [4] in chapter 1). Unfortunately, profound knowledge on this controversially discussed phenomenon of whisker-growth is still lacking. Therefore, particularly in recent years, the electronic industry promotes scientific activities to arrive at fundamental understanding of Sn whisker formation in order to implement industrially reliable (accelerated) whisker tests and/or mitigation strategies.

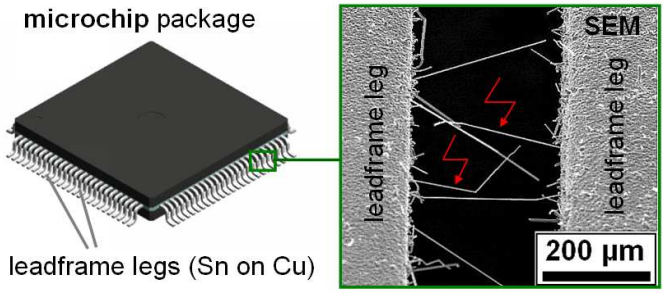

Figure 8.1: Schematic illustration of a common microchip package (left) with leadframe legs consisting of Sn-plated Cu. The spontaneous growth of Sn whiskers from the Sn-plated conductors (right; redrawn after Ref. [27] in chapter 1) can cause short-circuits between neighboring leadframe legs.

Against the above background, the present thesis focuses in particular on revealing the driving force for Sn whiskering in the system Sn on Cu during room temperature ageing and thus to devise a coherent understanding of the processes leading to the formation and growth of Sn whiskers. The obtained fundamental interrelations of microstructural evolution, phase formation, residual stress development and the associated whiskering of Sn thin films electro- and sputter-deposited on Cu as well as of SnPb thin films electrodeposited on Cu during ageing at room temperature have lead to a qualitative understanding of whisker growth in terms of localized Coble-creep. On this basis, whisker mitigation strategies can be proposed.

8.1. Compressive stresses and stress gradients; the driving force for whiskering

After (electro-) deposition of a Sn layer with columnar grain morphology on top of a Cu (bulk) substrate, and upon subsequent ageing at room temperature, Cu diffuses rapidly by an interstitial mechanism into the Sn layer and the formation of an intermetallic compound (IMC) Cu_6Sn_5 takes place along the Sn grain boundaries intersecting the Sn/Cu interface (see chapters 2 and 3). This ongoing IMC formation involving an irregular growth morphology (see Fig. 8.2 left) leads to the (continuous) development of residual compressive stress parallel to the Sn/Cu interface due to the constraint imposed by the (rigid) substrate upon increase of the specific volume associated with IMC formation at the Sn side of the Sn/Cu interface. Shortly after Sn deposition (i.e. for Sn films with a layer thickness of some micrometers), the residual (through-thickness averaged) stress attains a constant plateau value of about -8 MPa (see Fig. 8.3) and at the same time whiskering initiates (see Fig. 8.2 right).

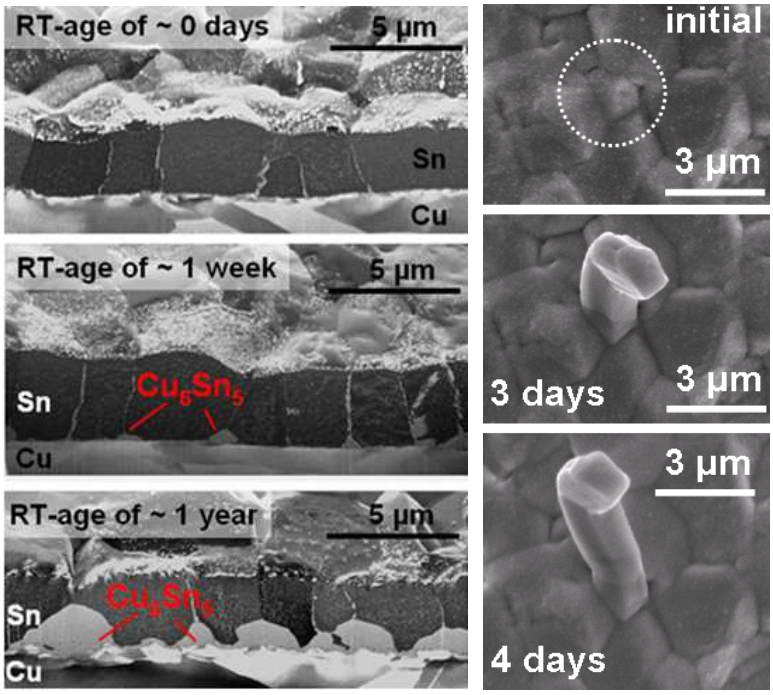

Figure 8.2: left: Microstructural evolution upon room temperature ageing of a Sn coating (thickness of about 3 µm) deposited on Cu as revealed in cross-sectional view by means of focused ion beam microscopy; right: Top-view SEM micrographs of the same specimen showing the onset of whiskering upon ageing.

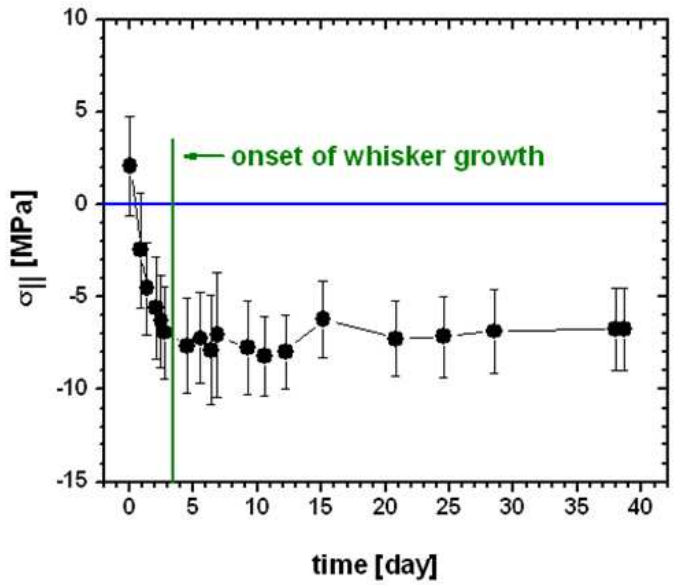

Figure 8.3: Residual through-thickness averaged stress of a Sn coating (thickness of about 3 µm) deposited on Cu as a function of ageing time at room temperature. The 321 diffraction line of Sn was employed for the stress analysis. The onset of whiskering is indicated by the green vertical line.

During continued ageing whisker growth proceeds while the residual stress remains more or less constant, even though the source for compressive stress generation, i.e. Cu_6Sn_5 growth, as described above, still operates (see Fig. 8.3); see also chapters 2 and 3. This can be understood as follows: Compressive-stress increase due to Cu_6Sn_5 growth can continue until the yield limit of Sn is exceeded.* Volume misfit due to further growth of Cu_6Sn_5 then induces plastic deformation, ultimately involving whisker growth (this work shows for the first time that whiskers formed on the surface of Sn coating deposited on Cu are composed of pure Sn and do not contain Cu, see chapter 3), as a localized stress-relaxation mechanism. This balance of stress generation and stress relief controls the whiskering behavior: Indeed, once the growth of Cu_6Sn_5 came effectively to a halt due slowed-down IMC growth kinetics upon long-time ageing at room temperature, whisker growth also stopped (see chapter 4).

On the other hand it is also shown in this work that Sn thin films subjected directly after layer deposition to a heat treatment at 150°C for 1 h (called "post-bake in industrial manufacturing) remain whisker-free for extended ageing times at room temperature (see chapter 2) because *(i)* the formation of a relatively thick, post-bake induced IMC layer (in this case consisting of the Cu_6Sn_5 and Cu_3Sn) acts effectively as diffusion barrier for Cu during subsequent ageing and thus significant irregular Cu_6Sn_5 growth at the Sn side of the Sn/Cu interface is avoided in the initial stage of ageing, i.e. a regular/planar growth morphology of Cu_6Sn_5 at the Sn/Cu interface results, which prevents effectively generation of compressive stress by the mechanism described above. However, after prolonged ageing at room temperature, once a sufficient amount of Cu is diffused through the IMC diffusion barrier at the Sn/Cu interface, (moderate) irregular growth of Cu_6Sn_5 along Sn grain boundaries takes place, which leads to a build-up of compressive stress. But despite the presence of (through-thickness averaged) compressive stress whisker formation does *not* occur because *(ii)* compressive stress by itself is not the driving force for whiskering (see chapter 6). Indeed, the present work provides the first experimental evidence that the occurrence of stress *gradients*, and not of compressive stresses, provides the driving force for

* The uniaxial yield limit is about 10-15 MPa for polycrystalline, isotropic bulk Sn; but note that the residual stress determined by conventional X-ray diffraction analysis represents a though-thickness averaged value. Contrary, the sputter-deposited Sn coating (thickness of about 350 nm) exhibits a significantly increased yield stress due to its fine-grained microstructure (see chapter 3).

whiskering (see chapters 6 and 7), i.e. whisker growth can occur even in the presence of a tensile state of stress provided that an appropriate stress gradient is established in a given specimen. In other words, the Cu_6Sn_5-induced compressive stress in the Sn layer is necessary in order to establish a negative stress gradient (from the surface towards the interface), but any other mechanism leading to a similar stress-depth distribution could as well trigger whiskering.

The origin for Sn whisker formation in the system Sn on Cu is ascribed to the development of stress *gradients* in the Sn layer as a direct consequence of the formation of Cu_6Sn_5 with an irregular growth morphology (see chapters 6 and 7): Negative out-of-plane stress gradients in the direction of increasing depth and negative in-plane stress gradients form the whisker nucleation site towards the surroundings drive the motion of Sn atoms to the whisker root in order to relax the mechanical stress. This picture of spontaneous Sn whiskering is confirmed by comparing the stress distribution of whisker-free (i.e. post-baked; see above) specimens which do *not* exhibit such stress gradients. Furthermore, it is recognized in this work that (active) whisker growth proceeds only as long as such whisker-driving stress gradients are developed in the Sn layer, particularly around the whisker root, i.e. as long as the driving force (in the system Sn on Cu it is the ongoing irregular formation Cu_6Sn_5) for Sn whiskering operates.

Furthermore, the comparison of microstructural evolution and residual stress development of high-purity Sn layers (with a thickness of about 350 nm) sputter-deposited both on Cu and Si substrates (see chapter 3) shows clearly for the first time that *(i)* Cu_6Sn_5 formation at the Sn/Cu interface is directly responsible for compressive stress generation (and thus for the creation of whisker-driving stress gradients, see above) in the system Sn on Cu (note that contrary, in the system Sn on Si, no intermetallic compound forms and thus compressive stress does *not* build-up, consequentially whiskering does *not* occur as the whisker-driving stress gradients are absent) and that *(ii)* impurities of organic and inorganic nature, possibly incorporated in the Sn film do not control whiskering (in the case of high-purity, sputter-deposited Sn films a possible presence of such impurities can be excluded, contrary to electrodeposited Sn coatings, for which the role of such impurities has been discussed controversially; see Ref. [38] in chapter 3).

Against the above discussed background it follows straightforwardly that Cu_6Sn_5 formation in the system Sn on Cu is directly connected to spontaneous whisker

formation. Particularly, the growth morphology of Cu_6Sn_5 at the Sn side of the Sn/Cu interface (i.e. irregular or regular) has been recognized as crucial parameter controlling generation of residual compressive stress (see above): Irregular (inhomogeneous) growth of Cu_6Sn_5 generates effectively compressive stress whereas regular/planar (homogeneous) growth of Cu_6Sn_5 prevents the build-up compressive stress (see chapters 2, 4-6). In order to provide a coherent understanding of such (whisker-initiating) intermetallic phase formation in the system (polycrystalline) Sn on (polycrystalline) Cu during ageing at room temperature, results obtained from detailed microstructural analyses of intermetallic phase evolution are interpreted in terms of interface thermodynamics and interdiffusion kinetics (see chapter 4). It is shown in this work that the observed irregular formation of Cu_6Sn_5 along Sn grain boundaries intersecting the Sn/Cu interface is in agreement with predictions derived from interface thermodynamics; the formation of Cu_6Sn_5 along Sn grain boundaries is energetically preferred among other possible scenarios (see Fig. 8.4 left), and the (whisker-inducing) irregular growth of Cu_6Sn_5 at these sites is controlled by interdiffusion kinetics of the system Sn on Cu, i.e. Cu diffuses into Sn, not vice versa (see Fig. 8.4 right). On this basis a whisker-mitigation treatment is proposed in section 8.4 (see also chapter 4).

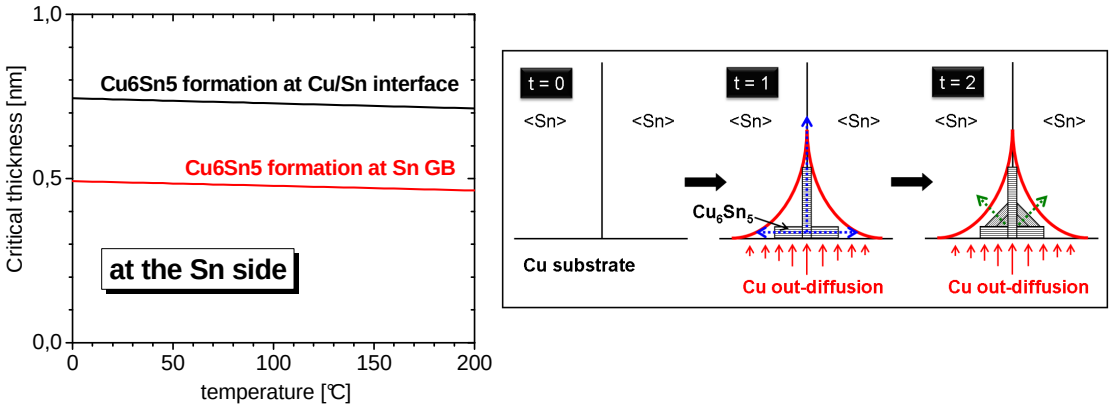

Figure 8.4: left: Critical thicknesses for formation of Cu_6Sn_5 at a Sn grain boundary and at the interface between Sn and Cu. right: Schematic illustration of Cu diffusion and Cu_6Sn_5 formation processes during room temperature ageing (for successive ageing time steps t = 0, 1 and 2) at a Sn grain boundary intersecting the *<Sn>/<Cu>* interface, leading to the formation of Cu_6Sn_5 with an irregular growth morphology.

8.2. Mechanisms of stress relaxation; the role or grain morphology

The above presented picture of spontaneous whiskering holds for a columnar Sn grain morphology with a native Sn-oxide layer on top of the Sn coating (the surface oxide forms immediately upon room temperature ageing and has a thickness of several nanometres, see chapter 2) deposited on a rigid substrate. Such a Sn microstructure can be considered as strongly immobile: The grain boundaries, running from top to bottom, are strongly pinned at the *(i)* the Sn/oxide interface and *(ii)* the Sn/Cu interface. Consequently, the Cu_6Sn_5-induced compressive stress cannot be relaxed by some mechanism requiring mobile grain boundaries in the coating and thus stress relaxation (by transport of Sn atoms) occurs *only* at some suitable surface locations (i.e. whisker-nucleation sites). This work shows that these potential whisker-nucleation sites are created already during Sn layer deposition and that these surface locations exhibit a specific (rigid) grain boundary arrangement, i.e. inclined (with respect to the surface normal) grain boundaries prevail (see chapter 5). Once appropriate stress-depth gradients (compressive stress in the bottom part and tensile stress in the top part of the Sn coating) have developed, in particular by pronounced Cu_6Sn_5 formation underneath such surface grains, whisker formation can occur by growth from these already pre-existing surface grains. As the stress-depth gradient is associated with a vacancy concentration-depth gradient (more vacancies in the tensily stresses part), mass transport of Sn via grain boundaries (note that the homologous temperature of Sn at room temperature equals about 0.6) occurs. Thus whiskering can be discussed as a local Coble-creep-like phenomenon: To prevent porosity/void formation upon Coble creep, as the consequence of the change of grain shape by the diffusional mass transport (via grain boundaries), grain-boundary sliding takes place. For the largely columnar Sn coating such grain-shape change does not occur globally but only locally; at locations where a grain-boundary arrangement with inclined grain boundaries is present shear stresses develop along such inclined grain boundaries (note the planar nature of the state of stress in the Sn coating) allowing outward “growth” of the surface grains concerned by facilitating the required grain-boundary sliding. Thereby this local process of Sn transport establishes relaxation of the stress (and thereby vacancy concentration) gradients in the entire Sn coating.

Coatings with an equiaxed grain morphology (e.g. SnPb or Sn; see chapter 5) exhibit a relatively large number of suitable locations (i.e. with inclined grain boundaries) where Coble-type creep of Sn can be accommodated: Sn transport by diffusional creep can occur at each inclined grain boundary (more or less equally distributed over the entire film) where shear stresses can develop leading to a rather uniform swelling of the coating in the out-of-plane direction, yet without forming locally whiskers. The grain-shape change occurs globally, not only locally as observed in columnar Sn coatings, and thus such coatings with an equiaxed grain morphology remain whisker-free in the presence of compressive stress.

This work also shows that the whisker-preventing effect of Pb (in SnPb coatings) is only attributed to the formation of an equiaxed grain morphology which enables to relax the compressive stress in the coating at each inclined grain boundary leading to uniform grain growth. Pb is "just" an agent to prevent Sn from its inherent columnar growth during layer deposition (see chapter 5) and this knowledge allows to propose the whisker-mitigation treatment descried in section 8.4 (see also chapter 5).

8.3. Model of whisker formation

On the basis of the above presented parameters controlling spontaneous Sn whiskering in the system Sn on Cu, the model of whisker formation shown in Fig. 8.5 results (see chapters 5 and 7):

After deposition of the Sn thin film (thickness of several micrometers) with columnar grain morphology on Cu and upon subsequent ageing at room temperature, Sn and Cu react to form (only) the intermetallic compound Cu_6Sn_5 at the Sn side of the Sn/Cu interface. The energetically preferred penetration of Cu_6Sn_5 along the Sn grain boundaries intersecting the Sn/Cu interface into the Sn layer induces in-plane compressive stress due to the constraint imposed by the (rigid) substrate upon increase of the specific volume associated with IMC formation, particularly in the depth range where Cu_6Sn_5 formation proceeds (note also that the formation of a native, stable Sn-oxide on top of the Sn layer prevents surface diffusion which imposes as further constraint on this system). Then in-plane tensile stress occurs in the Sn layer close to the surface; most pronouncedly at those surface locations where penetration of Cu_6Sn_5 along Sn grain boundaries is most distinctive, as observed underneath a whisker. Such surface grains, which are already formed during layer deposition, exhibit inclined (with

respect to the surface normal) grain boundaries, in contrast to columnar grain boundaries of the adjacent Sn grains constituting the Sn film. As a consequence of the above processes taking place in this strongly pinned system regarding (in-plane) grain boundary mobility, both negative out-of-plane residual stress gradients, in the direction of increasing depth and negative in-plane residual stress gradients in the direction from the whisker-nucleation site (i.e. surface grains with inclined grain boundaries) towards the whisker surroundings occur. These out-of-plane and in-plane negative stress gradients provide the driving force for the directional transport of Sn atoms to the whisker nucleation site, as stress-relief mechanism, and thus control Sn whisker growth. It is the negative nature of such stress gradients that drives whiskering, not the compressive stress by itself. Consequently, whisker growth can occur even in the presence of tensile stress parallel to the surface, provided that a negative nature of the stress gradients is developed. During ongoing stress relaxation via localized whiskering material depletion around the whisker root does not take place (even not for “extremely” long whiskers) which indicates clearly that whiskering is associated with long-range diffusion of Sn. This understanding of the processes controlling Sn whiskering at room temperature allows considering the formation and growth of Sn whiskers as a special form of localized diffusional creep (Coble-type creep) driven by stress gradients.

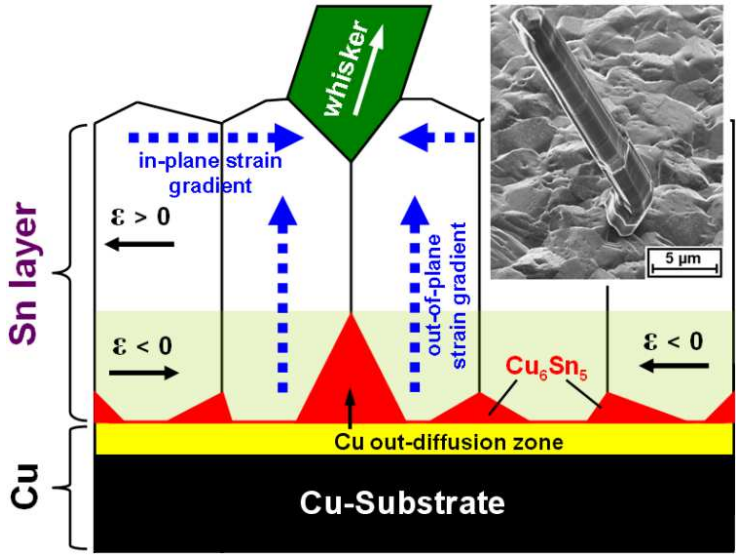

Figure 8.5: Schematic model, on the basis of the results of the present work, of the whisker-formation process in Sn thin films deposited on Cu substrates upon ageing at room temperature. The focused ion beam micrograph illustrates the growth morphology of a Sn whisker.

8.4. Whisker-mitigation treatments

The results of the present work allow proposing the following whisker-mitigation treatments:

(i) On the basis of the results discussed in chapter 4 it is proposed to avoid whisker formation by applying the knowledge of interface thermodynamics in order to change the growth morphology of Cu_6Sn_5 from "irregular" to "regular" upon favoring energetically the growth of Cu_6Sn_5 along the Sn/Cu interface as compared to irregular growth along Sn grain boundaries. This can be realized by a decrease of the grain boundary energy of Sn and/or by an increase of the interface energy between Sn and Cu. For example, the incorporation of a component in Sn that reduces the Sn grain-boundary energy is one possibility; Pb is such a component (wetting of Sn grain boundaries by Pb leads to Sn/Pb interfaces of energy about half of that of Sn/Sn interfaces, see Ref. [48] in chapter 4).

(ii) On the basis of the results discussed in chapter 5 it is proposed to suppress spontaneous whiskering on pure Sn coatings via microstructural control, i.e. to bring about an equiaxed grain morphology which enables relaxing compressive stress globally (at each inclined grain boundary leading to uniform grain growth), not locally (in the form of filamentary whiskers) as typically observed in columnar Sn coatings with only a few surface locations with inclined grain boundaries. This can be done, e.g. by appropriate choice of the chemistry of the electrolyte, the substrate material and/or the deposition routine.

9. Zusammenfassung

Das Materialsystem Sn auf Cu wird heutzutage sehr häufig in der Verbindungstechnologie modern elektronischer Systeme eingesetzt (siehe [14-15] im Kapitel 1), d.h. zur Realisierung mechanischer, thermischer und elektrischer „Integration“ elektronischer Komponenten (z.B. bestehend aus Cu) auf festen Substraten (d.h. Leiterplatten) mittels (z.B. Sn) Löttechnologie. Der momentan favorisierte Einsatz von reinem Sn für diesen Zweck liegt darin begründet, dass die vor Kurzem sehr häufig und erfolgreich eingesetzten SnPb Legierungen seit dem 01. Juli 2006 aus Umwelt-relevanten Gründen verboten sind (Pb-frei und „grüne“ Gesetzgebung). Es ist jedoch seit fast 60 Jahren bekannt, dass Sn Dünnschichten abgeschieden auf Cu Substraten sehr stark zur spontanen Bildung von nadelförmigen Sn Einkristallen, sogenannten Whiskern, während der Alterung an Raumtemperatur neigen (siehe [2-3] im Kapitel 1). Diese filamenthaften Sn Whisker, die Wachstumsraten von ungefähr 1 Å/sec aufweisen, sind von großer technologischer Bedeutung im Zusammenhang mit der Zuverlässigkeit von Sn-beschichteten Anschlusskontakten moderner mikroelektronischer Bauteile, weil elektrische Kurzschlüsse, ausgelöst durch das Wachstum von solchen Whisker, bereits zu Ausfällen verschiedenster elektronischer Bauteile und somit zu einem enormen finanziellen Schaden geführt haben; Beispiele hierfür sind Ausfälle von Satelliten, Computerzentren sowie militärischen und medizinischen Geräten (siehe Abb. 9.1) (siehe [2] und [4] im Kapitel 1). Leider fehlt bis heute ein fundierter Wissensstand zu diesem kontrovers diskutierten Phänomen des Whiskerwachstums. Das ist auch der Grund, warum insbesondere in jüngster Zeit die Industrie wissenschaftliche Aktivitäten auf diesem Gebiet unterstützt. Das Ziel ist ein fundiertes Verständnis zum Thema Whiskerbildung aufzubauen, so dass im industriellen Umfeld verlässliche (beschleunigte) Whiskertests und/oder Whiskervermeidungsmaßnahmen eingeführt werden können.

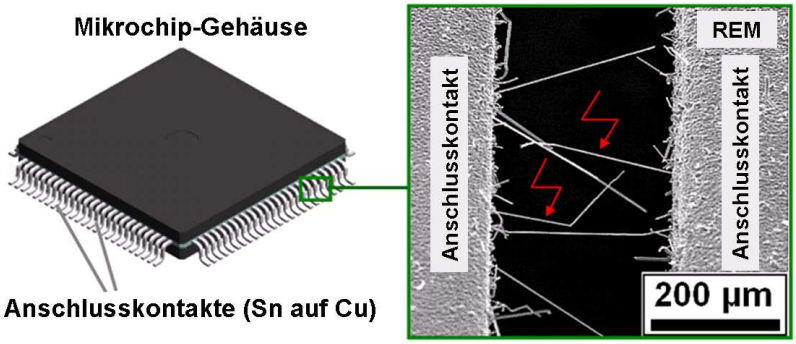

Abbildung 9.1: Schematische Darstellung eines gewöhnlichen Mikrochipgehäuses (links) mit Anschlusskontakten, die aus einem Sn-beschichteten Cu Basismaterial bestehen. Das spontane Wachstum von Sn Whiskern aus der Oberfläche der Sn-beschichteten Anschlusskontakte (rechts; verändert nach [27] im Kapital 1) kann elektrische Kurzschlüsse beim Überbrücken benachbarter Kontakte auslösen.

Vor diesem Hintergrund beschäftigt sich die vorliegende Arbeit insbesondere mit der Aufklärung der Triebkraft für Sn Whiskerbildung im System Sn auf Cu während der Alterung an Raumtemperatur, um basierend auf diesen Erkenntnissen ein in sich schlüssiges Verständnis der Vorgänge abzuleiten, die zur Bildung und zum Wachstum von Whiskern führen. Die aufgedeckten, grundlegenden Wechselwirkungen zwischen Mikrostrukturentwicklung, Phasenbildung und Eigenspannungsentwicklung für Whiskerbildung von Sn Dünnschichten auf Cu (galvanisch sowie mittels Kathodenzerstäubung abgeschieden) und von SnPb Dünnschichten auf Cu (galvanisch abgeschieden), während der Alterung bei Raumtemperatur, ermöglichten die Identifizierung der Triebkraft für das Whiskerwachstum sowie die Aufstellung eines qualitativen Modells und die Ausarbeitung möglicher Ansätze zur Vermeidung von Whiskerbildung. Im Folgenden werden die wichtigsten Aspekte der spontanen Sn Whiskerbildung besprochen.

9.1. Druckspannungen und Spannungsgradienten; die Triebkraft für Whiskerbildung

Nach der (galvanischen) Abscheidung der Sn Dünnschicht mit einer kolumnaren Kornmorphologie auf einem (bulk) Cu Substrat, und während anschließender Alterung an Raumtemperatur, beginnt Cu interstitiell in Richtung Sn Dünnschicht zu diffundieren und es kommt zur Bildung einer intermetallischen Phase

(IMP) Cu_6Sn_5 entlang von Sn Korngrenzen, die im Kontakt mit der Sn/Cu Grenzfläche stehen (siehe Kapitel 2 und 3). Diese fortlaufende Bildung der IMP, die eine irreguläre Wachstumsmorphologie aufweist (siehe Abb. 9.2 links), führt zum kontinuierlichen Aufbau von Druckeigenspannungen parallel zur Sn/Cu Grenzfläche, bedingt durch die durch das feste Substrat auferlegten geometrischen Randbedingungen in Folge der spezifischen Volumenausdehnung, die mit der Bildung der IMP auf der Sn Seite der Sn/Cu Grenzfläche einhergeht. Innerhalb kurzer Zeit nach der Abscheidung der Sn Dünnschicht (bei Sn Dünnschichten mit einer Schichtdicke von wenigen Mikrometern) erreichen die (durch die Schichtdicke gemittelten) Eigenspannungen einen konstanten Plateaubetrag von ca. – 8 MPa (siehe Abb. 9.3) und zur gleichen Zeit kommt es zur Bildung der ersten Whisker (siehe Abb. 9.2 rechts).

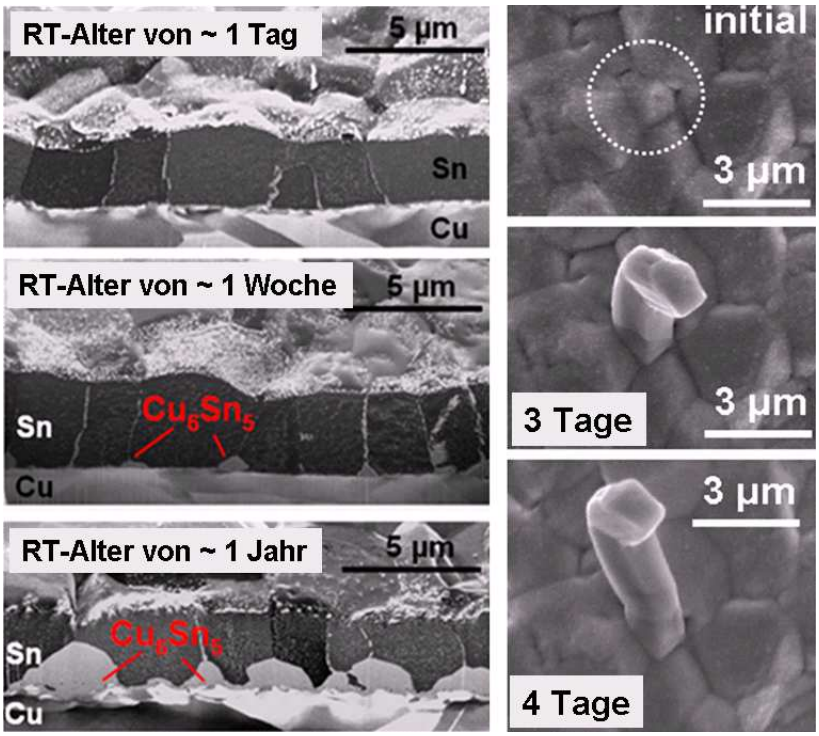

Abbildung 9.2: links: Entwicklung der Mikrostruktur einer Sn Dünnschicht (Schichtdicke von ca. 3 µm) auf Cu während der Alterung an Raumtemperatur beobachtet im Querschnitt mittels Ionenstrahlmikroskopie; rechts: Rasterelektronenmikroskopische Abbildungen in Aufsicht der gleichen Probe zur Veranschaulichung des Anfangsstadiums der Whiskerbildung während der Alterung an Raumtemperatur.

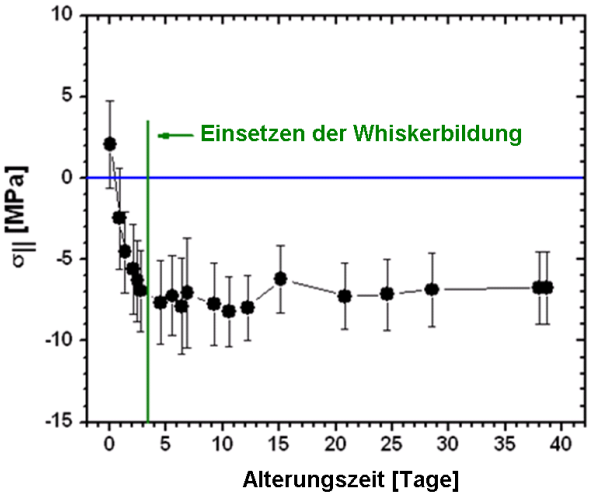

Abbildung 9.3: Eigenspannungen (durch die Schichtdicke gemittelt) einer Sn Dünnschicht (Schichtdicke von ca. 3 µm) auf Cu als Funktion der Alterung an Raumtemperatur. Die 321 Beugungslinie von Sn wurde zur Spannungsanalyse verwendet. Der Beginn der Whiskerbildung ist durch die grüne vertikale Linie angezeigt.

Während fortdauernder Alterung an Raumtemperatur geht auch das Whiskerwachstum weiter, wobei die Eigenspannung mehr oder weniger konstant bleibt, auch wenn die Quelle für den Aufbau von Druckspannungen, d.h. Wachstum von Cu_6Sn_5, nach wie vor aktiv ist (siehe Abb. 9.3; siehe auch Kapitel 2 und 3). Dieser Zusammenhang ist wie folgt zu verstehen: Der Anstieg der Druckspannung, bedingt durch das Wachstum von Cu_6Sn_5, erfolgt bis zum Erreichen der Fließspannung von Sn.[*] Die Volumenfehlanpassung, bedingt durch weiteres Wachstum von Cu_6Sn_5, induziert plastische Deformation, die letztendlich zum Whiskerwachstum (die vorliegende Arbeit zeigt zum ersten Mal, dass Whisker, die auf der Oberfläche von Sn Dünnschichten abgeschieden auf Cu wachsen, aus reinem Sn bestehen und kein Cu enthalten; siehe Kapitel 3) als lokalem Spannungsrelaxationsmechanismus führt. Dieses Gleichgewicht zwischen Spannungsaufbau und Spannungsabbau kontrolliert den Verlauf der Whiskerbildung: sobald das Wachstum von Cu_6Sn_5 in Folge verlangsamter IMP Wachstumskinetik während der Langzeitalterung an

[*] Die einachsige Fließspannung von polykristallinem, isotropen (bulk) Sn liegt bei ca. 10-15 MPa; es ist anzumerken, dass die röntgenographisch ermittelten Eigenspannungen einen durch die Schichtdicke hindurch gemittelten Wert darstellen. Es soll ebenso erwähnt werden, dass im Gegensatz zu den galvanisch abgeschiedenen Dünnschichten (Schichtdicken von wenigen Mikrometern), die gesputterten Sn Dünnschichten (Schichtdicke von ca. 350 nm) eine deutlich erhöhte Fließspannung auf Grund ihrer sehr feinkörnigen Mikrostruktur aufweisen (siehe Kapitel 3).

Raumtemperatur zum Stillstand kommt, erfolgt auch kein weiteres Whiskerwachstum (siehe Kapitel 4).

In der vorliegenden Arbeit wurde auch gezeigt, dass Sn Dünnschichten, die direkt nach Schichtabscheidung bei 150 °C für 1 Stunde ausgelagert wurden (sogenannte „post-bake"-Behandlung im industriellen Fertigungsprozess), während eines langen Alterungszeitraums an Raumtemperatur frei von Whiskern bleiben, weil *(i)* die Bildung einer relative dicken, „post-bake"-induzierten IMP Schicht (in diesem Fall bestehend aus Cu_6Sn_5 und Cu_3Sn) als effektive Diffusionsbarriere für Cu während anschließender Alterung dient. Folglich ist signifikantes, irreguläres Wachstum von Cu_6Sn_5 auf der Sn Seite der Sn/Cu Grenzfläche im initialen Alterungsstadium verhindert, d.h. eine reguläre/planare Wachstumsmorphologie von Cu_6Sn_5 resultiert, was effektiv dem Aufbau von Druckspannungen durch den oben beschriebenen Mechanismus entgegenwirkt. Nach einer ausgedehnten Raumtemperaturalterung kann jedoch weiteres, irreguläres Wachstum von Cu_6Sn_5 einsetzen, sobald eine ausreichende Menge an Cu durch die IMP Diffusionsbarriere an der Sn/Cu Grenzfläche hindurch diffundiert ist; folglich werden Druckspannung aufgebaut. Doch trotz vorhandener (durch die Schichtdicke gemittelter) Druckspannungen kommt es nicht zur Bildung von Whiskern, weil *(ii)* Druckspannungen an sich nicht die Triebkraft für Whiskerbildung sind (siehe Kapitel 6). Die vorliegende Arbeit erbrachte erstmalig den experimentellen Beweis dafür, dass das Vorhandensein von *Spannungsgradienten*, und eben nicht das Vorhandensein von Druckspannungen, die Triebkraft für Whiskerbildung darstellt (siehe Kapitel 6 und 7), d.h. Whiskerwachstum kann sogar in der Gegenwart von Zugspannungen auftreten, vorausgesetzt dass sich in der jeweiligen Probe ein geeigneter Spannungsgradient entwickelt hat. Mit anderen Worten: der durch das Wachstum von Cu_6Sn_5 induzierte Aufbau von Druckspannungen in der Sn Dünnschicht ist notwendig, damit sich ein negativer Spannungsgradient (von der Schichtoberfläche in Richtung Sn/Cu Grenzfläche) aufbauen kann, jedoch ist jeder andere Mechanismus ebenso in der Lage Whiskerbildung hervorzurufen, sobald ein ähnlicher Spannungstiefengradient realisiert werden kann.

Der Grund für Whiskerbildung im System Sn auf Cu liegt in der Entwicklung von Spannungsgradienten in der Sn Dünnschicht begründet, die als direkte Konsequenz der Bildung von Cu_6Sn_5 mit einer irregulären Wachstumsmorphologie zu verstehen sind (siehe Kapitel 6 und 7). Negative, senkrecht zur Oberfläche orientierte

Spannungsgradienten in Richtung zunehmender Tiefe und negative, horizontale zur Oberfläche orientierte Spannungsgradienten von der Whiskerwurzel in Richtung Whiskerumgebung sind für den Transport von Sn Atomen an die Whiskerwurzel verantwortlich, um die mechanische Spannung in der Sn Dünnschicht abzubauen. Dieses Bild der spontanen Whiskerbildung wird durch eine Untersuchung der Spannungsverteilung von Whisker-freien (d.h. mit „post-bake“ behandelten) Proben bestätigt, die solche Spannungsgradienten nicht aufweisen. Darüber hinaus konnte in der vorliegenden Arbeit gezeigt werden, dass (aktives) Whiskerwachstum nur solang andauert, wie Whisker-treibende Spannungsgradienten in der Sn Dünnschicht vorhanden sind, v.a. um die Whiskerwurzel herum, d.h. nur so lange wie die Triebkraft (im System Sn auf Cu ist es die fortlaufende, irreguläre Bildung von Cu_6Sn_5) für Sn-Whiskerbildung aufrecht gehalten wird.

Des Weiteren zeigte erstmalig der Vergleich der Mikrostrukturentwicklung und der Eigenspannungsentwicklung von hochreinen Sn Dünnsichten (mit einer Schichtdicke von ca. 350 nm), abgeschieden mittels Kathodenzerstäubung sowohl auf Cu als auch auf Si (siehe Kapitel 3), sehr deutlich, dass *(i)* die Bildung von Cu_6Sn_5 an der Sn/Cu Grenzfläche direkt verantwortlich ist für den Aufbau von Druckspannungen (und somit für den Aufbau von Whisker-treibenden Spannungsgradienten, siehe oben) im System Sn auf Cu (es sei angemerkt, dass im System Sn auf Si intermetallische Phasenbildung nicht stattfindet und somit auch Druckspannungen nicht auftreten; folglich tritt auch Whiskerbildung nicht auf, weil die Whisker-treibenden Spannungsgradienten nicht vorhanden sind) und dass *(ii)* organische und anorganische Verunreinigungen in der Sn Dünnschicht (die möglicherweise enthalten sind) Whiskerbildung nicht steuern (im Fall von hochreinen, mittels Kathodenzerstäubung abgeschiedenen Sn Dünnschichten kann das Vorhandensein von solchen Verunreinigungen ausgeschlossen werden, im Gegensatz zu galvanisch aufgebrachten Sn Dünnschichten, für die dieser Punkt kontrovers diskutiert wurde; siehe [38] im Kapitel 3).

Vor dem soeben dargestellten Hintergrund kann die Schlussfolgerung gezogen werden, dass die Bildung von Cu_6Sn_5 im System Sn auf Cu im direkten Zusammenhang mit der spontanen Whiskerbildung steht. Insbesondere die Wachstumsmorphologie von Cu_6Sn_5 auf der Sn Seite der Sn/Cu Grenzfläche (d.h. irreguläres oder reguläres, planares Wachstum) wurde als entscheidender Parameter zur Steuerung des Aufbaus von Druckspannungen erkannt (siehe oben): Irreguläres

(inhomogenes) Wachstum von Cu_6Sn_5 erzeugt effektiv Druckspannungen wobei ein reguläres/planares Wachstum von Cu_6Sn_5 den Aufbau von Druckspannungen verhindert (siehe Kapitel 2, 4-6). Um ein in sich schlüssiges Verständnis von solcher (Whisker-treibenden) Bildung der intermetallischen Phase im System (polykristallines) Sn auf (polykristallinem) Cu während der Alterung an Raumtemperatur aufstellen zu können, wurden die Ergebnisse von detaillierten Untersuchungen der Mikrostruktur während der Entwicklung der intermetallischen Phase im Vergleich mit theoretischen Ansätzen zur Grenzflächenthermodynamik und Interdiffusionskinetik interpretiert (siehe Kapitel 4). Die beobachtete, irreguläre Bildung von Cu_6Sn_5 entlang von Sn Korngrenzen, die im Kontakt zur Sn/Cu Grenzfläche stehen, ist in guter Übereinstimmung mit den grenzflächenthermodynamischen Vorhersagen; die Bildung von Cu_6Sn_5 entlang von Sn Korngrenzen ist energetisch begünstig im Vergleich zu anderen Konfigurationen (siehe Abb. 9.4 links) und die (Whisker-treibende) irreguläre Bildung von Cu_6Sn_5 ist durch die Interdiffusionskinetik im System Sn auf Cu gesteuert, d.h. Cu diffundiert in Richtung Sn, nicht umgekehrt (siehe Abb. 9.4 rechts). Basierend auf diesen Erkenntnissen ist im Abschnitt 9.4 eine Whiskervermeidungs-maßnahme vorgeschlagen (siehe auch Kapitel 4).

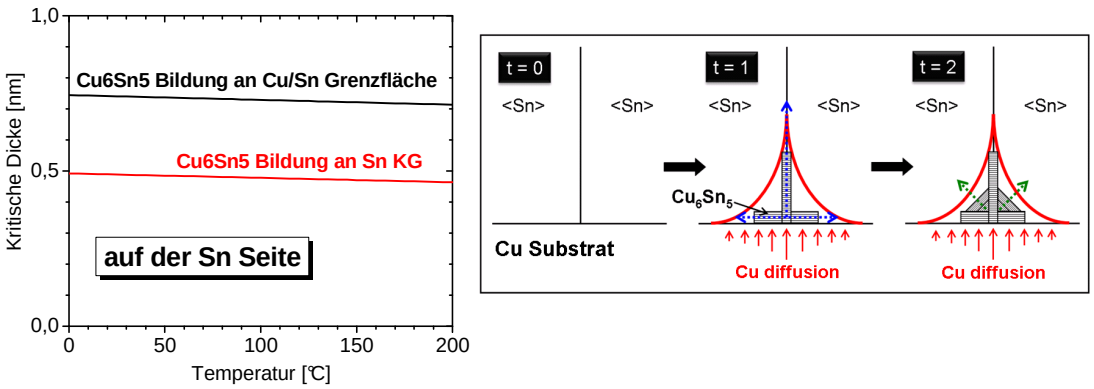

Abbildung 9.4: links: Kritische Dicke, die erforderlich ist zur Bildung von Cu_6Sn_5 an Sn Korngrenzen und an der Grenzfläche zwischen Sn und Cu. rechts: Schematische Darstellung der Vorgänge von Cu Diffusion und Cu_6Sn_5 Bildung während der Alterung an Raum-temperatur (für aufeinander folgende Alterungsschritte t = 0, 1 and 2) an einer Sn Korngrenze im Kontakt mit der Sn/Cu Grenzfläche, die zur irregulären Bildung von Cu_6Sn_5 führen.

9.2. Mechanismen der Spannungsrelaxation; die Rolle der Kornmorphologie

Das bisher vorgestellte Bild der spontanen Whiskerbildung beinhaltet das Vorhandensein einer kolumnaren Sn Kornmorphologie mit einer natürlichen Sn Oxidschicht auf der Sn Oberfläche (das Oberflächenoxid bildet sich sofort während der Alterung an Raumtemperatur und hat eine Dicke von wenigen Nanometern, siehe Kapitel 2) abgeschieden auf einem festen Substrat. Solch eine Sn Mikrostruktur kann als sehr stabil betrachtet werden: Die Korngrenzen, die von der Oberfläche zur Grenzfläche der Sn Dünnschicht verlaufen sind effektiv immobilisiert an *(i)* der Sn/Oxid Grenzfläche sowie an *(ii)* der Sn/Cu Grenzfläche. In Folge dessen kann die Cu_6Sn_5-induzierte Druckspannung nicht durch einen Mechanismus relaxiert werden, der mobile Korngrenzen in der Schicht erfordert, so dass Spannungsrelaxation (durch Transport von Sn) nur an wenigen, passenden Oberflächenstellen (d.h. Whiskerkeimstellen) erfolgen kann. Die vorliegende Arbeit zeigt, dass diese potentiellen Whiskerkeimstellen bereits während der Abscheidung der Sn Dünnschicht angelegt werden und dass diese Oberflächenstellen eine spezielle Anordnung von Korngrenzen aufweisen, d.h. geneigte (im Bezug zur Probennormalen) Korngrenzen (siehe Kapitel 5). Sobald sich entsprechend Spannungstiefengradienten (Druckspannung im unteren Teil und Zugspannung im oberen Teil der Dünnschicht) entwickeln, insbesondere durch signifikantes Wachstum Cu_6Sn_5 unterhalb solcher oberflächennaher Körner, kann Whiskerbildung direkt aus den bereits vorhandenen Oberflächenkörnern hervorgehen. Da der Spannungstiefengradient mit einem Leerstellenkonzentrationsgradient in Verbindung steht (mehr Leerstellen befinden sich im Bereich, der unter Zugspannung steht), kommt es zum Massetransport von Sn entlang von Sn Korngrenzen (die homologe Temperatur von Sn bei Raumtemperatur entspricht ca. 0.6). Daraus folgt, dass Whiskerwachstum als ein lokales Coble-ähnliches Kriechphänomen diskutieren werden kann: Um Porosität/Hohlraumbildung während des stattfindenden Coble-Kriechens zu verhindern, die eine direkte Konsequenz der Kornformänderung in Folge des Massetransport durch Diffusion (entlang von Korngrenzen) ist, kommt es zum Korngrenzengleiten. In größtenteils kolumnaren Dünnschichten erfolgt diese Kornformänderung nicht global sondern lokal; an Stellen, wo eine Korngrenzenanordnung mit schrägen Korngrenzen vorliegt, entwickeln sich Scherspannungen entlang dieser schrägen Korngrenzen (es sei

anzumerken, dass es im vorliegenden Fall ein planarer Spannungszustand in der Sn Dünnschicht vorherrscht), die ein „Herauswachsen“ des Oberflächenkorns bewirken, indem das erforderliche Korngrenzengleiten erleichtert wird. Hierdurch ermöglicht dieser lokale Transportprozess von Sn, dass die Spannungs-, und dadurch Leerstellenkonzentrationsgradienten in der gesamten Sn Dünnschicht relaxieren.

Dünnschichten mit einer globularen Kornmorphologie (z.B. SnPb oder Sn; siehe Kapitel 5) weisen eine verhältnismäßig große Anzahl an passenden Stellen (d.h. mit schrägen Korngrenzen) auf, wo Coble-ähnliches Kriechen von Sn aufgenommen werden kann: Sn Transport durch Diffusionskriechen kann an jeder schrägen Korngrenze (mehr oder weniger gleichmäßig in der gesamtem Dünnschicht verteilt) erfolgen, wo sich entsprechend Scherspannungen ausbilden können, so dass ein eher gleichförmiges „Anschwellen“ der Dünnschicht senkrecht zur Oberfläche erfolgt, jedoch ohne die Notwendigkeit lokal Whisker zu bilden. Die Kornformänderung erfolgt global, nicht lokal wie im Fall von kolumnaren Sn Dünnschichten, und aus diesem Grund verbleiben Dünnschichten mit einer globularen Kornmorphologie auch im Vorhandensein von Druckspannungen frei von Whiskern.

Die vorliegende Arbeit zeigt, dass der Whisker-unterdrückende Effekt des Pb (in SnPb Dünnschichten) nur der Bildung einer globularen Kornmorphologie zuzuschreiben ist, die Spannungsrelaxation in der Dünnschicht an jeder schrägen Korngrenze ermöglicht, was zu einem gleichmäßigen Kornwachstum führt. Pb ist „lediglich“ eine Substanz, um während der Dünnschichtabscheidung von Sn das kolumnare Schichtwachstum zu stören. Dieses Wissen führt zu der im Abschnitt 9.4 beschriebenen Whiskervermeidungsmaßnahme (siehe auch Kapitel 5).

9.3. Modell der Whiskerbildung

Basierend auf den bisher vorgestellten Parametern, die im System Sn auf Cu die spontane Whiskerbildung steuern, kann das in Abb. 9.5 gezeigt Whiskermodell vorgeschlagen werden (siehe Kapitel 5 und 7):

Nach der Abscheidung der Sn Dünnschicht (Schichtdicke von wenigen Mikrometern) mit einer kolumnaren Kornmorphologie auf Cu und während anschließender Alterung bei Raumtemperatur, reagieren Sn und Cu mit (nur) der Bildung einer intermetallischen Phase Cu_6Sn_5 auf der Sn Seite der Sn/Cu Grenzfläche. Das thermodynamisch bedingte, bevorzugte „Hineinwachsen“ von Cu_6Sn_5 in die Sn

Dünnschicht entlang von Sn Korngrenzen, die im Kontakt mit der Sn/Cu Grenzfläche stehen, induziert Druckspannungen parallel zur Sn/Cu Grenzfläche auf Grund der durch das dicke Substrat auferlegten geometrischen Randbedingungen in Folge der spezifischen Volumenausdehnung durch die Bildung der IMP, insbesondere in dem Tiefenbereich wo Cu_6Sn_5 Bildung stattfindet (es sei auch angemerkt, dass die native Sn Oxidschicht auf der Oberfläche von Sn Oberflächendiffusion verhindert, was eine weitere Einschränkung im System bedeutet). Nahe der Sn Oberfläche kommt es zur Ausbildung von Zugspannungen parallel zur Sn/Cu Grenzfläche; Zugspannungen sind v.a. an den Stellen besonders ausgeprägt, wo auch das Wachstum von Cu_6Sn_5 entlang der Sn Korngrenzen besonders signifikant ist, so wie es unterhalb eines Whiskers zu beobachten ist. Solche Oberflächenkörner, die bereits während der Schichtabscheidung gebildet werden, weisen schräge (im Bezug zur Probennormalen) Korngrenzen auf, im Gegensatz zu den kolumnaren Korngrenzen der angrenzenden Sn Körner der Dünnschicht. In Folge der oben geschilderten Prozesse, die sich in dem äußerst immobilen (im Bezug auf Korngrenzenmobilität) System abspielen, kommt es zur Entwicklung von negativen, senkrecht zur Oberfläche orientierten Eigenspannungsgradienten in Richtung zunehmender Tiefe und negativen, horizontal zur Oberfläche orientierten Eigenspannungsgradienten von der Whiskerkeimstelle (d.h. Oberflächenkörner mit schrägen Korngrenzen) in Richtung Whiskerumgebung. Diese beiden Typen von Spannungsgradienten stellen die Triebkraft für den gerichteten Transport von Sn Atomen in Richtung Whiskerkeimstelle dar – als Spannungsrelaxationsmechanismus – und kontrollieren somit das Sn Whiskerwachstum. Es ist die negative Natur solcher Spannungsgradienten, die das Whiskerwachstum antreibt, nicht die Druckspannung an sich. Folglich kann Whiskerwachstum sogar bei Vorhandensein von Zugspannung erfolgen, vorausgesetzt dass eine negative Ausprägung des Spannungsgradienten vorliegt. Während anhaltender Spannungsrelaxation mittels lokalem Whiskerwachstum kommt es nicht zur Ausbildung von Materialabreicherungen an der Whiskerwurzel (nicht einmal bei „extrem“ langen Whiskern), was deutlich darauf hindeutet, dass Whiskerwachstum mit einer weitreichenden Sn Diffusion in Verbindung steht. Dieses Verständnis der Prozesse, die Whiskerbildung bei Raumtemperatur kontrollieren, erlaubt es die Bildung und das Wachstum von Sn Whiskern als eine spezielle Form von durch Spannungsgradienten angetriebenem, lokalem Diffusionskriechen (Coble-Kriechen) zu deuten.

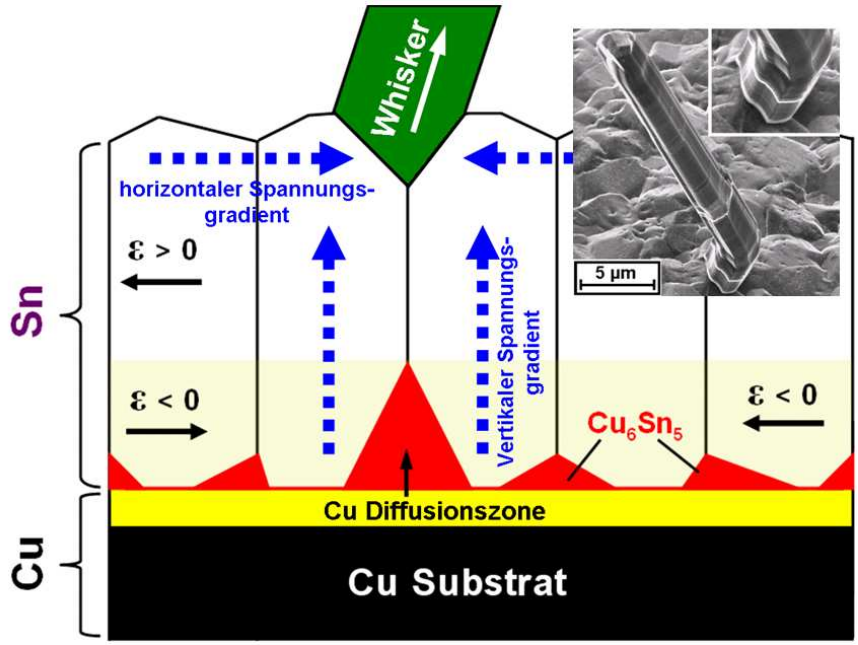

Abbildung 9.5: Schematisches Modell der Vorgängen in Sn Dünnschichten abgeschieden auf Cu Substraten, die während der Raumtemperaturalterung zur Whiskerbildung führen, basierend auf den Ergebnissen der vorliegenden Arbeit. Die Ionenstrahlabbildung stellt die Wachstumsmorphologie eines Whiskers dar.

9.4. Whiskervermeidungsmaßnahmen

Die Ergebnisse der vorliegenden Arbeit ermöglichen es die folgenden Whiskervermeidungsmaßnahmen vorzuschlagen:

(i) Basierend auf den Ergebnissen, die in Kapitel 4 vorgestellt wurden, wird vorgeschlagen spontanes Whiskerwachstum durch Anwendung der Erkenntnisse über Grenzflächenthermodynamik zu verhindern; hierdurch kann die Wachstumsmorphologie von Cu_6Sn_5 von „irregulär“ zu „regulär“ modifiziert werden, indem das Wachstum Cu_6Sn_5 entlang der Sn/Cu Grenzfläche energetisch bevorzugt wird im Vergleich zum irregulären Wachstum entlang von Sn Korngrenzen. Das kann realisiert werden, indem die Korngrenzenenergie von Sn erniedrigt und/oder die Grenzflächenenergie zwischen Sn und Cu erhöht wird. Das gezielte Hinzufügen einer Komponente zur Sn Dünnschicht, die die Sn Korngrenzenenergie reduziert, wäre zum Bespiel eine Möglichkeit; Pb ist eine solche Komponente (Benetzen der Sn Korngrenzen durch Pb führt zur Bildung von Sn/Pb Grenzflächen mit einer Energie, die in etwa der Hälfte von Sn/Sn Grenzflächen entspricht, siehe [48] im Kapitel 4).

(ii) Basierend auf den Ergebnissen, die in Kapitel 5 vorgestellt wurden, wird vorgeschlagen spontanes Whiskerwachstum in reinen Sn Dünnschichten mittels Kontrolle der Mikrostruktur zu unterdrücken, d.h. eine globulare Kornmorphologie zu realisieren, die in der Lage ist Druckspannungen global (an jeder schrägen Korngrenze, begleitet von Kornwachstum) zu relaxieren, nicht lokal (in Form von filamenthaften Whiskern), wie das typischerweise der Fall ist in kolumnaren Sn Dünnschichten mit nur wenigen Oberflächenstellen mit schrägen Korngrenzen. Das kann realisiert werden, z.B. durch entsprechende Wahl der Elektrolytchemie, des Substratmaterials und/oder der Abscheidungsroutine.

List of publications

1. Sobiech M., Wohlschlögel M., Welzel U., Mittemeijer E. J., Leineweber A., Hügel W. & Kirchner V. (2006): Investigation of mechanical stress gradients of Sn thin films, *Hasylab Annual Report* **1**, 591.
2. Sobiech M., Welzel U., Schuster R., Mittemeijer E. J., Hügel W., Seekamp A. & Müller V. (2007): The microstructure and state of stress of Sn thin films after post-plating annealing: an explanation for the suppression of whisker formation?, *Proceedings of the 57th Electronic Components and Technology Conference in Reno, USA*, 192.
3. Sobiech M., Welzel U., Mittemeijer E. J., Hügel W. & Seekamp A. (2008): Driving force for Sn whisker growth in the system Cu-Sn, *Appl. Phys. Lett.* **93**, 011906.
4. Sobiech M., Wohlschlögel M., Welzel U., Mittemeijer E. J., Hügel W., Seekamp A., Liu W. & Ice G. E. (2009): Local, submicron strain gradients as the cause of Sn whisker growth, *Appl. Phys. Lett.* **94**, 221901.
5. Sobiech M., Wohlschlögel M., Welzel U., Mittemeijer E. J., Hügel W., Seekamp A., Liu W. & Ice G. E. (2009): Avoiding short circuits by a whisker, *APS Annual Science Report*, 20.
6. Sobiech M., Krüger C., Welzel U., Wang J. Y., Mittemeijer E. J. & Hügel W. (2010): Evolution of microstructure and stress of and associated whisker growth on Sn layers sputter-deposited on Cu substrates, *J. Mater. Res.* **25**, 2166.
7. Sobiech M., Krüger C., Welzel U., Wang J., Mittemeijer E. J. & Hügel W. (2010): Phase formation at the Sn/Cu interface during room temperature ageing: Microstructural evolution, whiskering and interface thermodynamics, *J. Mater. Res.*, submitted.
8. Sobiech M., Teufel J., Welzel U., Mittemeijer E. J. & Hügel W. (2010): Stress relaxation mechnaisms of Sn and SnPb conatings electrodeposited on Cu: avoidance of whiskering, *Acta Mater.*, submitted.
9. Sobiech M., Welzel U., Mittemeijer E. J. & Hügel W. (2010): Room temperature evolution of microstructure and residual stress in Sn coatings deposited on Ni (on Cu) and FeNi substrates: The explanation for the absence of Sn whisker growth, in preparation.

Press releases (online)

1. *How tin whiskers grow (May 18th, 2009)*
   http://blogs.physicstoday.org/update/2009/05/how-tin-whiskers-grow.html
2. *Getting to the roots of lethal hairs (September 29th, 2009)*
   http://www.mpg.de/english/illustrationsDocumentation/documentation/pressReleases/2009/pressRelease20090929/index.html
3. *Haarwuchs durch Spannungsunterschiede (September 2009)*
   http://www.uni-stuttgart.de/uni-kurier/uk104/PDF/04_forschen.pdf
4. *Getting to the Roots of Lethal Hairs (October 9th, 2009)*
   http://www.aps.anl.gov/Science/Highlights/Content/APS_SCIENCE_20091008B.php

Danksagung

Die vorliegende Arbeit wurde am Max-Planck-Institut für Metallforschung (Abteilung Prof. Dr. Ir. E. J. Mittemeijer) in Stuttgart, bei der Robert Bosch GmbH (Geschäftsbereich Automotive Electronics) in Reutlingen sowie am Institut für Materialwissenschaft der Universität Stuttgart angefertigt.

An erster Stelle möchte ich Herrn Prof. Dr. Ir. E. J. Mittemeijer, meinem Doktorvater, dafür danken, dass er mich in seine Abteilung aufgenommen und mir dieses überaus spannende Thema überlassen hat. Sein außergewöhnliches Engagement während der regelmäßigen wissenschaftlichen Diskussionen, seine unermüdliche Bereitschaft zum freien Gedankenaustausch sowie sein volles Vertrauen in meine Person haben maßgeblich zum Erfolg der Arbeit beigetragen.

Herrn Prof. Dr. J. Bill danke ich für die freundliche Übernahme des Mitberichts, sowie Herrn Prof. Dr. E. Roduner für die Bereitschaft den Prüfungsvorsitz zu übernehmen.

Ich danke der Robert Bosch GmbH (Geschäftsbereich Automotive Electronics) in Reutlingen, sowie den Mitarbeitern der Abteilung „Quality Management Suppliers“, für die tatkräftige Unterstützung, das stets in mich gesetzte Vertrauen sowie für die Ermöglichung dieses einmaligen Kooperationsprojekts.

Besonders herzlich möchte ich mich bei meinem täglichen Betreuer am Max-Planck-Institut für Metallforschung, Dr. Udo Welzel, für die volle Unterstützung, die zahlreichen wissenschaftlichen Diskussionen sowie für die wertvollen Ratschläge bedanken. Sein außergewöhnlicher Einsatz war für die erfolgreiche Fertigstellung dieser Arbeit unerlässlich.

Bedanken möchte ich mich auch bei meinen täglichen Betreuern bei der Robert Bosch GmbH, Dr. Werner Hügel und Dr. Andrea Seekamp, für die zielstrebige Unterstützung dieses Kooperationsprojekts und für die intensiven Diskussionen.

Allen Mitarbeitern des Max-Planck-Insituts für Metallforschung, insbesondere den Kollegen der Abteilung Mittemeijer, gilt mein herzlicher Dank für die vertrauensvolle Zusammenarbeit und die angenehme Arbeitsatmosphäre.

Ich möchte mich besonders herzlich bei meiner Familie sowie meinem Freundeskreis bedanken. Ein ganz besonderer Dank gebührt jedoch meiner Frau Tanja, deren Unterstützung nicht in Worte zu fassen ist.

Curriculum Vitae

Persönliche Daten

Name	Matthias Lukas Sobiech
Geburtsdatum	19. Januar 1979
Geburtsort	Zakopane (Polen)
Staatsangehörigkeit	deutsch

Schulbildung

1986 – 1990	Grundschule in Möglingen und Ditzingen
1990 – 1999	Gymnasium Glemsaue in Ditzingen Abschluss: Allgemeine Hochschulreife

Zivildienst

1999 – 2000	Rettungsdienst beim Deutschen Roten Kreuz in Leonberg

Hochschulbildung

2000 – 2006	Studium der Geowissenschaften an der Universität Stuttgart; Diplomarbeit am Institut für Mineralogie und Kristallchemie der Universität Stuttgart in Zusammenarbeit mit dem Zentrum für Sonnenenergie- und Wasserstoff-Forschung in Stuttgart Thema: „*Mikro-Ramanspektroskopie zur Untersuchung von strukturellen und chemischen Inhomogenitäten in Dünnschicht-solarzellen Cu(In,Ga)Se_2*“ Hauptberichter: Prof. Dr. rer. nat. Paul Keller

Promotion

2006 – 2010	Max-Planck-Institut für Metallforschung in Stuttgart, Robert Bosch GmbH in Reutlingen und Institut für Material-wissenschaft der Universität Stuttgart Thema: „*Whisker formation on Sn thin films*” Hauptberichter: Prof. Dr. Ir. Eric J. Mittemeijer